

THESIS

NANOFIBER BASED SMART WOUND DRESSING COMBINED WITH BACTERIA
DETECTION AND DRUG DELIVERY

Submitted by

Faqrul Hassan

Department of Design and Merchandising

In partial fulfillment of the requirements

For the Degree of Master of Science

Colorado State University

Fort Collins, Colorado

Summer 2018

Master's Committee:

Advisor: Yan Vivian Li

Juyeon Park

Ketul Popat

Copyright by Faqrul Hassan 2018

All Rights Reserved

ABSTRACT

NANOFIBER BASED SMART WOUND DRESSING COMBINED WITH BACTERIA DETECTION AND DRUG DELIVERY

Since the emergence of Nanotechnology in the past decades, the development and design of nanofibers demonstrated the great potential for applications in wound treatment. Proliferation of bacteria in wound site is a major challenge in combating wounds. Bio-sensing wound dressing composed of nanofibers has proven to be an effective tool in detecting bacterial presence at wound sites. Though wound dressing with antibacterial property is available but they are not quite effective in terms of bioavailability and sustained release of drugs. Biodegradable polymeric nanoparticles have been proven to increase bioavailability, encapsulation, and control release of drugs with less toxic properties. In this study, poly diacetylene (PDA)-based composite nanofibers were prepared to study the microstructure and mechanical properties, and to investigate relationship between these two. It was found that mixing polyurethane (PU) polymer with the PDA yielded better mechanical properties as PU and PDA mixed homogeneously and this helped to form large crystalline regions in the fiber microstructure. In the second part of this thesis, poly(D, Lactide-co-glycolide) acid (PLGA) nanoparticles were synthesized by double emulsion solvent evaporation technique to encapsulate hydrophilic gentamicin antibiotics. The effects of different formulation parameters on the particle size and structure were examined thoroughly which included copolymer ratios of PLGA, molecular weight and concentration of stabilizing agents or surfactants, volume of both aqueous and organic phase, sonication and stirring rate and time. The molecular weight and concentration of surfactants had the most impact on the size and morphology of particles. Higher molecular weight of surfactants caused agglomeration of particles. Increasing the concentration of surfactants resulted in smaller particles. PLGA particles with different morphologies were obtained where the average size ranged 300 nm to several microns.

ACKNOWLEDGEMENTS

Firstly, I would like to express my sincere gratitude to my advisor Dr. Yan Vivian Li for the continuous support of my master's study and related research, for her patience, motivation, and immense knowledge. Her guidance helped me in all the time of research and writing of this thesis. The door to Dr. Li's office was always open whenever I ran into a trouble spot or had a question about my research or writing.

Besides my advisor, I would like to thank the members of my thesis committee: Dr. Juyeon Park and Dr. Ketul Popat for their insightful comments and encouragement, but also for the hard question which incited me to widen my research from various perspectives.

My sincere thanks also goes to Dr. Ogle for her continuous consultation and support throughout my master's program. No matter how hard or hostile the situation was she made it smooth for me.

With a special mention to Dr. Roy Geiss and Dr. Patrick McCurdy from Central Instrument Facility (CIF) at Colorado State University (CSU) for guiding me with the TEM and SEM and helping me in understanding the data.

Finally, I must express my very profound gratitude to my parents and to my sister for providing me with unfailing support and continuous encouragement throughout my years of study and through the process of researching and writing this thesis. This accomplishment would not have been possible without them.

Thank you all!

DEDICATION

I would like to dedicate this thesis to my dear mom Shamsun Naher.

TABLE OF CONTENTS

ABSTRACT	ii
ACKNOWLEDGEMENTS	iii
DEDICATION	iv
LIST OF TABLES	vii
LIST OF FIGURES	viii
Chapter 1 INTRODUCTION	1
Chapter 2 LITERATURE REVIEW	5
2.1 Introduction of Nanofibers in Wound Care	5
2.2 Coaxial Electrospinning	6
2.3 Polymers Used for Nanofiber Fabrication	8
2.4 Drug Delivery and Biodegradable Polymers	9
2.5 Nanoparticle Based Drug Delivery System	10
2.6 Poly Lactic-co-Glycolic Acid (PLGA)	11
2.7 Synthesis of PLGA Nanoparticles	12
2.8 Drug Release in Polymer System	13
2.9 Interaction of Bacteria with Nanofiber Structure	15
2.10 Evaluation of Antibacterial Efficacy	16
Chapter 3 MATERIALS AND METHODS	18
3.1 Materials	18
3.2 Nanoparticle Synthesis	18
3.3 Coaxial Spinning of Core-Shell Nanofibers	19
3.4 Nanoparticle and Nanofiber Characterization	20
3.4.1 Morphology	20
3.4.2 Mechanical strength	20
3.4.3 Drug-polymer interactions	20
3.4.4 Drug release study	21
3.4.5 Drug incorporation efficiency	21
3.4.6 Antibacterial test	21
Chapter 4 MANUSCRIPT	22
4.1 Introduction	23
4.2 Experimental Section	25
4.2.1 Materials	25
4.2.2 Methods	26
4.2.3 Fiber Characterizations	28
4.3 Results and Discussions	31
4.3.1 Colorimetric response of PDA fibers in bacterial solution	31
4.3.2 Fiber Structure and morphologies	32

4.3.3	TEM Analysis	36
4.3.4	Mechanical Properties Analysis	41
4.3.5	AFM Analysis	44
4.3.6	Contribution of PDA to the Fiber Structures and Strength	48
4.4	Conclusion	50
Chapter 5	SYNTHESIS OF PLGA NANOPARTICLES	51
5.1	Introduction	51
5.2	Methods	52
5.3	Results and Discussions	57
5.3.1	Mechanism of PLGA Nanoparticle Formation in Double Emulsion Method	60
5.3.2	Effects of Preparation Conditions on Particle Size and Morphology . .	63
Chapter 6	CONCLUSION	73
Chapter 7	FUTURE WORKS	74
Bibliography	76

LIST OF TABLES

4.1	Compositions of the prepared electrospinning solutions.	27
4.2	Summary of nanomechanical properties of pure and composite fibers	45
5.1	Formulation parameters used for PLGA (50:50) nanoparticle synthesis by double emul- sion technique.	55
5.2	Formulation parameters used for PLGA (75:25) nanoparticle synthesis by double emul- sion technique	56

LIST OF FIGURES

2.1	Coaxial electrospinning setup	7
2.2	Structure of poly lactic-co-glycolic acid	11
2.3	Drug release profile of PLGA particles	14
3.1	Set-up used for preparation of nanoparticles by the double emulsification method	19
4.1	Polydiacetylene (PDA) synthesis scheme.	26
4.2	Colorimetric response of PDA fibers in bacteria solution	31
4.3	SEM images of electrospun PEO control nanofibers and PEO-PDA composite nanofibers	33
4.4	SEM images of electrospun PU control nanofibers and PU-PDA composite nanofibers	34
4.5	Comparison line graph for average diameter of different composite nanofibers	35
4.6	TEM micrographs of PEO control nanofiber	37
4.7	TEM micrographs of PU control nanofiber	37
4.8	TEM micrographs of PEO-PDA composite nanofiber	39
4.9	TEM micrographs of PU-PDA composite nanofibers	40
4.10	Tensile stress-strain curves for 100% PEO and 100% PU fiber	41
4.11	Tensile stress-strain curves for PEO-PDA and PU-PDA composite nanofibers.	43
4.12	AFM topographical images and F-D curves obtained on PEO and PU control fibers	46
4.13	AFM topographical images and F-D curves obtained on PEO-PDA and PU-PDA composite fibers	47
4.14	TEM micrographs of PDA crystals	48
5.1	PLGA nanoparticles produced from high molecular weight (89,000-98,000 g/mol) PVA	57
5.2	SEM micrographs of A. PLGA NP18 and B. NP19 prepared from low molecular weight (13,000-31,000 g/mol) PVA	58
5.3	SEM micrographs of PLGA NP10 and PLGA NP11 prepared by the emulsion solvent evaporation method	59
5.4	Primary emulsion (w/o) with aqueous droplets dispersed into organic/continuous phase.	61
5.5	Double emulsion droplets with A. single and B. multiple aqueous droplets inside it.	62
5.6	PLGA microparticles with capsule and honeycomb structure observed under SEM.	62
5.7	Effect of PLGA monomer ratios on particle size and morphology	63
5.8	Effect of PLGA concentrations on particle size and morphology	64
5.9	Effect of surfactant (PVA) concentration on particle size and morphology	66
5.10	Effect of sonication time and power on particle size and morphology	67
5.11	Effect of second sonication of w/o/w double emulsion droplet	67
5.12	Effect of internal aqueous phase on particle size and morphology	69
5.13	Effect of external aqueous phase on particle size and morphology	69
5.14	Effect of high stirring speed and temperature on particle size and morphology	70
5.15	Effect of longer stirring period on particle size and morphology	71

Chapter 1

INTRODUCTION

A wound is defined as an injury or tear on the skin surface by physical, chemical, mechanical, and/or thermal damages. There are mainly two types of wounds: acute (healable within 8 to 12 weeks) and chronic wounds (healing takes more than 12 weeks) [Zahedi et al., 2010]. Wound healing is a complex biological process that consists of three major phases - inflammation, proliferation, and maturation [Cherreddy et al., 2016]. Wound dressings have been developed and used to facilitate the healing process. Wound dressing works as a protective barrier against infection to assist the wound healing process. Wound infection is a serious problem that mainly results from compromised immune systems, diabetes, or other chronic conditions. Chronic wound infections are common among the high-risk population such as the elderly. Wound infections can be fatal (causing sepsis), especially for a post-surgical patient [Tissue, 2015]. Recurrence of wound infections is quite common too [Ferreira et al., 2006]. Bacteria is one of major factors causing wound infections. Bacteria are ubiquitous in wound. Infection occurs when the cell count of the bacteria reaches to a critical threshold. Bacterial colonization in chronic wounds is a well-recognized factor contributing to impaired wound healing [Jockenhöfer et al., 2013, Renner et al., 2012]. In the United States, chronic wounds affect more than 6 million people annually and this number is anticipated to increase primarily due to the increase of aging population and the high prevalence of diabetes mellitus. According to American Academy of Dermatology Association (AADA) chronic wounds are the number 1 direct medical cost of all human skin diseases, costing \$9.7 billion in the United States every year [Bickers et al., 2006]. A severe infection may even require amputation, such as diabetes foot disease. Therefore, effective diagnosis and treatment of wound infections is critical in wound care and management.

Conventional wound dressings such as gauze, tulle, bandages, and low adherence dressings, may prevent bacterial infections to some extent [Heyer et al., 2013], but do not provide other functions such as diagnosis or treatment. Currently, no wound dressings are able to diagnose if infection

occurs without any further laboratory pathological procedures. In addition, current wound dressings are not able to automatically deliver treatment solutions to the infected wounds. Although antibiotics are commonly applied to reduce bacterial colonization, there are still many challenges with antibiotic treatment such as low bioavailability (the degree to which a drug or other substance becomes available to the target tissue and has an active effect after administration), poor penetration to bacteria infected intracellular compartment, and antibiotic resistance. Recently, antibiotics-encapsulated in nanoparticles or microparticles that are made up of biodegradable polymers have shown great potential in replacing the administration of antibiotics in their free form (without having any other surface modifying polymers) to improve treatment efficiency [Xiong et al., 2014]. Researchers are now more interested in developing bioactive wound dressing than conventional wound healing materials. In bioactive wound dressing materials, active ingredients (e.g., antibiotics, antimicrobial agents, and vitamin) are incorporated into wound dressing hence to facilitate wound healing process [Zahedi et al., 2010]. Recently, biopolymers containing active antibiotics have been used in wound dressing materials [Imbuluzqueta et al., 2013, Stebbins et al., 2014]. The purpose of applying antibiotics and other antibacterial in wound dressing is mainly to inhibit the bacterial growth and combat infections more rapidly especially for chronic wounds. The use of antibiotics into the dressing can provide tissue compatibility, low occurrence of bacterial resistance and reduced interference with wound healing [Doillon and Silver, 1986]. The use of lower antibiotic doses within the dressings also reduces the risk of systemic toxicity considerably. For example, gentamicin is an effective antibiotic and is used in many therapeutic treatments in vivo and in vitro. Convincing results of their efficacy against the bacteria have also been found [Imbuluzqueta et al., 2013, Sirc et al., 2012, Thein et al., 2013]. As most of the antibiotics including gentamicin are hydrophilic, they cannot reach the target molecule quite efficiently. The antibiotics also deteriorate fast in vivo because there is no protective layer to sustain for a long period of time. Nanoparticles have been used to improve the drug delivery system due to their controlled and sustained drug release properties, subcellular size, and biodegradability within our body without producing any toxic elements. Nanoparticles have become a part of sustained drug delivery as

it can reduce the amount of drug doses without compromising therapeutic effectiveness, preventing the possible toxic side effects that ultimately result in effective therapeutic outcomes for the patients [Wei, 2012]. These wound dressing materials are found to have a direct influence on the acceleration of the wound healing process without producing any toxics at the wound sites. Although these wound dressings have significantly improved wound management, a wound dressing that can effectively heal chronic wounds while providing bacterial diagnosis has been yet explored.

The proposed research focuses on design and development of novel dressing materials that can provide bacterial diagnosis as well as antibiotic treatment simultaneously. The dressing materials will compose of nanofibers with a core-shell structure produced by coaxial electrospinning. The shell of the nanofibers will be a composite of polyurethane (PU) and polydiacetylene (PDA). The PDA is a conjugative polymer that demonstrates interesting bio-sensing properties including detecting bacteria via colorimetric changes. The core of the nanofibers will be constructed with antibiotics such as gentamicin-loaded nanoparticles that is able to kill and clean wide-spectrum bacteria. Gentamicin is an antibiotic that is used to treat moderate to severe bacterial infections and often used for the initial stages of the infection at clinics. Poly (lactic-co-glycolic acid) (PLGA) nanoparticles will be used as drug carrier because PLGA has high biodegradability and biocompatibility (approval from The U.S. Food and Drug Administration (FDA)), capability of encapsulating both hydrophilic or hydrophobic drug particles, protection of drug from degradation, sustained release, possibility of surface modifications and target delivery to specific organs or cells [Cherreddy et al., 2016, Kumari et al., 2010].

The core-shell nanofibers will potentially monitor the presence of bacteria in wounds and simultaneously deliver antibiotic treatment. The objective of this project is to develop uniform core-shell nanofibers in the range of 100-300nm in diameter and the nanofibers consist of PU-PDA in the shell and gentamicin in the core. The PDA will be mixed with PU allowing it to be directly electrospun, resulting in uniform nanofibers. A coaxial electrospinning method will be used to develop the core-shell nanofibers. Coaxial electrospinning has been proven as a very dynamic process to produce the core-shell fiber structure. There are many factors that can influence the

entrapment of core components and also various shell structures is possible in this method [Sun et al., 2003, Chakraborty et al., 2009]. A variety of electrospinning parameters such as- solution concentration, applied voltage, tip-to-collector distance, injection rate etc. will be investigated. Electrospun fibers will be characterized using scanning electron microscope, transmission electron microscopy, and atomic force microscopy.

This thesis has been arranged in the following four chapters. A literature review of nanofiber in wound care, coaxial electrospinning, PLGA polymer properties, various nanoparticle synthesis methods, and their characterizations have been provided in chapter 2. In chapter 3, the proposed research and experiments include the synthesis and characterization of gentamicin-loaded PLGA nanoparticles, the fabrication and characterizations of core-shell nanofibers, and the release study of gentamicin from nanofibers. Chapter 4 includes a manuscript thoroughly investigating the microstructure and macromechanical properties of PDA based composite fibers. Synthesis of PLGA nanoparticles and the effects of various formulation parameters on nanoparticles' size and morphology have been discussed in detail in chapter 5.

Chapter 2

LITERATURE REVIEW

2.1 Introduction of Nanofibers in Wound Care

One of the principal research drivers in the field of wound care technology focuses on the development of wound dressings in the form of nanofibrous meshes [Zhang et al., 2005]. These nanofiber structures are made of non-woven, ultra-fine polymeric fibers with diameters ranging from several micrometers down to a few nanometers. Nanofibrous meshes have several intrinsic properties (e.g., high-surface area, nanoporosity, absorbability, semi-permeability, conformability, and functional ability) [Zahedi et al., 2010], which make them particularly attracting in wound dressing preparation. Extracellular matrix (ECM) is the largest component of normal skin tissue and gives the skin its unique properties of elasticity, tensile strength and compressibility. ECM plays an important role during the wound healing process by acting as a scaffold for physically supporting cells and providing conditions for cell attachment, proliferation, migration, and differentiation [Martins et al., 2007]. Nanofibrous meshes offer a good starting point toward the development of a synthetic scaffold that is able to reproduce the structure of the natural ECM. Due to the nanostructures of the mesh and random alignment within the mesh, the fibers tend to imitate the fibrous architecture of the natural ECM. In addition, nanofibrous meshes have shown the promotion of the hemostasis (the stoppage of blood flow through a blood vessel or organ of the body) of injured tissues owing small interstices and the high-surface area of the fibers [Zhang et al., 2005]. The high-surface area of nanofibrous meshes is also essential for fluid absorption, enhanced dermal drug and antimicrobial delivery, providing the opportunity to modify the surface of the fibers with specific chemical functionalities. Nanofiber structures show high inter-connected porosity (60-90%), allowing cell respiration, high-gas permeation, and prevention of wound desiccation and dehydration [Zhang et al., 2005].

Nanofibers are also used in drug delivery systems. Two basic delivery designs are common: matrices and reservoirs. In the matrix carriers, the drug is homogeneously dispersed in the material of the nanofiber, and the release of the drug is based on solid-state diffusion or a desorption mechanism [Thakur et al., 2008, Srikar et al., 2008]. Such a drug-loaded system tends to have a strong burst release within the first hours, followed by slow release of remaining drug. In the second design, reservoir structures consist of a drug-loaded core and a covering polymer shell [Srikar et al., 2008, Huang et al., 2006]. The core-shell structure enables good control of the drug release profile by adjusting the shell properties, such as the microstructure, the thickness, and the degradability of the shell [Sirc et al., 2012]. The core-shell nanofibers can be developed for the loading of growth factors, vitamins, and other bio-molecules that are able to enhance the healing processes.

2.2 Coaxial Electrospinning

In the past two decades, electrospinning has been extensively used to produce microfibers and nanofibers [Reneker and Chun, 1996, Huang et al., 2003]. This technique utilizes a high electrical charge to draw very fine fibers from a polymer solution. This simple technique of nanofiber fabrication has undergone many variations. One advanced development is the coaxial electrospinning. In this method, double-layered composite nanofibers can be produced with unique properties. A typical coaxial electrospinning set-up consists of three main components including coaxial needle, syringe pump, and high voltage source. During spinning, two different polymer solutions are fed simultaneously in the outer and inner channels of the coaxial needle. High voltage is applied to charge the polymer solutions. A syringe pump maintains a constant flow rate of the polymer solutions through the needle while a droplet of the polymer solutions is formed at the tip of the needle. The high voltage induces a charge on the surface of the polymer droplet that is subjected to two opposing forces- the electrostatic repulsion force and the surface tension of the solution. At high voltage, the charged droplet overcomes the surface tension and elongates to form a Taylor cone. The Taylor cone continues to develop into a liquid jet that is continuously stretched to be thin due to the electrostatic repulsion present in the polymer solution and the whipping process they undergo

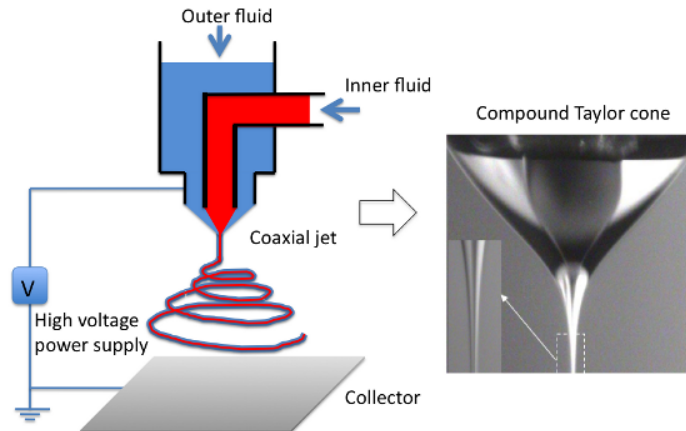


Figure 2.1: The basic setup for coaxial electrospinning and fabrication process of common core-shell nanofibers [Li et al., 2010].

before reaching the collector. The thin fibers dry rapidly and are collected on a collecting plate [Li et al., 2010]. Figure 2.1 shows a basic setup of a coaxial electrospinning. Two different fluids are fed simultaneously and separately through a coaxial spinneret needle including an inner channel and outer channel, providing a core-shell fiber structure. Recently, the core-shell fibers have been used as a novel technique in drug delivery and wound healing system [Nguyen et al., 2011, Liang et al., 2007]. Using a coaxial electrospinning, Lee et al. have achieved nearly 100% drug entrapment [Nguyen et al., 2012]. It has been possible to control the drug release profile by tuning the size of nanoparticles that entrap drugs and polymer concentration in the coaxial electrospinning. The flow rate in the electrospinning of polymer solutions is a primary parameter that can affect the core/shell structure of the nanofibers and hence the performance of the nanofibers [Sun et al., 2006b]. Low core feed rates resulted in discontinuous core/shell composite nanofibers. The fluid jet could be broken into droplets or split into core and shell jets when the core feed rate exceeds a suitable range. Diaz et al. have found that the stability of this compound jet of two liquids is strongly affected by the viscosity, core/sheath interface tension, as well as the feed rates [Díaz et al., 2006]. When fabricating the core/shell nanofibers, Nguyen et al. observed that a stable Taylor cone was developed when a sufficiently high viscosity of the shell fluid and a low

value of the core/shell interfacial tension were satisfied [Nguyen et al., 2012]. However, using dual capillary system in the coaxial electrospinning can increase the fiber diameter significantly in comparison to the single nozzle electrospinning [Maleki et al., 2013].

2.3 Polymers Used for Nanofiber Fabrication

Nanofibers can be formed from various polymers depending on the end uses. When developing nanofibers for wound dressing applications, biocompatible polymers are used such as poly-L-lactide (PLLA), polyvinyl chloride (PVC), polyacrylonitrile (PAN), polycaprolactone (PCL), polyethylene oxide (PEO), and poly diacetylene (PDA) [Chen et al., 2012]. PDAs are attracting because they have responsive chromogenic properties. PDAs exhibits color changes in presence of external stimuli, such as pH, temperature, bacteria etc. [Chae et al., 2007]. The external stimuli disturb the sidechain packing that affects the electronic absorption of the conjugated backbone of PDA, which ultimately result in its color transition [Chae et al., 2007]. PDAs usually have absorption at 650 nm, exhibiting a blue color. When the blue phase PDAs are exposed to external stimuli, the absorption is switched to 550 nm and the color of PDAs becomes red [Jelinek and Ritenberg, 2013]. The color transition properties have made PDAs as a potential material to be used in bacterial detection such as biosensors (a device that is sensitive to a biological element and generates and transmits signal regarding a physiological change of that element). Jeon et al. have studied the color transformation properties of PDA electrospun fibers and their results suggested superior sensitivity of PDA fibers compared to the thin films produce from the same solution [Jeon et al., 2012]. This was mainly attributed to the roughness and higher surface area of the nanofibers [Verstraete et al., 2016]. PDA monomers such as 10,12-pentacosadyonic acid (PCDA) molecules in an electrospinning solution are randomly distributed before electrospinning. They can self-assemble when the solution is drawn to fibers upon the solvent evaporation [Chae et al., 2007]. The self-assembly of diacetylene (DA) molecules is primarily promoted by two types of intermolecular interactions: directional hydrogen bonding between the carboxylic acid moieties and van der Waals interactions between neighboring alkyl chains of diacetylene monomers [Radke and Alocilja, 2005]. Due to the

low viscosity of PDA dissolved in organic solvents, it is difficult to electrospinning 100% PDAs. Previously, PDA electrospun fibers have been developed with a matrix polymer (that works as a supportive component in fibers), such as polymethyl methacrylate (PMMA), polystyrene (PS), tetraethyl orthosilicate (TEOS), and poly (ethylene oxide) (PEO) [Chae et al., 2007]. Alam et al. incorporated biocompatible PEO and PU with PDA to fabricate PDA composite nanofibers and showed that PDA nanofibers can be a great diagnostic tool for detecting the bacterial presence visually [Alam et al., 2016]. They observed that PDA composite fibers with higher matrix polymer to PDA ratio exhibited faster and pronounced color transition. Chae et al. also worked with the PDA-embedded composite fibers and investigated the application as chemosensors [Chae et al., 2007]. They found that PDA-embedded electrospun fibers could be a potential sensor material as they demonstrated fluorescence generation upon specific ligand receptor interaction.

2.4 Drug Delivery and Biodegradable Polymers

Drugs are critical in clinical wound treatment. A drug delivery system is necessary for effective clinical treatment. In the past few decades, significant medical advances have been made in the area of drug delivery especially in controlled drug delivery systems (CDD). In a CDD system, therapeutic agents are released at a predetermined rate to a specific site or system. For example, a polymer is combined with a drug or other active agent in such a way that the active agent is released from the polymeric shell in a predesigned manner [Chae et al., 2007]. The release of the active agent may be constant in a long period. It may be also cyclic in a long period, or it may be triggered by the environment or other external events. CDD is able to provide effective therapies while eliminating the potential for both low dosing and overdosing in drug management.

3000 years ago, natural biodegradable materials such as plant fibers, hair, tendons, and wool fibers have been used as suture material [Goldenberg, 1959]. As there was no practical drug delivery system at that time, suture materials had been used to close the wound site and to prevent it from bacterial infections. The need to develop safer biodegradable sutures led to investigations of synthetic biodegradable polymers [Muffly et al., 2011]. Since 1960s, synthetic biodegradable poly-

mers such as polyesters poly (glycolic acid) (PGA), poly(D,L-lactic acid) (PLA), and poly(D,L-lactic-co-glycolic acid) (PLGA) have been used for biodegradable suture for wound treatment applications [Kulkarni et al., 1971]. The use of degradable polymers in drug delivery applications has become prominent since then because they can degrade inside the body without producing toxic natural byproducts [Fredenberg et al., 2011]. The biomaterials commonly used in drug delivery can be broadly classified into two categories: (1) synthetic biodegradable polymers that includes relatively hydrophobic materials such as the α -hydroxy acids (a family that includes poly lactic-co-glycolic acid, PLGA), polyanhydrides, and others, and (2) naturally occurring polymers, such as complex sugars (hyaluronan, chitosan) and inorganics [Kamaly et al., 2016].

2.5 Nanoparticle Based Drug Delivery System

Advances in nanotechnology have introduced innovative nanomaterials to revolutionize the field of drug delivery [Ravichandran, 2009]. The nanoparticles made from polymers have received great interest in controlled drug delivery due to high stability and ease of surface modification. This stability is attributed to the smaller size and reduced surface area of the nanoparticles [Singh and Lillard Jr, 2009]. The particles are stable either at room or body temperature. Various site-specific ligands can be attached to the nanoparticle surface for localized delivery. Nanoparticles can be tailored for controlled drug release and disease-specific localization by tuning the polymer characteristics and surface chemistry [Kreuter, 1994]. The advantages of using nanoparticles have been resulted from two main properties: small size and biodegradable materials. The nano size of these particles allows for efficient uptake in a variety of cell types and selective drug accumulation at target sites [Desai et al., 1997]. In addition, the enormous surface area of nanoparticles helps to increase the dissolution rate of the drugs that have poor solubility. The use of biodegradable materials in nanoparticle preparation allows for sustained drug release over a period of days or even weeks. The system also helps to protect therapeutic agents against enzymatic degradation [Ge et al., 2002]. Till now, various polymer-based nanoparticles have been investigated for drug delivery applications [Liechty et al., 2010]. PLGA nanoparticles have been preferred for

antibiotic treatment as they present many advantages over other polymers for drug delivery systems [Cheredy et al., 2016]. PLGA nanoparticles can load antibiotics and release them at a molecular level, which can directly reach the intracellular locations to which traditional drugs cannot reach [Pinto-Alphandary et al., 2000]. When entrapped in the nanoparticle, antibiotics show a better and sustained efficacy against bacteria because these nanoparticles degrade slowly and release required amount of drugs for a long period without producing any toxic products. For these reasons PLGA nanoparticles have been used for cancer treatment, treatment of cerebral diseases, inflammatory diseases, vaccination, infection treatment [Danhier, 2012].

2.6 Poly Lactic-co-Glycolic Acid (PLGA)

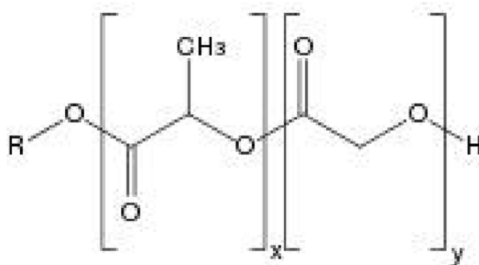


Figure 2.2: Structure of poly lactic-co-glycolic acid (x is the number of lactic acid units and y is number of glycolic acid units).

PLGA is a copolymer of poly lactic acid (PLA) and poly glycolic acid (PGA). It has been used for therapeutics entrapment with a wide range of molecular weights and can be fabricated into particles of various sizes and shapes [Champion et al., 2007]. The drug release capability using PLGA can be tuned by varying molecular weights (MW) of the polymer, ratio of lactide to glycolide, and drug concentration. For example, the extra methyl groups in the side chain of PLA make the polymer more hydrophobic compared to PGA, resulting in slow degradation rate. An increase of methyl groups in the PLA content lead to low water absorption, resulting in slow degradation rates [Makadia and Siegel, 2011]. Other parameters such as crystallinity, glass transition temperature (T_g), solubility, and MW can also influence the rate and release behaviors of incorporated

drug molecules. The effect of these polymer properties on the rate of drug release from biodegradable polymeric matrices has been widely studied. The change in PLGA properties during polymer biodegradation influences the drug release as well as the degradation rates of incorporated drugs.

2.7 Synthesis of PLGA Nanoparticles

A number of articles have been published focusing on the synthesis methods of PLGA nanoparticles [Desgouilles et al., 2003], the choice of which depends on the polymer and drug properties. Nanoparticles can be prepared by both polymerization methods and synthesis with preformed polymers, which can for the core-shell structure to entrap various ingredients. These techniques can be employed for manufacturing PLGA nanoparticles (nanospheres and nanocapsules) by adjusting the processing parameters. The size and size distribution of the PLGA nanoparticles are affected by the technique used for the nanoparticle production and the pertinent synthesis parameters, i.e. PLGA molecular weight, the addition of active components, surfactants, and other additives. The following section is designed to present a comprehensive information on various synthesis methods and control of nanoparticle properties by manipulation of the synthesis parameters.

The available methods of PLGA nanoparticle synthesis can be classified in two categories: (1) bottom-up techniques (emulsion polymerization, interfacial polymerization, and precipitation polymerization) and (2) top-down techniques (emulsion evaporation, emulsion diffusion, solvent displacement, and salting out techniques). In bottom-up approach the polymerization is used to form nanoparticles from individual molecules. The drawback of this method is the presence of residual sub-products in the final nanoparticles that can induce toxicity and affect the drug release properties. To overcome this limitation top-down methods are developed where size reduction of polymer particles is used to obtain controlled-size particles [Astete and Sabliov, 2006].

Emulsion evaporation is a conventional top-down method that is used to develop nanoparticles from polymers including PLGA. The method is based on the emulsification of an organic solution of the polymer in an aqueous phase followed by the evaporation of the organic solvent. First the polymer is dissolved in a suitable organic solvent, resulting in an organic phase. The organic phase

is poured into an aqueous phase, in which a surfactant is used to impart stability to the emulsion. Emulsification is carried out under high-shear stress by stirring to reduce the size of the emulsion droplet (directly related with the final size of the nanoparticles). The process of emulsification is followed by evaporation of the organic solvent under vacuum, which leads to polymer precipitation and nanoparticle formation. Common emulsions such as oil in water (o/w) or water in oil (w/o) and double emulsions (w/o/w) can be used to accommodate the entrapment of active components (antibiotics, proteins etc.) with different properties. The o/w emulsion is usually used for entrapment of hydrophobic compounds, whereas w/o/w double emulsion is used for the entrapment of hydrophilic compounds [Astete and Sabliov, 2006]. The main drawback of the double emulsion method is the large size of the nanoparticles formed and the leakage of the hydrophilic active component [Ficheux et al., 1998], responsible for low entrapment efficiencies. The coalescence and Ostwald ripening are the two mechanisms that destabilize the double emulsion droplets. One strategy followed by Song et al. to reduce the nanoparticle size was to apply a second strong shear rate [Song et al., 1997]. The leakage effect can be reduced by using a high polymer concentration, and a high polymer molecular weight, accompanied by an increase in the surfactant molecular weight.

2.8 Drug Release in Polymer System

Drug release in a polymeric system typically refers to how a drug molecule is transported from a starting position in a polymeric matrix to the polymer matrix's outer surface and, finally, how it is released into the surrounding environment. Drug molecules can be transported out of drug delivery systems via diffusion through water-filled pores, which is a process governed by random movements of the drug and driven by chemical potential gradients and convection produced by osmotic pressure. In addition to diffusion, drug molecules can be released from the polymer matrix by erosion, which leads to pore formation and erosion effects and can be observed after an initial diffusion-controlled lag period. The main controlled-release mechanisms can be summarized

as (A) drug diffusion through water-filled pores, (B) diffusion through the polymer matrix, (C) osmotic pumping, and (D) erosion [Fredenberg et al., 2011].

PLGA copolymer undergoes degradation by hydrolysis or biodegradation through cleavage of its backbone ester linkages into oligomers and, finally monomers. Since there are many variables that influence the degradation process, the release rate pattern is often unpredictable. The biodegradation rate of the PLGA copolymers are dependent on the molar ratio of the lactic and glycolic acids in the polymer chain, molecular weight of the polymer, the degree of crystallinity, and the T_g of the polymer. The release of drug from the homogeneously degrading matrix is more complicated. A biphasic curve for drug release as a result of PLGA biodegradation has been shown to display the following pattern:

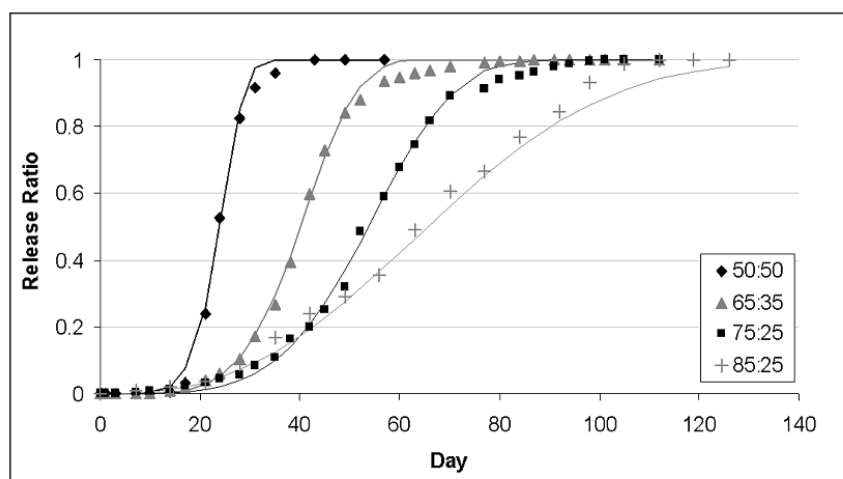


Figure 2.3: Modeled in vivo release profiles for 50:50, 65:35, 75:25 and 85:15 poly lactic-co-glycolic acid. Notation 65:35 PLGA means 65% of the copolymer is lactic acid and 35% is glycolic acid [Makadia and Siegel, 2011].

A biphasic release profile with an initial zero release period followed by a rapid drug release has been observed. In the first phase initial burst of drug release is happened which depends on drug concentration and polymer hydrophobicity. Drug on the surface, in contact with the medium, is released as a function of solubility as well as penetration of water into polymer matrix. In the second phase, drug is released progressively through the thicker drug depleted layer. The

water inside the matrix hydrolyzes the polymer into soluble oligomeric and monomeric products. This creates a passage for drug to be released by diffusion and erosion until complete polymer solubilization. Drug type also plays an important role here in attracting the aqueous phase into the matrix.

Degradation of polymer and drug release

To enhance the desirable properties of PLGA, it is essential to understand the factors affecting the PLGA degradation and design a drug delivery device accommodating all these factors to make it efficient and efficacious. Some of the major factors influencing polymer degradation are: size and shape of the matrix, drug type, drug load, crystallinity, and pH. The ratio of surface area to volume has shown to be a significant factor for degradation of large devices. High surface area ratio results in high degradation of the matrix. It has also been reported that bulk degradation is faster than surface degradation for PLGA, which makes the release of the drug fast from the devices with high surface area to volume. The presence of hydrophilic or hydrophobic drug may change the degradation mechanism from bulk erosion to surface degradation, hence affecting the rate of matrix degradation. A drug release profile that is defined by the time required for 100% release and the steady-state rate also varies significantly. Amount of drug loading in the drug delivery matrix plays a significant role on the rate and duration of drug release. Matrices with high drug content exhibit a larger initial burst release than those with low content. Tsuji et al. have proposed that the crystallinity of lactic acid (PLLA) increases the degradation rate because the degradation of semi-crystalline polymer is accelerated due to an increase in hydrophilicity [Tsuji et al., 2000]. In addition, in vivo and in vitro biodegradation/hydrolysis of PLGA showed that both alkaline and strongly acidic media accelerate polymer degradation [Astete and Sabliov, 2006].

2.9 Interaction of Bacteria with Nanofiber Structure

A good understanding of the interaction of bacteria with antibacterial nanofibers is essential to develop nanofiber-based wound care products that can effectively reduce the risk of infection. In

a wound healing process, effective antibacterial nanofibers would get involved in dynamic interaction with the bacteria [Said et al., 2011] that destroys the bacteria cells and deters the bacterial growth. If active drug components are incorporated into the fibers, they can be able to damage the cell wall or cell membrane of bacteria, denature proteins, inhibit enzyme activity or lipid synthesis [Gao and Cranston, 2008]. The attachment of the bacteria to the nanofibers can be utilized to reduce the bacterial concentration in the wounds. When a nanofiber mesh is used on a wound, bacterial adhesion is initiated in surface irregularities of the fibers that serve as microenvironments where bacteria take shelter to promote their survival. The surface roughness of nanofiber that is much smaller than the bacterium can work as an initial driver for this bacterial attachment [Mitik-Dineva et al., 2008]. Amna et al. developed the Zn-doped titania nanofibers and investigated the antimicrobial activity against *Escherichia coli* (Gram negative) and *Staphylococcus aureus* (Gram positive) in liquid growth medium [Amna et al., 2012]. They proposed a mechanism of the interaction between the fiber and the bacteria and how the fiber may damage the structure of the bacterial cell membranes. The mechanism includes three steps- a) attachment of nanofiber to the bacteria cell wall b) cleavage/piercing of nanofibers inside the cells and c) disintegration of the bacteria cells.

2.10 Evaluation of Antibacterial Efficacy

The evaluation of antibacterial efficacy is important to assess the effectiveness of the nanofiber mats for wound care applications. Various evaluation methods have been developed in the textile industry. These methods generally fall into three categories: the agar diffusion test, dynamic contact test, and intimate contact test [Gao et al., 2014].

In agar diffusion test (AATCC (American Association of Textile Chemist and Colorist)-147-2004), a dilute bacterial inoculum is spread or streaked on nutrient agar plates. Nanofiber membranes, typically in squares or circular discs of 10 mm, are firmly laid over the agar before the plates are incubated at 37°C for 18-24 h. It allows the antibacterial agent incorporated in the membrane to diffuse into the surrounding agar. After the local concentration reaches the minimum

inhibitory concentration (MIC), the sample can generate a zone of inhibition to bacteria. The size of the zone is indicative of the level of antibacterial activity in the membrane [Rujitanaroj et al., 2010, Mahapatra et al., 2012].

A dynamic contact test (ASTM E2149) determines antibacterial activity of immobilized (insoluble in water) antibacterial agents under dynamic contact condition. In the test, an antibacterial fiber specimen is immersed in a dilute bacterial solution and shaken for a given time. During the shaking, a dynamic contact between the bacteria and the specimen is able to deactivate the bacteria. A small volume of the suspension is withdrawn at designated times to determine bacterial concentration [Gao et al., 2014].

An intimate contact method (AATCC 100-2004) is often used for nonleaching biocides on fibers where the biocides act from the outside of the bacterial cells. Typically, a small volume of dilute bacterial inoculum is fully absorbed into a small amount of testing specimen to ensure the intimate contact between the material and the bacteria. After incubating, the inoculated samples in humidified jars at 37°C for up to 24 h, the bacteria are eluted and counted by serial dilution and plating on nutrient agar plates to determine the antibacterial efficacy.

Chapter 3

MATERIALS AND METHODS

3.1 Materials

10, 12-Pentacosadiynoic acid (PCDA, 98%) will be used as monomer to prepare polydiacetylene (PDA) nanofibers. Polyethylene oxide (PEO) and Polyurethane (PU) will be the matrix polymers. Chloroform, tetrahydrofuran (THF, 99%) and N, N-dimethylformamide (DMF, 99.8%) will be used as solvents to prepare the electrospinning solutions. Gentamicin sulphate will be used as the antibiotic drug. PLGA 502H (Resomer RG 502H, PLGA 50:50) and PLGA 752H (Resomer RG 752H, PLGA 75:25) will be procured to use as nanoparticle forming polymer. Polyvinyl alcohol (PVA) will be used as surfactant. For organic solvent dichloromethane and ethyl acetate would be used.

3.2 Nanoparticle Synthesis

PLGA nanoparticles will be prepared via double emulsion evaporation method. First, two liquid phases will be separately prepared. Organic phase will be prepared by dissolving PLGA into the organic solvent. Aqueous phase will be prepared by dissolving the hydrophilic gentamicin into the water/other aqueous phase. Second, PVA surfactant will be mixed with the two phases to prepare the emulsion. Third, high shear stress will be applied to the emulsion via ultrasonication to obtain mini-emulsion of nanodroplets. The mini-emulsion will then be poured into a large container containing second surfactant solution under stirring. The mixing will allow the solvent to diffuse through the polymer matrix to the outer liquid phase. The mixing will result in precipitation of nanoparticles. The synthesis method is illustrated in Figure 3.1. Nanoparticle precipitates will be collected via centrifugation ($10,000\text{--}20,000\text{ g}$, where $\text{g} = (1.118 \times 10^{-9}) \times \text{diameter of rotor} \times \text{rpm}^2$). The collected nanoparticles will be washed via centrifugation to completely remove any traces of solvent from the particles. Without an efficient cleaning, the solvent

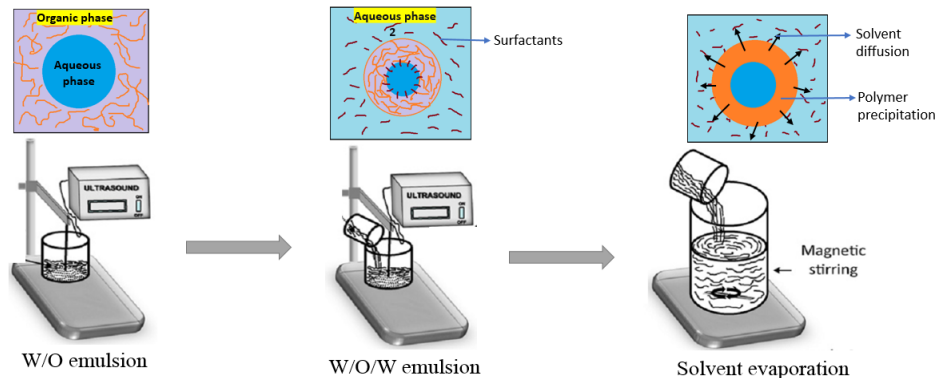


Figure 3.1: Set-up used for preparation of nanoparticles by the double emulsification method [Mora-Huertas et al., 2010].

residues will develop agglomeration of nanoparticles. Hence the washing should be done carefully because it will directly influence the nanoparticle aggregation and size distribution. Lyophilization of the washed nanoparticles will be done subsequently to preserve the particles. In lyophilization, a suitable cryoprotectant such as mannitol will be mixed with the washed nanoparticles and will be freeze-dried. During freeze-drying, ice crystals are developed and can damage the particles and cause agglomeration. Addition of cryoprotectant has been proven to improve the uniformity and complete resuspension of nanoparticles [Zhou et al., 2013]. Then the sample will be placed in a lyophilizer at a low temperature and pressure (below 80°C, pressure~0.005 Torr) for at least 24 hours.

3.3 Coaxial Spinning of Core-Shell Nanofibers

Coaxial electrospinning solution will be prepared following the methods described by Alam et al. [Alam et al., 2016]. Two different polymer concentrations will be used for the matrix polymer (PU). Different polymer to nanoparticle ratio will be tested to find out an optimum value to produce good nanofiber samples. A customized electrospinning device with two nozzle apparatus will be used for the coaxial electrospinning. We will use two syringes to feed the "Inner fluid" (PLGA nanoparticles suspended in solution) into the inner capillary and "Outer fluid" (PU polymer solution) into the outer capillary of the spinneret. For tip to collector distance we will start with 25 cm and then adjust the voltage accordingly (15~25 kV) to maintain a stable Taylor cone.

In the electrospinning the stability of core-shell Taylor cone will be a decisive factor to control the overall fiber structures. Flow rates in the capillaries will be controlled using two separate pumps in the electrospinning apparatus. As the viscosity of the matrix polymer will be higher (10~15 w/w%) than the nanoparticle solution (5-10 w/v%) we will use a higher flow rate (0.5~1.5 mL/h) for the shell solution and lower flow rate (0.01~0.5 mL/h) for the core solution.

3.4 Nanoparticle and Nanofiber Characterization

3.4.1 Morphology

Scanning Electron Microscopy (SEM) and Atomic Force Microscopy (AFM) will be used to measure the size and surface properties of the nanoparticles and nanofibers. Transmission Electron Microscopy (TEM) will give us information about the core-shell structure of the prepared nanofibers. TEM will also help to understand the microstructure of the nanoparticles and the nanofibers as well.

3.4.2 Mechanical strength

AFM will be used to measure the Young's modulus of the particles and nanofibers, and obtain the force-distance curve by using non-contact mode. Instron will be used to obtain the stress-strain curve for the nanofibers. This will help us to have an understanding of the durability of the nanofiber mats.

3.4.3 Drug-polymer interactions

To evaluate the drug encapsulation we need to collect information about the inner structure of the nanoparticles. We will use Fourier Transmission InfraRed spectroscopy (FTIR) to observe the different vibration bands. As each type of molecules have their own intrinsic properties, they will only vibrate at a certain wavelength. By measuring the variations in the vibration of the reflective bands of different molecules will be identified at the surface and inside of the nanoparticles.

3.4.4 Drug release study

UV-vis spectroscopy will be used to evaluate the drug release from the nanoparticles as well as from the nanofibers. The preformed nanoparticles will be suspended into a phosphate-buffered saline (PBS) solution and then solution will be analyzed over time. To determine the gentamicin amount an O-phthaldialdehyde assay (OPA) assay will be used as described by Taha et al. and Anhalt et al. [Taha et al., 2013, Anhalt, 1977].

3.4.5 Drug incorporation efficiency

Dried PLGA nanoparticles will be dissolved in a common solvent (both polymer and drug will dissolve, e.g., acetonitrile [Govender et al., 1999]). The solution will be measured using UV-Vis spectroscopy at a couple of fixed wavelength (292 nm and 286 nm) for the polymer (PLGA) and gentamicin. The amount of polymer and gentamicin particles observed on the solution over a specific period will be used to evaluate the drug release property. Drug incorporation efficiency will be expressed both as drug content (% w/w) and drug entrapment (%) by using the following formula:

$$DrugContent(\%w/w) = \frac{massofdruginnanoparticles \times 100}{massofnanoparticlesrecovered}$$

$$DrugEntrapment(\%) = \frac{massofdrugsinnanoparticles \times 100}{massofdrugusedin formulation}$$

3.4.6 Antibacterial test

The antibacterial activity of the non-woven mats of the PDA/NP core/shell composite nanofibers will be evaluated against the common bacterium *Escherichia coli* (Gram negative) and *Staphylococcus aureus* (Gram positive) as model organisms. The bacterial inhibition rate and efficacy of nanofiber membranes will be investigated following the agar diffusion and dynamic contact method as described previously [Gao et al., 2014, Rujitanaroj et al., 2010]. A spectrophotometer will be used to analyze the bacterial growth in the suspension medium.

Chapter 4

MANUSCRIPT

Synopsis

10,12-Pentacosadiynoic acid (PCDA) monomers were mixed with polyethylene oxide (PEO) or polyurethane (PU) and the mixtures were used to produce composite nanofibers via an electrospinning. PDA composite nanofibers were prepared in UV light. The composite nanofibers demonstrated color-changing properties in the presence of bacteria, which exhibited a potential use in wound care. The structural and mechanical properties of composite nanofibers were investigated using scanning electron microscopy (SEM), transmission electron microscopy (TEM), atomic force microscopy (AFM), and tensile tests. The PU-PDA fiber surface was found to be smoother and more uniform in the diameter than the PEO-PDA fibers. Surface flakes were also observed in both fibers with low concentrations which is attributed to the PDA component in the fibers. Phase separation was observed in the PEO-PDA fibers with the PEO accumulated at the outside layer. The PEO-PDA fibers were primarily amorphous at the outside layer and were slightly crystalline at the center of the fibers, where the PDA took an important role of molecules alignment. On the other hand, the PU-PDA fibers demonstrated a homogeneous crystal structure present throughout the fibers, suggesting no phase separation. Tensile test results suggested that well-developed molecular orientation in the PU-PDA fibers significantly improved the mechanical properties of the composite fibers. The presence of PDA in the matrix polymer reduced the overall strength and breaking elongation of both PEO-PDA and PU-PDA composite nanofibers. Mechanical properties of the nanofibers were also measured using a force spectrometer in AFM. The results are in good agreement with the tensile tests. The PEO-PDA fibers showed significantly higher stiffness and modulus than the PU-PDA fibers. The AFM force-distance curve suggested that the PU-PDA fibers had an elastic deformation due to an external force and also exhibited flexibility. In a comparison, the PEO-PDA fibers were stiff and brittle and the PU-PDA fibers showed

smooth surface structures and elastic behaviors, suggesting the PU-PDA nanofibers is a promising composite for non-adherent, durable, flexible, and elastic (to cope with stress exerted by body contours) wound dressing materials.

4.1 Introduction

Wound care is a continuously evolving industry with many opportunities for innovation and improvement. The practice of dressing and treating wounds has been around for as long as human kind and will continue to be used so long as humans have exposed wounds. Wound dressings aid in restoration of a wound by using natural and/or synthetic materials [Felgueiras and Amorim, 2017]. The main purposes of the use of wound dressings are to remove exudate and to protect from outside interference as well as against dehydration [Selig et al., 2012]. Conventional wound dressings are made of natural or synthetic materials such as cotton or polyurethane that is able to keep a wound moist and then to protect from pathogenic bacteria [Lazcka et al., 2007]. Although wound care technology increasingly develops, the demand for an effective wound dressing continues to increase. New materials are constantly being studied to contribute effective wound care technology. Some of the latest technological advances include introducing biosensors into wound care practices. Biosensors are the devices containing a biological recognition component that can trigger a response signal to pathogens, virus, and other biological stimuli [Kissinger, 2005].

One of the attractive materials used for biosensor developments is polydiacetylene (PDA). PDA is a family of conjugated polymers potentially to be beneficial in chromogenic sensors. When the PDA is stimulated by environmental stimuli, it undergoes a colorimetric change and a transition from blue to red [Jianrong et al., 2004]. The environmental stimuli include bacteria, proteins, glucose, DNA, enzymes, and microorganisms. The colorimetric response that the PDA demonstrates is significant for the development of colorimetric detection biosensors. Kim et al. reported that PDA is made via the polymerization of the monomers of 10,12-pentacosadiynoic acid (PCDA) [Yoon et al., 2009]. When PCDA is in a solution and under external forces, the PCDA molecules are able to self-assemble and then polymerized at the condition of UV irradiation, re-

sulting in PDAs. One of methods to facilitate the polymerization of PDA is electrospinning that can structure fibers containing PDA [Subbiah, 2004].

Electrospinning applies a high voltage electric field to a hollow needle where a polymer solution droplet is subjected to very high surface tension until a tiny jet stream occurs. As the spinning solution containing PCDA is stretched to make fibers via electrostatic forces during electrospinning, the electrostatic forces also initiate self-assembling of PCDA [Ramalingam and Ramakrishna, 2017]. The self-assembles of PCDA in the fibers polymerize via UV irradiation, resulting in PDA fibers. Although PDA is an exceptional biosensor polymer, it is difficult to be electrospun on its own due to low viscosity and therefore usually is mixed with other polymers (matrix polymer) used in the electrospinning to produce composite fibers [Alam et al., 2016, Peng et al., 2009]. In two-phase fiber composites, the first phase is a matrix polymer (such as PU, PVA, PEO) and is the backbone of the composite [Ramalingam and Ramakrishna, 2017]. The second phase is a reinforcing material (such as PCL, chitosan, PEG, collagen, nanoclay etc.) that imparts additional strength or functionalities to the matrix polymer. The two-phase fiber composites have been studied extensively due to their unique properties that cannot be achieved by either phase material only [Alemdar and Sain, 2008]. For example, Peng et al. have developed carbon nanotube/ polydiacetylene (CNT/PDA) composite fibers that reversibly change color in response to electrical current and mechanical stress with negligible elongation [Peng et al., 2009]. In the PDA-contained nanofiber composites, the PDA phase imparts the sensing property to the composites. The chemical properties have been studied previously [Yoon et al., 2009, Alam et al., 2016, Lee et al., 2014]. However, the mechanical properties of PDA composite nanofibers have not been reported, which has given opportunity to the current study. The desire to explore the mechanical properties in wound dressing materials is significant because the mechanical properties of the materials determine the strength, elasticity and absorption ability of wound dressings.

In this paper, polyethylene oxide (PEO) (a hydrophilic polymer) and polyurethane (PU) (a hydrophobic polymer) were used as a matrix polymer to make PDA-containing composite fibers. Both PEO and PU are bio-friendly and safe to be used in wound dressings [Chen et al., 2008, Khil

et al., 2003]. PEO-PDA and PU-PDA composite nanofibers were made via electrospinning. The microstructures and morphology of the composite nanofibers were investigated using scanning electron microscopy (SEM) and transmission electron microscopy (TEM). The mechanical properties of the composite nanofibers were studied using an Instron tensile tester and atomic force microscope (AFM). SEM images demonstrate that the PEO-PDA fibers with irregular surface had diameters ranging from 561 nm to 1222 nm. On the other hand, the PU-PDA fibers showed smooth and regular surface and diameters ranging from 779 nm to 1655 nm. In TEM analysis, the PU-PDA fibers showed more prominent molecular alignment than the PEO-PDA fibers. Tensile tests showed that the addition of PDA in PEO and PU reduced the overall strength and elasticity of the composite nanofibers. In addition, the PU-PDA nanofibers exhibited higher tensile strength and Young's modulus than the PEO-PDA fibers. In AFM force spectrometry, a large adhesion hysteresis was observed in the F-D curve of PEO-PDA fibers, suggesting a plastic deformation occurring in the PEO-PDA fibers. PU-PDA fiber has almost three times higher modulus (448.34KPa) than the PEO-PDA fiber (155.53 KPa) suggesting excellent mechanical properties of PU-PDA composite fibers. It was found that 16% (w/w) PU-PCDA solution with 6:1 blend ratio has the highest tensile strength with significantly high elongation at break. Our results show the potential applications for PU-PDA blend nanofiber mats as wound dressing material with good structural and mechanical properties that will be further investigated.

4.2 Experimental Section

4.2.1 Materials

10, 12-Pentacosadiynoic acid (PCDA, 98%) was purchased from GFS Organics (Columbus, OH, USA) and was used as monomer to prepare polydiacetylene (PDA). Polyethylene oxide (PEO, Mw = 300,000 g/mol) was purchased from Sigma-Aldrich (St. Louis, MO, USA). Polyurethane (PU) Tecoflex™ SG-80A was purchased from Lubrizol Corporation (Brecksville, OH, USA). Chloroform ($\geq 99.8\%$) was purchased from Sigma-Aldrich (St. Louis, MO, USA). Tetrahydrofuran (THF, 99%), Diethyl ether and N, N-dimethylformamide (DMF, 99.8%, extra dry, AcroSeal®

were purchased from Fisher Scientific (USA). The chloroform, DMF, and THF were the solvents used to prepare the electrospinning solution. No further purification was done for all the polymers and solvents used in this experiment.

4.2.2 Methods

4.2.2.1 Synthesis of PDA

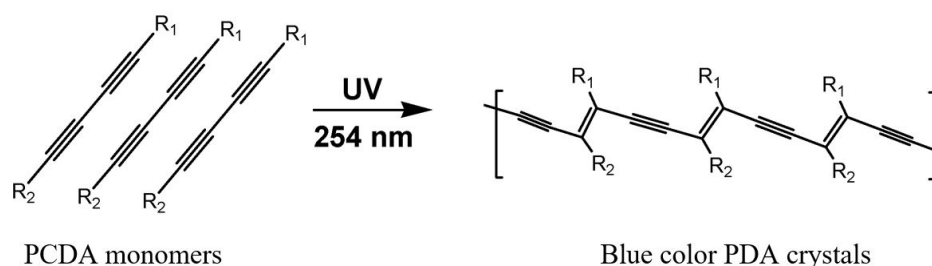


Figure 4.1: Polydiacetylene (PDA) synthesis scheme.

Polydiacetylene vesicles were synthesized from the diacetylene monomer, PCDA, following our previously reported procedure [Alam et al., 2016]. Diethyl ether (35 mL) was added to PCDA, 2.5g (6.8 mmol) to isolate any contaminants by vacuum filtration. Millipore water (18.2 MΩcm) was added to the filtrate to yield a 1.0% w/v suspension, which was sonicated at 65°C for 30 min. The suspension was allowed to reach room temperature, then cooled at 4°C overnight. The suspension was photo-polymerized with UV-light (254 nm) for 8 min in a crystallizing dish equipped with a magnetic stir bar [Alam et al., 2016]. A deep blue suspension was obtained from the photo-polymerization. The suspension was transferred to a round bottom flask protected from light to remove the solvent under vacuum. The solid PDA was stored at -20°C.

4.2.2.2 Preparation of Electrospinning Solution

Two matrix polymers including polyethylene oxide (PEO) and polyurethane (PU) were used and each was combined with 10, 12-Pentacosadiynoic acid (the monomer of PDA) to produce PDA nanofiber composites. The solutions were prepared by using two different concentrations for each matrix polymer (PEO and PU) and two mass ratios (2:1 and 6:1) (w/w%) of matrix polymer to

PCDA at each concentration. Two control samples of 100% PEO and PU were also electrospun from 2% and 10% polymer concentration (w/w) respectively. Table 4.1 shows the composition of the prepared solutions. The solutions for fabricating PEO-PDA nanofibers were prepared by adding required amount of PEO and PCDA in chloroform, followed by stirring overnight at room temperature at 600 revolutions per minute (rpm) until a homogeneous light-pink solution was obtained. The solutions for fabricating PU-PDA nanofibers were prepared by mixing the PU pellets in THF and kept overnight at room temperature under constant stirring at 600 rpm, and then the same amount of DMF (DMF:THF 1:1 (v/v)) was added on the next day to confirm the required polymer concentration. The stirring continued for an hour to make a homogeneous light-pink solution.

Table 4.1: Compositions of the prepared electrospinning solutions.

Composition	Concentration%(w/w)	Polymer Ratio	PEO or PU%(w/v)
PEO:PDA	2	2:1	2.30
		6:1	2.70
	3.75	2:1	3.87
		6:1	4.97
PU:PDA	10.83	2:1	7.22
		6:1	9.20
	16	2:1	10.67
		6:1	13.71

4.2.2.3 Electrospinning of PEO-PDA and PU-PDA Nanofiber Composites

A customized vertical electrospinning apparatus was used to prepare nanofiber composites of PEO-PDA and PU-PDA. The apparatus primarily consisted of a Gamma High Voltage Research ES50P power supply, a 5ml plastic syringe, a stainless steel 18gauge needle, a Harvard PHD 2000 syringe pump, and a copper coated plate collector (36x24 cm²). The fiber preparation was adopted from the electrospinning method reported by Alam et al., [Alam et al., 2016]. Briefly, an electrospinning solution was extruded through the electrically charged needle at required potential (15-25 kV) between the solution and the grounded collector. The solution was delivered with the

syringe through the needle at various flow rates ranging from 0.01-0.2 mL/h using the syringe pump (Li et al., 2013). Fibers were collected on an aluminum foil paper taped to the grounded plate. The collection distance was fixed at 25 cm. The spinning time varied depending upon the solution concentration and injection rates. The as-spun fibers were kept in the dark overnight for the solvent to evaporate completely. Then, Spectroline (Longlife™ filter, New York, USA) UV lamp was used to induce photo-polymerization of PCDA in the fibers, resulting PDA-contained nanofibers. Under the UV irradiation, the fibers became blue quickly within 30 seconds and then turned deep blue in 3 minutes, which indicated the PCDAs were photo-polymerized to macromolecule of PDAs [Alam et al., 2016]. All the fiber mats were prepared under identical conditions. All the experiments were performed at room temperature in atmosphere.

4.2.2.4 Preparation of Bacteria Solution for Colorimetric Detection

The chromatic change of the PDA fibers was evaluated in the presence of Escherichia coli (E. coli) bacteria. The bacteria were grown aerobically at 37°C on a sterilized solid Luria Bertani (LB) medium composed of 10g tryptone, 5g yeast extract, and 5g NaCl were added to 1L deionized water. The mixture was autoclaved at 121-124°C for 20min to prepare LB media. After culture of E.coli for 24h at 37°C, the bacteria solution was centrifuged at 10k rpm at 4°C for 10 min. Then filter the supernatant with a 0.2µm filter, and half of the filtered supernatant was taken to be autoclaved, the other part was stored for further use. 5ml solution was added to the petri dish, and then the membrane was immersed thoroughly into the solution in the petri dish. Photos were taken at regular intervals as the membrane starts to change its color. Also, the color before and after experiment was tested by Color Quest XE dual beam spectrophotometer (Hunter lab™).

4.2.3 Fiber Characterizations

4.2.3.1 Scanning Electron Microscope (SEM)

The size distributions and morphologies of the nanofiber mats were analyzed using scanning electron microscope (SEM) (JEOL, JSM 6500F, Tokyo, Japan) at an accelerating voltage of 15 kV with a 10mm working distance. The fiber samples were first kept overnight under vacuum to

evaporate any residual solvent or moisture. After the solvents have evaporated completely, a small section of the fiber mat attached to aluminum foil was cut out and mounted on a metal sample stub by means of double-sided carbon tape. The fiber mat was sputter-coated with 10nm layer of gold (Au) for 33s with Denton Vacuum - DESK 2 sputter-coater to improve conductivity of the samples for good imaging quality. Images of the nanofibers were taken at 1,600x magnification to obtain a general understanding of the size distribution of the nanofiber samples. For a good understanding of the morphology of the nanofibers, enlarged images were taken at higher magnification (15,000x to 20,000x). The average diameter and size distribution of the nanofibers were obtained using DiameterJ plugin through ImageJ software (National Institutes of Health, Maryland, USA). The samples had diverse fiber diameters and for this reason super pixel data in ImageJ were used for determining the average diameter. Histogram data were also used to represent the size distribution of the nanofiber samples. As there are still some limitations in segmentation algorithm used by Diameter J [Hotaling et al., 2015], the results of average diameter from both super pixel and histogram data were obtained. Diameter variations across all the samples characterized was confirmed by measuring at least ten different fiber diameters for each sample.

4.2.3.2 Transmission Electron Microscope (TEM)

In order to understand the morphologies and microstructures thoroughly, the 100% PDA, 100% PEO and 100% PU control fibers, and the two PDA composite nanofibers were examined under a JEM 2100F field-emission transmission electron microscope (TEM; JEOL, Tokyo, Japan) at an accelerating voltage of 200 kV. 100% PDA powder was dissolved into a 1M KOH solution (at pH 13.0). The PDA solution was dropcasted onto a copper grid in open air. The grid was kept overnight to completely dry out the sample before it was examined in the TEM. The fibers (100% PEO and 100% PU control fibers, and the two PDA composite fibers) were electrospun directly onto the carbon coated copper TEM grids (400 mesh, Ted-Pella Inc.) over the aluminum foil in the electrospinning chamber and then was imaged in TEM. The selected TEM images were analyzed using GATAN Digital Micrograph (version 2.3.2) software.

4.2.3.3 Mechanical Properties Analysis

Tensile Test

Tensile properties of the electrospun nanofiber mats were determined using an Instron Universal Testing machine (model 4442, Universal Testing Systems, Norwood, MA, USA) following the guidelines of ASTM D638-14. The tests were based on the testing conditions using a 50N load cell with a crosshead speed at 50 mm/min for the PU-PDA composite fibers and 100 mm/min for PEO-PDA composite fibers. Fiber mat specimens were cut into a doge-bone shape using a standard ASTM D-638-5 cutting device. The length and width of each specimen were 7.62 mm and 3.18 mm respectively. The thickness of the specimens was varied from 0.9mm to 0.22mm. At least five specimens from each sample were tested. Mean values and standard deviations are reported in the Bluehill 2 software attached to the Instron.

Atomic Force Microscope- Force Spectrometry

Nanomechanical properties of the nanofibers were studied using a Park AFM XE-7 (Suwon, Korea). To avoid the vibrational noise and thermal drift from the environment, the AFM was placed on a vibration reduction control device in a damping isolation chamber. Fiber mats collected on aluminum foil were cut in square pieces. A square fiber mat was then attached onto a circular magnetic disc using a double-sided tape. The magnetic disc was mounted on the AFM sample stage. An OMCL-AC160TS (Olympus Opt. Inc., Tokyo, Japan), non-contact cantilever with aluminum reflex coating was used for imaging in the AFM. Topographical images were first obtained in the non-contact mode and the topographical image was later used as reference image to obtain force-distance (F-D) curves in AFM spectrometry. The F-D curves were obtained using a silicon-tipped probe cantilever with a frequency of 300 kHz and spring constant of 26 N/m. The shape of the cantilever tip was tetrahedral and the tip radius was 7nm. For each sample at least ten points were selected on the topographical image to produce multiple F-D curves. The approach (when the cantilever comes close to the sample surface) and retraction (when cantilever deflects away from the surface) curves were obtained at a speed of 0.33 $\mu\text{m/s}$ with the maximum load set

at 3.5 nN. In the XEI image processing software attached with AFM, The Hertzian model was applied to the loading curves to obtain Young's modulus (at 200nm depth) at the selected points assuming the Poisson's ratio of PEO and PU as 0.49 and 0.45 respectively [R. W. Warfield, 1972]. As the Young's modulus is the intrinsic property of materials it will give us information on the resistance of the fibers to elastic deformation under load. The F-D curves taken at different points of the fiber had different shape to some extent and from the array of curves we selected the shape of the mostly occurred curve as a standard to analyze and compare the nano-mechanical properties of the samples.

4.3 Results and Discussions

4.3.1 Colorimetric response of PDA fibers in bacterial solution

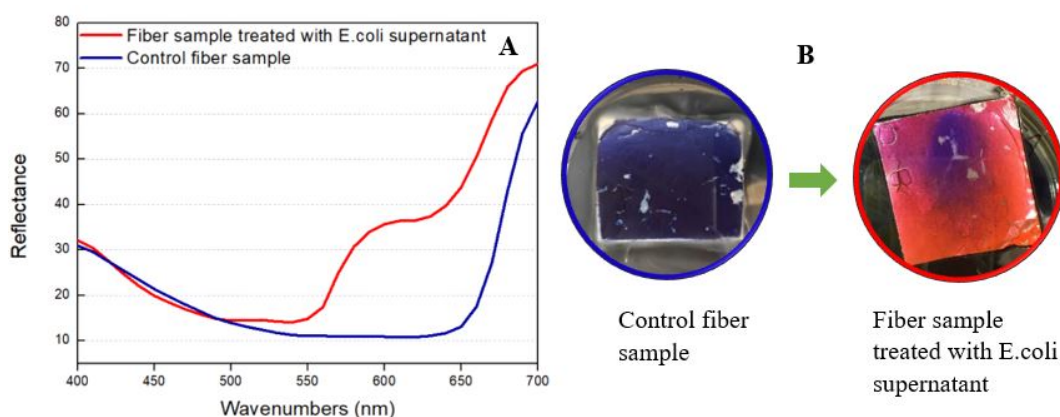


Figure 4.2: A. Reflectance spectra of the PDA composite fibers show the chromatic transformations induced by bacterial E.coli bacterial supernatant. B. Photographs showing the color transitions of the fibers after 24 hrs. of treatment.

PDA fibers have been shown to exhibit unique chromatic properties in bacterial solution, undergoing visible blue-red transformations. The fiber mat sample spun for 1h started to change color as soon as it was immersed into the supernatant solution and the color changed to complete bright red in 20 minutes. The color transition from blue ($\lambda_{max} \sim 640\text{nm}$) to red ($\lambda_{max} \sim 540\text{ nm}$) was also observed in the reflectance spectra. Figure 4.2A demonstrates that the spectral component at around

550 nm progressively increases for the treated fiber sample until it reaches 700 nm which is the red region in the visible electromagnetic spectrum. This spectral change corresponds to the blue-red transformation of the fibers. The colorimetric transformation of PDA fibers is ascribed to the structural transformations of the C-C bond of PDA backbone. When the rotation of the C-C bond changes few degrees of the π -orbital overlap, it results in a significant redshift of the reflectance spectrum [Lee et al., 2014, Chae et al., 2007, Menzel et al., 2000]. The chromatic reactions induced in PDA composites by bacteria is not well understood. The color changes are most likely due to fiber-surface interactions of bacterially secreted amphiphilic compounds (membrane-active peptides and toxins) that bind to PDA fiber surface, thereby inducing chromatic transformations in PDA [Scindia et al., 2007].

4.3.2 Fiber Structure and morphologies

Electrospinning parameters can determine overall structural morphology and diameter of the electrospun fibers. Fiber size, size distribution, and surface roughness are discussed according to three parameters of electrospinning solutions, including (i) solution concentration (ii) mass ratio of PCDA to matrix polymer (PEO or PU), and (iii) matrix polymer.

4.3.2.1 Fiber size and size distribution

Figure 4.3 shows SEM images of 100% PEO fibers and PEO-PDA composite fibers obtained at different concentrations and polymer ratios. Figure 4.4 shows SEM images of 100% PU fibers and PU-PDA composite fibers obtained at different concentrations and polymer ratios. Fiber size distributions are presented in a histogram figure next to the SEM image of corresponding fibers. In addition, a high magnification SEM image is inserted to each corresponding image. Figure 4.3A and Figure 4.4A suggest that the PEO control nanofibers are much smaller. The average diameters of the 100% PEO and PU sample were found to be 678.6 ± 130.6 nm and 1467.3 ± 518.6 nm, respectively. The average diameter of different PEO-PDA composite fibers (Figure 4.3B, 4.3C, 4.3D, 4.3E) was determined from 561.9 nm to 1222.8 nm. The average diameter for the PU-PDA composite fibers (Figure 4.4B, 4.4C, 4.4D, and 4.4E) was observed from 779.0 nm to 1655.0 nm.

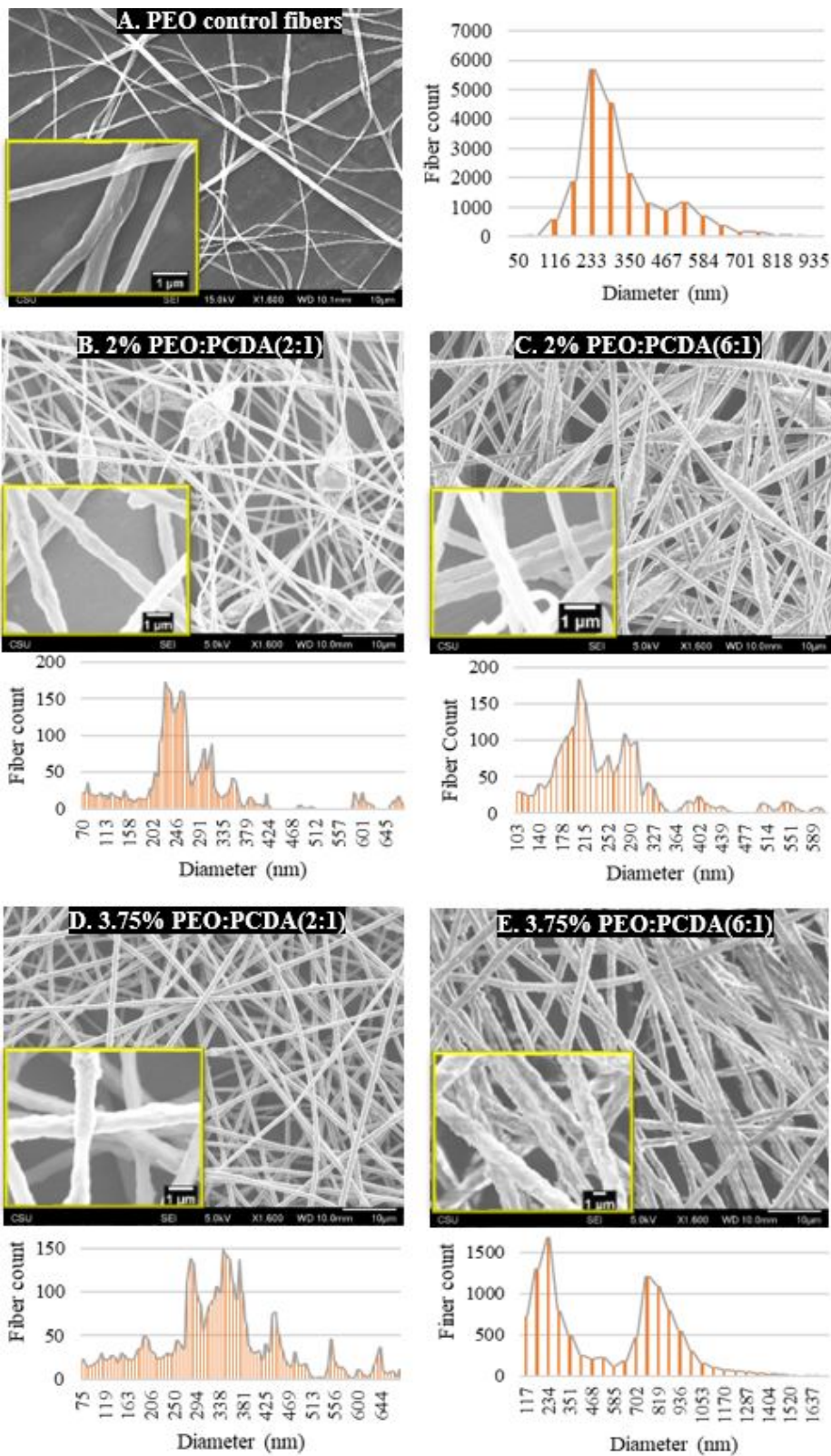


Figure 4.3: SEM images of electrospun nanofibers with their size distribution bar chart. (A) PEO control nanofiber. (B-E) PEO-PDA composite nanofibers with PEO concentration of 2.03%, 2.7%, 3.87%, and 4.97% respectively.

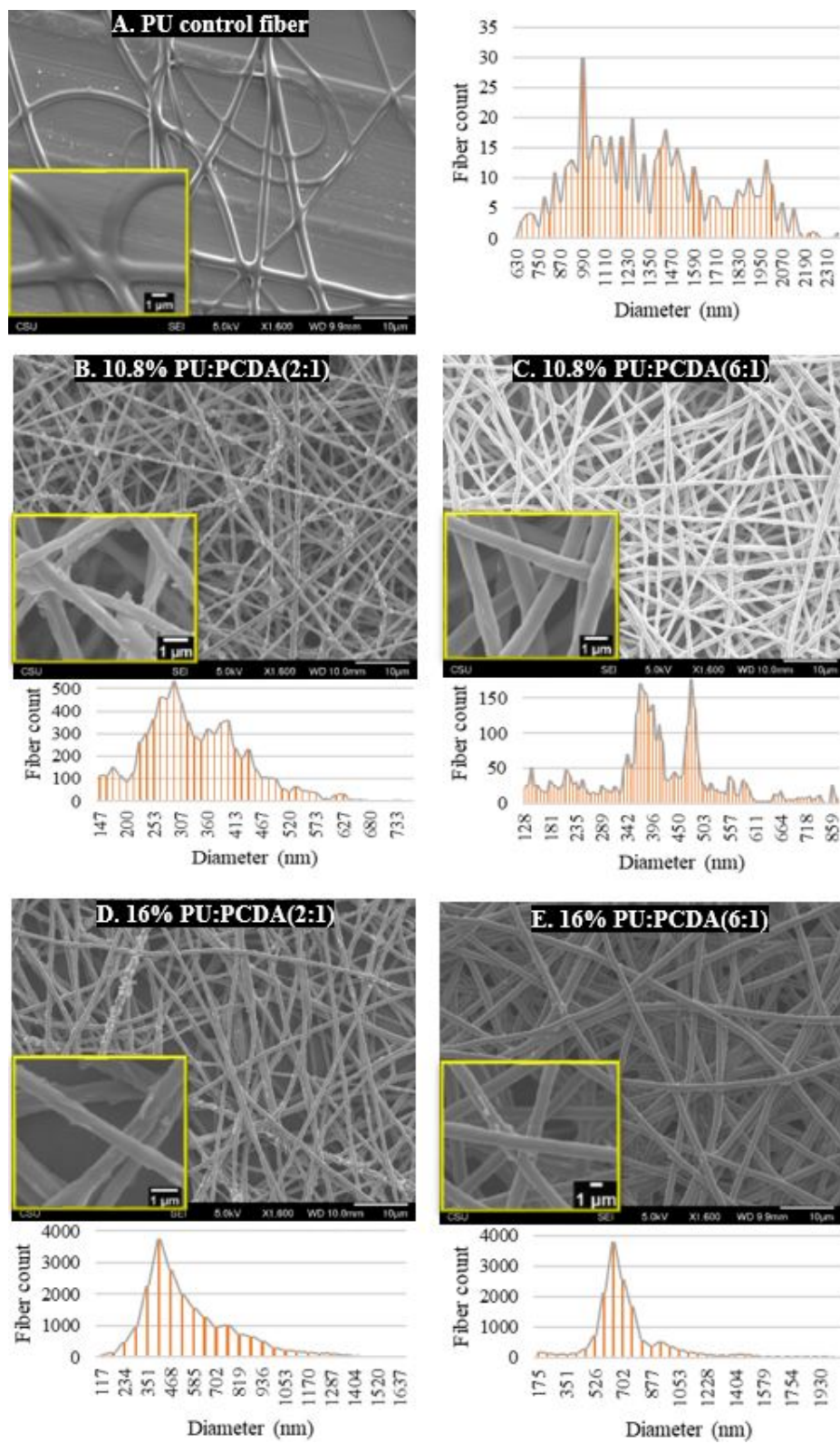


Figure 4.4: SEM images of electrospun nanofibers with their size distribution bar chart. (A) PU control nanofiber. (B-E) PU-PDA composite nanofibers with PU concentration of 7.22%, 9.20%, 10.65%, and 13.71% respectively.

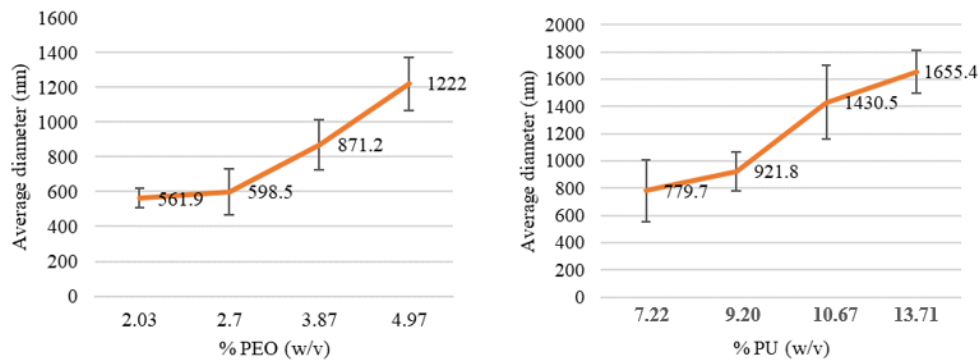


Figure 4.5: The average diameter of composite nanofibers as a function of (A) PEO and (B) PU concentration (w/v) in the spinning solution.

Figure 4.5 shows the average diameter of composite nanofibers as a function of matrix polymer concentration. It suggests that an increase in matrix polymer concentration results in the increase of the average diameter for both the PEO-PDA and PU-PDA nanofibers. In Figure 4.5A, the average diameters of PEO-PDA nanofiber containing 2.7% PEO (w/v) and 3.87% PEO (w/v) was found to be 598.5 ± 131.8 nm and 871.2 ± 145.4 respectively. The SEM images shown in Figure 4.3B and Figure 4.3C suggested that low concentration solutions produced discontinuities and beads in PEO-PDA fibers. The formation of beads is primarily due to cumulative effect of viscosity and surface tension [Fong et al., 1999]. At a low concentration, the viscosity of the solution is low but the surface tension is relatively high. As a result, the spinning jet could not maintain its own shape under high surface tension and formed spindle shaped beads to maximize surface area in the fibers. When the concentration was increased, the spinning jet overcame the surface tension, resulting a continuous fiber.

4.3.2.2 Fiber surface morphology

Close observation at Figure 4.3 and Figure 4.4 reveals two different surface morphologies in PEO-PDA and PU-PDA composite nanofibers. The PU-PDA composite nanofibers are more uniform and smoother on surface than the PEO-PDA composite nanofibers. PU is a di-block copolymer that contains both soft and hard blocks. The soft block is responsible for the high extension and elastic recovery of the PU, while the hard segment contributes high modulus and strength [Petrović and Ferguson, 1991]. The flexibility and elasticity are in favor of smooth surface in the PU-PDA

fiber morphology. In addition, the PEO-PDA spinning solutions were more dilute than the PU-PDA solutions. The solvent might not completely evaporate before the PEO-PDA fiber reached the collector. Because the solvent residue was still present in the fibers, the fiber morphology continued to change on the collector due to stress relaxation of the polymer chains, resulting in rough and irregular surfaces as seen in Figures 4.3A and 4.3E [Yao et al., 2014]. Another factor that may have a contribution to smooth surfaces of the PU-PDA fibers is the high dielectric constant of the solvents (THF and DMF) used in PU-PCDA solutions. The dielectric constant of THF and DMF is 7.58 and 36.7 respectively, whereas the dielectric constant of chloroform (used in PEO-PCDA solution) is 4.81 [Peng et al., 2009]. In the PU-PDA fibers, the high conductivity of the jet due to high dielectric constant promoted sufficient elongation of solution jet and alignment of molecular chains, resulting in a uniform and smooth surface structure of the PU-PDA fibers [Tan et al., 2005]. In addition, a flake-like structure was observed on the fiber surfaces of both PEO-PDA and PU-PDA nanofibers obtained at low concentration. Interestingly, no such flakes were observed on both the 100% PEO and PU control fibers, strongly suggesting that the surface irregularity of flake structures are mainly due to the addition of the PDA in the composite nanofibers.

4.3.3 TEM Analysis

The 100% PEO and PU fibers and PDA composite nanofibers were analyzed in a TEM. The TEM analysis was to investigate how the PDA interacted with the matrix polymers (PEO or PU) and thus influence the overall structures and properties of the composite nanofibers. The TEM image analysis software provides image analysis tools of Selected Area Electron Diffraction (SAED) patterns and Fast Fourier Transform (FFT) images that are able to provide assessment of molecular structures of the fibers, such as chain alignment and crystallinity.

PEO and PU Control Nanofibers

Figure 4.6 shows the TEM images of the 100% PEO nanofiber. Figure 4.6A reveals a smooth surface with a few dark spots on the fiber. Figure 4.6B shows a close look of the fiber and a FFT pattern of circle diffraction, suggesting no particular chain alignment in the PEO fiber. A close

look of the dark spots (10-20 nm in diameter) on the fiber is shown in Figure 4.6C. A FFT pattern of circle diffraction is also found, suggesting no chain alignment either. The results suggest a highly amorphous structure in the PEO fibers. Deitzel et al. reported that although PEO usually demonstrates good crystalline behavior, crystalline regions might not well developed in electrospun PEO nanofibers [Deitzel et al., 2001]. The lack of crystallinity is pronounced when the nanofibers are produced under elongational flow, such as electrospinning. Su et al. (2012) have attributed the lack of crystallinity to the short crystallization time and the highly unstable whipping of the electrospun jets during electrospinning [Su et al., 2012].

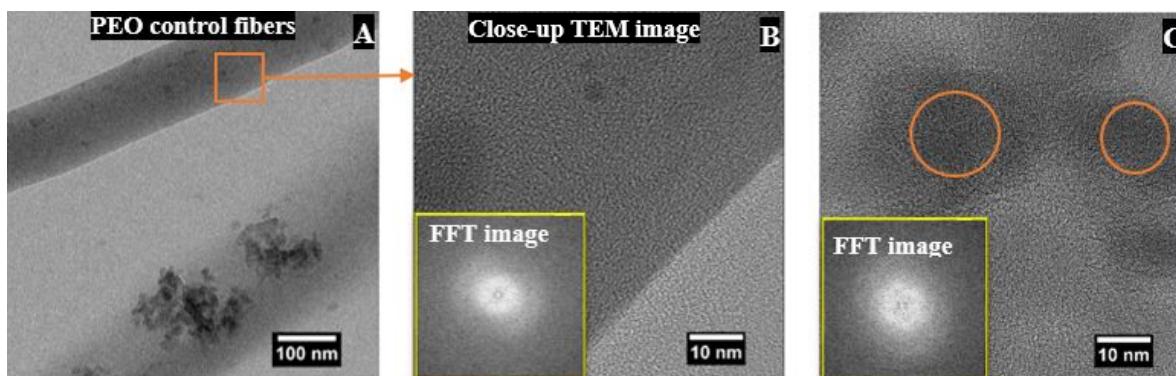


Figure 4.6: TEM micrographs of PEO control nanofiber A. Longitudinal view B. Close-up image with FFT image C. FFT image (inset) on dark spots of PEO nanofiber.

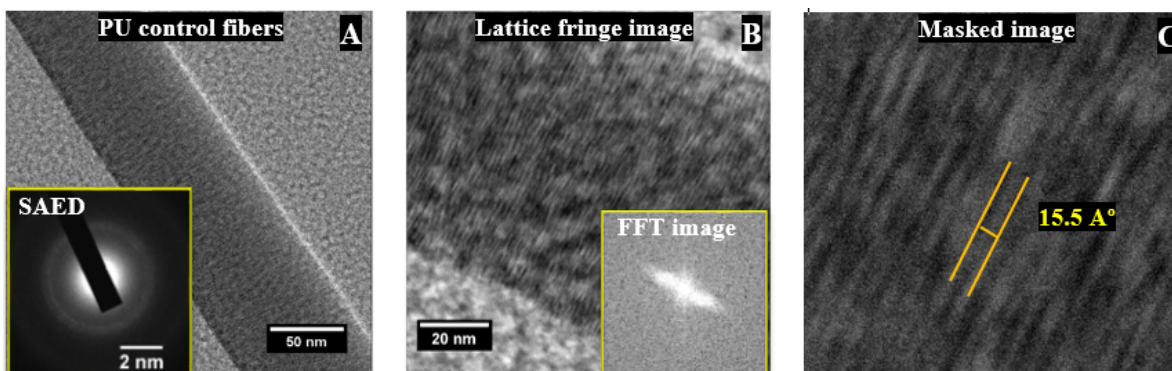


Figure 4.7: TEM micrographs of PU control nanofiber A. Longitudinal view B. Lattice fringe image with FFT image (inset) C. Masked image to understand the molecular alignment.

The TEM images of 100% PU fibers are shown in Figure 4.7. A bright and sharp diffraction ring was found in SAED pattern on a single PU nanofiber shown in Figure 4.7A. It implies a well-oriented crystal structure present across the fiber diameter. Ziabicki and Kedzierska (1962) also observed similar sharp x-ray diffraction pattern in PU fiber that confirmed an ordered structure of PU molecules [Ziabicki and Kedzierska, 1962]. An enlarged lattice fringe image is shown in Figure 4.7B. Clear lines on the lattice fringe image are evidences that the PU fiber has higher degree of molecular orientation and crystallinity. In order to gain a good understanding of the orientation and crystallinity in the PU fibers, a masking tool of image analysis was applied to the image of Figure 4.7B. The masking tool is able to remove unwanted noise or frequency and hence enhance the periodic elements of an image. Application of mask on FFT image (shown in Figure 4.7B) results in an inverse FFT image. Inverse FFT function determines the spatial distribution of periodic contents in a material [Tanaka, 2008]. The inverse FFT was then combined with the raw image to produce a masked image that is demonstrated in Figure 4.7C. Molecular alignment was magnified in the masked image. The crystalline regions of PU fibers were formed by aligned lamellae structures (bright lines) that were densely packed and stacked upon each other. The lattice spacing was 15.5 \AA . The lamellar crystal structure in polymer was first proposed by Flory [Flory et al., 1981]. The lamellar crystal consists of polymer chains randomly folding back into the same lamella or even participating in adjoining lamellae. The amorphous regions (dark lines) mostly consist of relaxed tie molecules that are random polymer chains that connect crystal lamellae) [Lim et al., 2008]. Saito et al. (1972) investigated the crystal structures of PU fibers and found the d-spacing of 2,6-polyurethane 16.8 \AA [Saito et al., 1972] that is comparable with the current lattice spacing (15.5 \AA). The large lattice spacing might explain the flexible structure of PU fibers. No lattice spacing could not be measured in the PEO fibers due to the random molecular packing across the fiber.

PEO-PDA Nanofibers

Figure 4.8A shows the TEM images of a PEO-PDA nanofiber and an inserted corresponding SAED pattern. The fiber demonstrates a rough and translucent edge and a dark center, suggesting

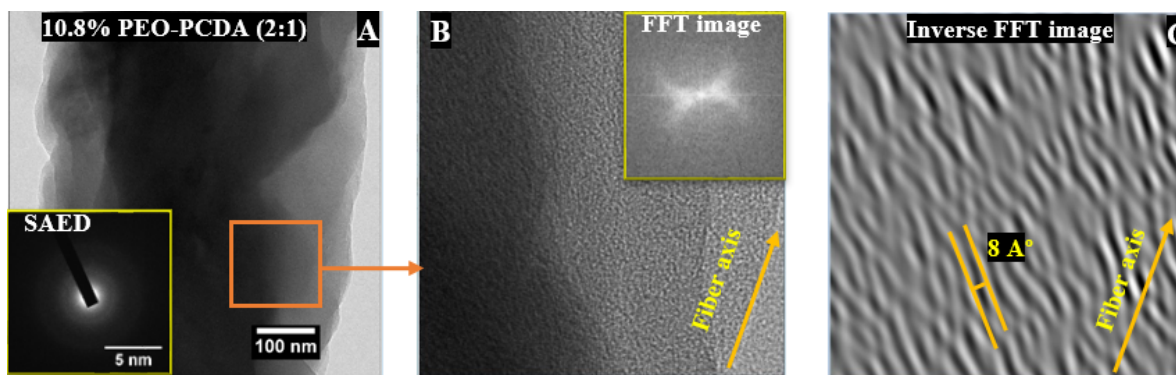


Figure 4.8: TEM images with corresponding selected-area electron diffraction (SAED) of PEO-PDA composite nanofibers A. Longitudinal view B. FFT image observed at the center of fiber (inset) C. Showing inverse FFT image based on the FFT pattern.

possibly a phase separation in the PEO-PDA composite nanofibers. The phase separation might be due to differences in solubility and electrical conductivity of the two components [Zhang et al., 2009, Deitzel et al., 2001]. For example, a mixture of poly(lactic acid) and chitosan was electrospun [Li et al., 2012] and chitosan was found accumulating in the shell layer. Moreno et al. (2011) reported a low conductivity of PEO as 1.2×10^{-9} and 2.5×10^{-9} $\text{ohm}^{-1}\text{cm}^{-1}$ (with molecular weight 600,000 and 4,000,000 respectively) [Moreno et al., 2011]. Whereas polydiacetylene crystals are classified as electrical insulators with room-temperature conductivities in the range 10^{-16} to 10^{-12} $\text{ohm}^{-1}\text{cm}^{-1}$ [Day and Lando, 1981]. During electrospinning, the charged PEO ions were pushed to the edge of the solution jet due to the high repulsive forces. The ions of PDA due to nearly zero conductivity resist moving far and remain close to the center [Zhang et al., 2009]. The results favor a hypothesis that the PEO wraps up the PDA in the composite nanofibers.

Further, the edge of the PEO-PDA nanofibers is rough as shown in Figure 4.8A. The TEM image displays wavy and layer structures. A SAED pattern is made on the wavy fiber edge as shown in Figure 4.8B. The SAED is an image analysis technique that can provide information of microstructures such as amorphous (represented by diffuse rings), crystalline (represented by bright spots), or polycrystalline (represented by small spots making up a ring) [Tanaka, 2008]. The SAED pattern on the wavy fiber edge shows diffuse rings, suggesting no crystalline formation. To investigate the microstructure of dark region FFT image taken in Figure 4.8B. The FFT image in

Figure 4.8B shows two identical but oppositely oriented diffraction pattern, suggesting that there are twinned crystal lattices oriented in a different direction relative to each other. More interestingly, these conjugated diffraction patterns rotate around their axis when the FFT imaging location was moving on the dark region of the PEO-PDA fiber. The FFT images that have similar diffraction rings but different orientations along the center of the fiber are able to justify the assumption that the polymer lattices have same geometrical structure but they are not oriented in one particular direction [Parsons, 2003]. Rather they are oriented in different directions forming a weave-like structure of molecular chains, which gives a unique anisotropic property of the nanofibers. Inverse FFT function was applied on FFT pattern of Figure 4.8B in order to determine the spatial distribution of periodic contents in the fiber as shown in Figure 4.8C. Inclined and misaligned lines were clearly seen, suggesting that the macromolecules were stacked in a spiral form along the axis of the fiber. Lim et al. (2009) also observed the misaligned polymer lamellae formation across polycaprolactone (PCL) nanofibers, resulting in low crystallinity [Lim et al., 2008].

PU-PDA Nanofibers

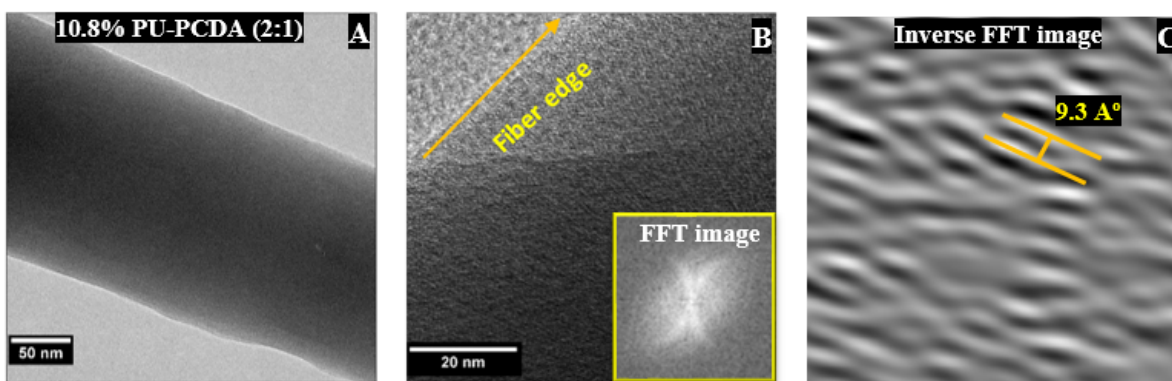


Figure 4.9: TEM images of PU-PDA composite nanofiber A. Longitudinal view B. Lattice fringe image with FFT image (inset) C. Inverse FFT image to understand the molecular alignment.

Figure 4.9A shows the TEM image of a PU-PDA nanofiber. It reveals that the fiber was smooth on the surface as well as homogeneous cross the diameter, suggesting no phase separation in the PU-PDA nanofiber composites. A zoom-in image of the fiber and the corresponding FFT image is

shown in Figure 4.9B where macromolecular alignment across the width of the fiber was observed. The close-up TEM image and the FFT image show that there were well oriented crystal lattices across the fiber diameter. Conjugated diffraction patterns were seen repeatedly throughout the core of the PU-PDA nanofibers. Figure 4.9C is the inverse FFT image produced from the FFT pattern shown in Figure 4.9B. Figure 4.9C demonstrates an enlarged view of the molecular packing. The molecular chains composed a lamellar structure across the fiber diameter at an angle, which is similar to the structure observed in PEO-PDA nanofibers (Figure 4.8C). Another important feature; lattice spacing was recorded from the inverse FFT image. The spacing between the crystal lattices was found to be 9.3\AA , suggesting an open structure at molecular level in the PU-PDA fibers. The large lattice spacing and regular ordering at molecular level increases the size of crystallites in PU-PDA fiber microstructure [Hindeleh and Johnson, 1978].

4.3.4 Mechanical Properties Analysis

Mechanical performance of composite nanofibers is important for potential use in wound dressings. Overall strength of the nanofiber mats was represented by the cumulative strength of individual nanofibers due to a combined effect of fiber size, size distribution, polymer concentration, fiber microstructure, and thickness of the fiber mats.

PEO vs PU Fiber

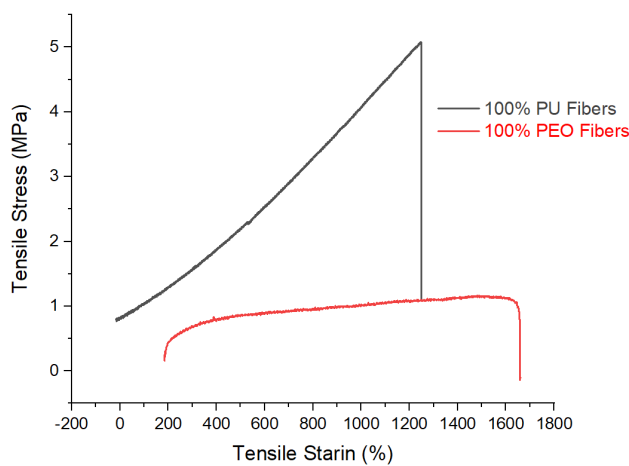


Figure 4.10: Tensile stress-strain curves for 100% PEO and 100% PU fiber.

Figure 4.10 shows stress-strain curves of 100% PEO and PU fibers. The PU fibers showed large area under the stress-strain curve (energy required for complete fracture), suggesting high strength and high impact resistance of the PU fibers [Roylance, 2001]. The tensile stress of the PU fibers increased proportionally with an increase in strain, indicating that the PU is an elastomer [Sonnenschein, 2015]. Physical cross-links (H-bonds) among the hard segments and the extension of soft segments at stretch explains the good elastic property of PU [Sonnenschein, 2015, Smith, 1974]. During the elastic deformation the extended polymer chains can go back to their initial position and hence retain original shape of the fibers after an external force is removed. The PU fiber breaks after the elastic limit that is the highest magnitude of stress up to which the stress and strain remain proportional.

A short but steep increase in the stress-strain curve of the 100% PEO fibers is observed when the fibers started deformation, indicating high stiffness in the fibers. After the very small strain of about 0.8% was completed, the stress in the fibers started to decrease. The PEO fibers yielded without significant increase in stress, resulting in a long plateau on the curve. After the yield point, the PEO fibers experienced a strain hardening where the random polymer chains tended to orient and aligned in the loading direction. The strain hardening was able to increase the strength and stiffness of the PEO fibers in the loading direction. A small but constant increase in the stress was observed in a large range of strain after the yield point at which the fibers started a plastic deformation. No plateau or necking on the stress-strain curve were observed in 100% PU fibers, suggesting no plastic deformation in the PU fiber [Pedicini and Farris, 2003]. The tensile strength of the 100% PU fibers (4.4 ± 0.51 MPa) is twice more than that of the 100% PEO fibers (1.3 ± 0.90 MPa). The PU has soft and hard segments that may crosslink in the chain backbone, resulting in high tensile strength [Staudinger, 1960]. At the maximum stress, the soft segments of the PU were extended and the hard segments of the PU clustered and yielded before the soft segments broke, resulting extra strength in the PU fibers [Spathis, 1991].

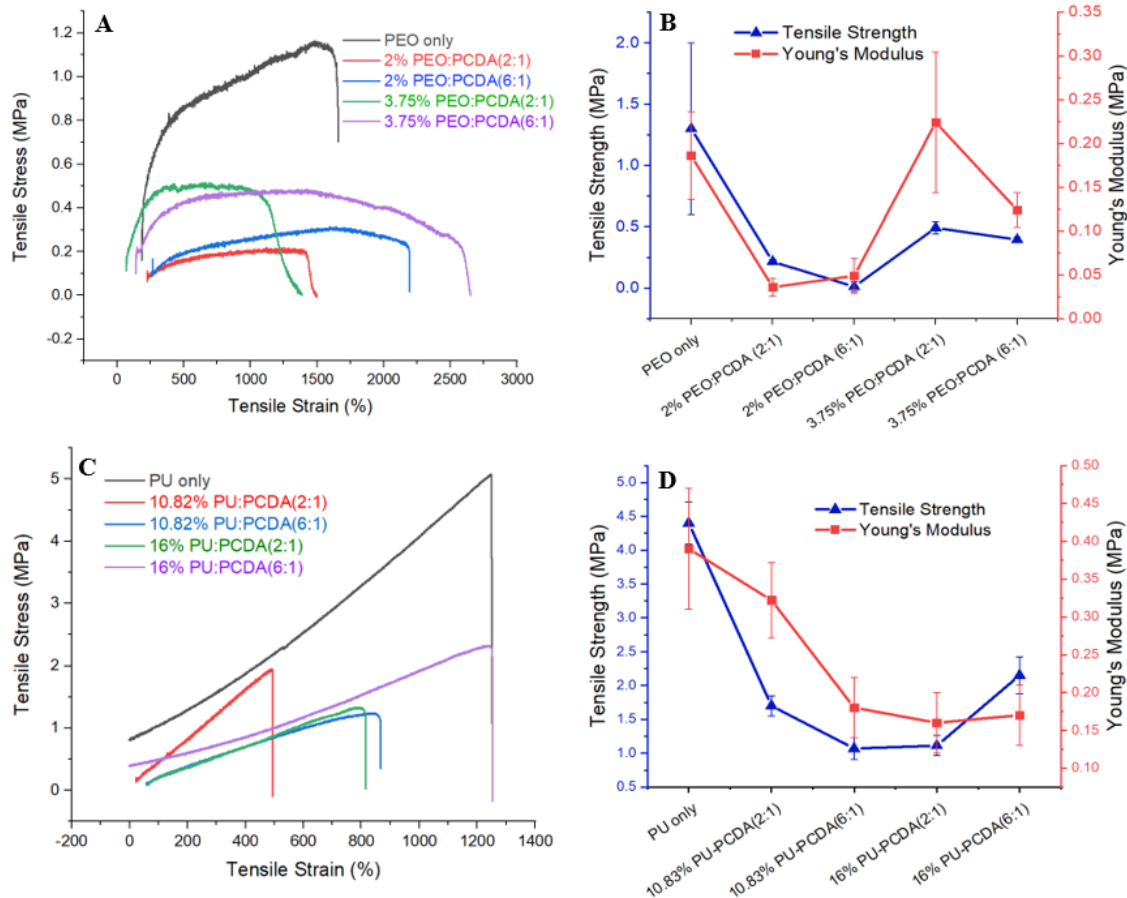


Figure 4.11: Tensile stress-strain curves (left) for A. 100% PEO and PEO-PDA fibers C. 100% PU and PU-PDA composite fibers. Corresponding comparison line graphs of their mechanical properties for different polymer concentrations and mass ratio are shown on the right (B,D).

PEO-PDA vs PU-PDA Composite Fibers

Figure 4.11A and 4.11C shows stress-strain curves of PEO-PDA and PU-PDA composite fibers, respectively. The shapes of the stress-strain curves measured from PEO-PDA and PU-PDA composite fibers are in a similar fashion as the 100% PEO and PU fibers. However, the overall strength of both PEO-PDA and PU-PDA composite fibers are lower than the 100% PEO and PU fibers. PDA has rigid macromolecular chains that very likely hinder the molecular alignment and orientation in the fibers. Tong et al. reported heterogeneous dispersion of PDA in mixture may increase the free volume inside the fiber structure and ultimately reduces their structural stability [Tong et al., 2011]. The highest tensile strength obtained in the PEO-PDA composite fibers was 0.49 ± 0.05 MPa (3.75% PEO-PCDA (2:1)) that is 62% less than the tensile strength of the 100%

PEO fibers. The highest tensile strength obtained in the PU-PDA composite fibers was 2.15 ± 0.27 MPa (16% PU: PCDA (6:1)) that is 51% less than the tensile strength of the 100% PU fiber. In addition, the breaking elongation decreases with an increase of PDA in the composite fibers. It is because of the rigid PDA chains impart the crystal regions in the fibers and reduce the mobility of polymer mixture. The increase in the PDA content ultimately increases the Young's modulus but reduces the elastomeric behavior of the PU-PDA fibers simultaneously. Large areas under the stress-strain curves were found in the PU-PDA composite nanofibers, suggesting flexibility and toughness in the fibers. High stress at the beginning of the stress-strain curves at a very small increase in strain was observed in the PEO-PDA composite nanofibers, indicating stiffness and brittleness in the fibers.

Figure 4.11B and 4.11D shows the Young's modulus and tensile strength of the PEO-PDA and PU-PDA fibers with respect to the polymer concentrations. The tensile strength and Young's modulus of the PU-PDA fibers are generally higher than that of the PEO-PDA fibers. However, the breaking elongation of PEO-PDA fibers is generally higher than the PU-PDA fibers. It is because there is contribution of both elastic and plastic deformations in the PEO-PDA fibers, but only elastic deformation in the PU-PDA fibers. The results are in good agreement with the TEM analysis that suggested no phase separation and crystalline structures in the PU-PDA composite nanofibers, resulting in good mechanical properties.

4.3.5 AFM Analysis

Force-Distance (F-D) spectrometry in an Atomic Force Microscope can measure interaction between an AFM tip and a material surface. The AFM tip first approached to the material surface and then retract from the surface, resulting in a F-D curve that exhibits the interfacial forces as a function of distance between the tip and the surface [Weisenhorn et al., 1989]. The F-D curve consists of two regions: approach and retraction. The slopes of the approach and retraction region can be used to measure stiffness and adhesion of the material, respectively [Cappella et al., 2005]. Young's modulus of the material can be also accessed using a viscoelastic model such as Hertzian,

Derjaguin-Muller-Toporov (DMT) and Johnson-Kendall-Roberts (JKR) model [Lin et al., 2007]. In the F-D curve, the area difference in the approach and retraction represents adhesion hysteresis that can be used to estimate adhesion energy. Force spectrometry can evaluate mechanical properties of a material such as hardness, adhesion, and elastic modulus [Gavara, 2017]. The maximum indentation force applied by the cantilever tip onto the sample surface gives us information about the sample stiffness while tracking how the sample deforms in response to said force. Table 4.2 shows average load, adhesion energy and Young's modulus of PEO, PU, PEO-PDA, and PU-PDA composite nanofibers.

In table 4.2, the Young's modulus of the 100% PU fibers (798.79 ± 21.77 KPa) was slightly higher than that of the 100% PEO fibers (775.27 ± 11.75 KPa). The PEO fibers exhibited slightly higher loading force (3.47 nN) than the PU fibers, suggesting a high rigidity in the PEO fibers.

Table 4.2: Summary of nanomechanical properties of pure and composite fibers

Fiber Sample	Average Maximum Load (N)	Average Adhesion Energy (J)	Average Young's Modulus (KPa)
PEO fiber	3.47×10^{-9}	6.25×10^{-17}	775.27 ± 11.75
PU fiber	3.41×10^{-9}	318.20×10^{-17}	798.79 ± 21.77
PEO-PDA fiber	0.65×10^{-9}	2.35×10^{-17}	155.53 ± 142.22
PU-PDA fiber	1.52×10^{-9}	3.07×10^{-17}	448.34 ± 118.57

The average Young's modulus of the PU-PDA composite fibers is 448.34 ± 118.57 KPa that is nearly twice higher than the modulus of the PEO-PDA fibers (155.53 ± 142.22 KPa). The force spectroscopy results are in good agreement of previous tensile tests. Also, the maximum indentation force recorded on the PU-PDA sample is 172% larger than the PEO-PDA surface. This indicates the ability of PU-PDA composite to sustain large force before deformation. It can be attributed to the moderately oriented crystalline region observed throughout the structure of PU-PDA fibers in TEM.

The F-D curves obtained on both 100% PEO and 100% PU control sample are presented in Figure 4.12 which gives us interesting insights in terms of their strength at molecular level. Close

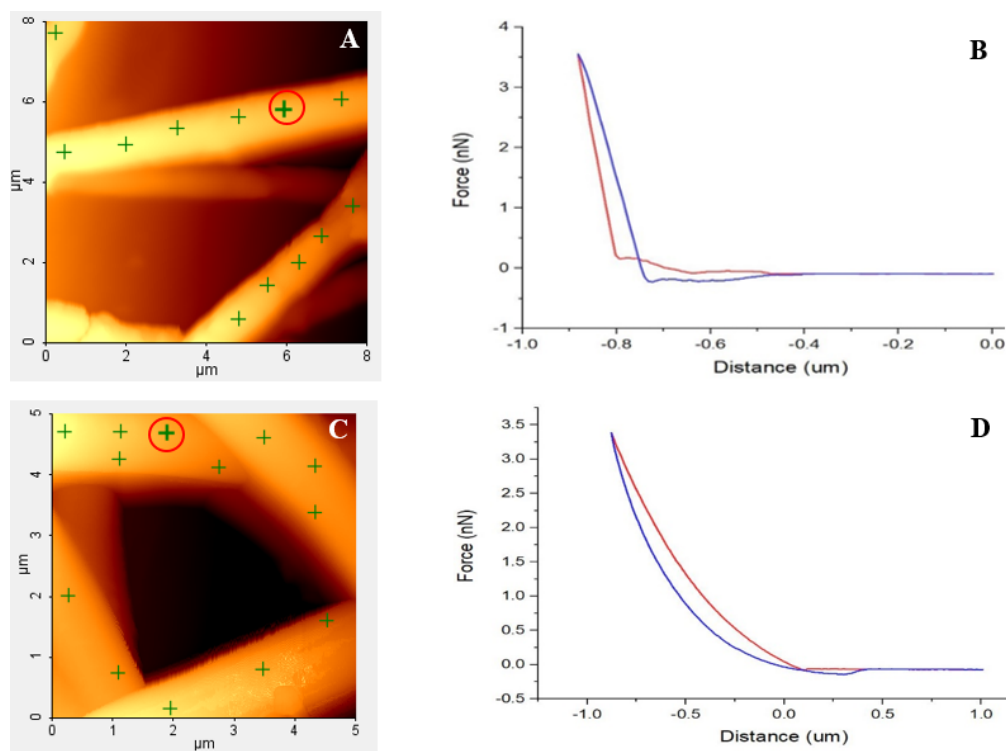


Figure 4.12: AFM topographical images (A and C) and the corresponding F-D curves (B and D) obtained on PEO and PU control sample. Cross mark enclosed in white circle shows the point at which the corresponding F-D curve was taken.

correlation was observed between absolute values of elastic moduli determined by AFM and values obtained from tensile tests for bulk fiber mats. From figure 4.12B and 4.12D it is evident that the slope of the approach curve for PEO sample is steeper than the PU sample. This steeper slope indicates the higher stiffness of the PEO fiber at molecular level [Weisenhorn et al., 1993]. This high rigidity of PEO polymer can be attributed to the glassy amorphous structure (random alignment of polymer chains) observed in PEO fiber under TEM. Under indentation force random polymer chains rearrange themselves and becomes compact. This reduction in free volume and compactness enhanced the hardness and modulus of amorphous components of semi-crystalline PEO fibers [Klapperich et al., 2001]. On the other hand, the slope of the F-D curve for PU fiber increases gradually. This less steep slope indicates the elastic deformation of soft PU fiber surface [Weisenhorn et al., 1993]. PU fiber showed higher Young's modulus and elastic response than

the PEO fiber due to more regular alignment of PU chains which forms large crystalline region in 100% PU fibers.

Force curves taken at different locations of PEO-PDA and PU-PDA fibers representing the tip-sample interaction force are shown in Figure 4.13. The F-D curves of PEO-PDA and PU-PDA highlight the difference in adhesion hysteresis and deformation behaviors. A large adhesion hysteresis in the force curves of the PEO-PDA fiber indicated a large plastic deformation [Butt et al., 2005]. The results are in a good agreement of tensile tests and TEM analysis. On the other hand, small adhesion hysteresis is found in the PU-PDA fibers, suggesting that the indentation on fiber surface is small and the fiber surface undergoes an elastic deformation rather than a plastic deformation. A large lattice spacing (15.5\AA) is found in PU-PDA fiber. Therefore, when the cantilever tip approach and indent the surface at molecular level, the polymer chains are able to m-

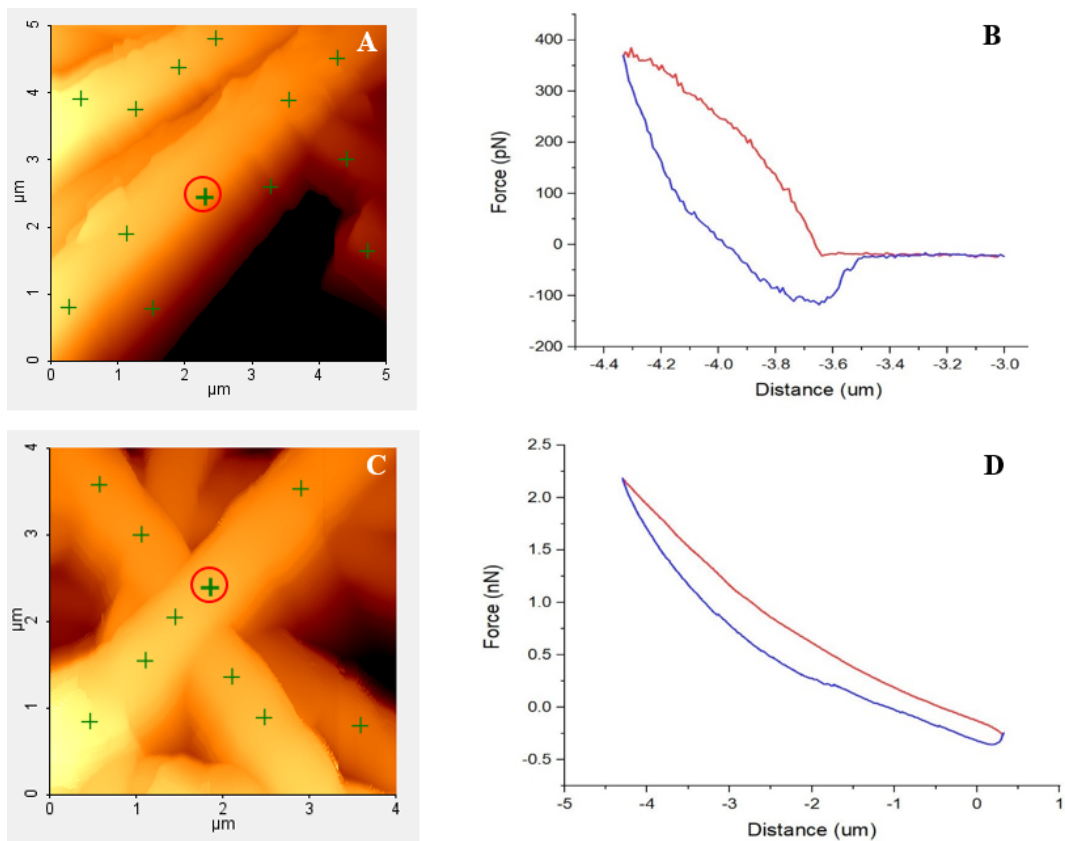


Figure 4.13: AFM topographical images (A and C) and the corresponding F-D curves (B and D) obtained on PEO-PDA and PU-PDA composite fiber sample. Cross mark enclosed in white circle shows the point at which the corresponding F-D curve was taken.

ove and slide due to large lattice spacing and hence recover to original positions at retraction. It is also confirmed on the approach region. In the PEO-PDA fibers, the loading curve starts to decline after an indentation depth of $0.25\mu\text{m}$. The declining point is defined as a yielding point [Butt et al., 2005] suggesting a characteristic plastic deformation of the material. However, no yielding point is found in the PU-PDA fibers at approach region. In a summary, the PU-PDA composite fibers are found stronger than PEO-PDA composite fibers. Both composite fibers were weaker than the 100% control fibers.

4.3.6 Contribution of PDA to the Fiber Structures and Strength

Previous studies suggest that the monomers of diacetylene (DA) are able to self-assemble due to external forces such as electrostatic forces and hence construct lamellar plate-like structure [Lee et al., 2014]. The self-assembly of DAs is largely promoted by directional hydrogen bonding between the carboxylic acid moieties as well as van der Waals interactions between neighboring alkyl chains of DAs. In addition, large attractive forces between DA monomers, number of methylene units between the DA unit and carboxylic acid group have been proposed to aid the ordered nanostructures of PDA [Chae et al., 2007, Menzel et al., 2000, Jorgensen, 1993]. Self-assemblies of DAs can be polymerized via to UV radiation to produce the supramolecules of PDA.

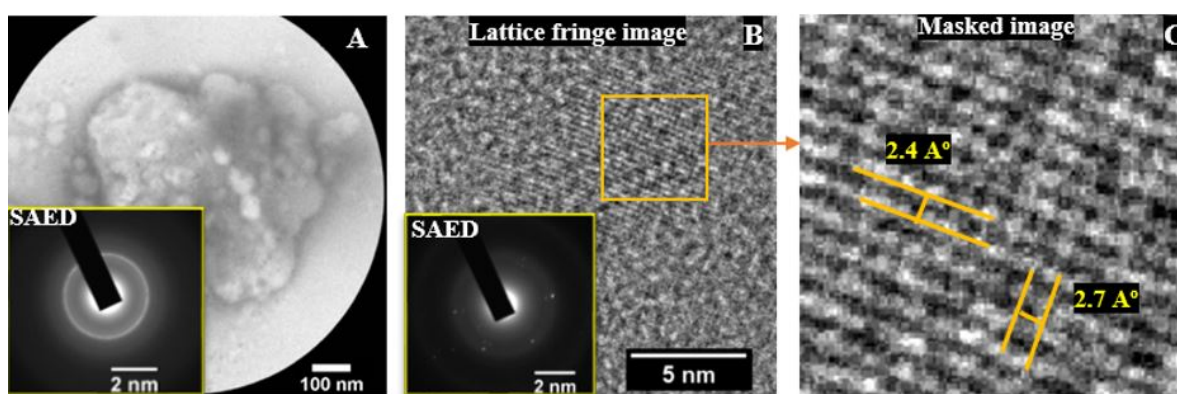


Figure 4.14: TEM micrographs (A) with corresponding selected-area electron diffraction (SAED) of PDA crystals (B). (C) Molecular alignment micrographs form masked image

In the current study, PCDA was used as the DA monomer to produce polydiacetylene (PDA). The PCDA molecules were mixed with PEO or PU and dispersed in the organic solvent. After high electrostatic force was applied to produce fibers during electrospinning, the PCDA was able to self-assemble due to the electrostatic force [Chae et al., 2007]. After the fibers were made, UV light was applied to polymerize PCDA self-assemblies, resulting in PDA in the fiber composites. In addition, 100% PDA was synthesized in a solution and studied in TEM. The results shown in Figure 4.14. of self-assembled PDA supramolecules confirm that PDA polymers have a high degree of crystallinity in their microstructure, which contributed to the crystal lattices observed at the center of the PEO-PDA composite nanofibers. In Figure 4.14A, a bright diffraction ring from the SAED pattern was found, suggesting highly ordered lamellar structure of the PDA molecules. Figure 4.14B shows a lattice fringe image of PDA and a SAED diffraction image. The SAED diffraction is a ring and a hexagonal spot pattern on the edge of the ring, suggesting a monoclinic crystal structure of PDA. The monoclinic crystal structure in PDA was previously reported by Kobayashi et al. (1987) and Tachibana et al. (2001) [Tachibana et al., 2001, Kobayashi et al., 1987]. The masking tool of image analysis was applied on a spot in Figure 4.14B, resulting in a masked image shown in Figure 4.14C. The average d-spacing (interplanar-spacing between the atomic planes arranged in any crystal structure) for the lattice planes was approximately 2.5\AA , suggesting a highly packed structure. Figure 4.14 demonstrates that the PDA primarily consists of highly packed crystals with great molecular alignment. Galiotis et al. (1984) reported the theoretical strength of PDA single crystal to be 3 GPa which is due to the stiffness of the diacetylene polymer backbone [Galiotis et al., 1984]. They also found the Young's modulus from the stress-strain curve to be 45 ± 2 GPa which confirmed a high-modulus PDA fiber. PDA are rigid-chain polymers due to owing the conjugated double and triple bonds in their polymeric backbone [Sun et al., 2006a] and they do not have the flexibility to conform a chain folded lamellar structure. In our experiment the packing of PDA monomers and thus the formation crystal structure was hindered by the flexible matrix polymer molecules in the composite fibers. Therefore, when the PDA was mixed in the composite

nanofibers, crystallinity of PDA decreased which resulted in a lower mechanical strength of the composite fibers.

4.4 Conclusion

PEO-PDA and PU-PDA composite nanofibers were successfully produced via an electrospinning method. The morphologies of the composite nanofibers were determined by polymer concentration, blend ratio of PDA, and matrix polymer. The presence of PDA introduced flake-like surfaces to the composite fibers. The surface flakes were reduced at high concentration of polymer in the spinning solution, resulting in smooth surfaces. TEM results showed that the PDA was homogeneously dispersed in the PU matrix and also promoted a high molecular orientation and alignment, resulting in large crystal regions in the fibers. On the other hand, no significant molecular orientation was observed in PEO-PDA fibers due to poor mixtures of PEO and PDA. The relationship between the structural and mechanical properties was significant. Tensile test results suggested the PU-PDA composite nanofibers showed superior mechanical properties to the PEO-PDA composite nanofibers. Due to the rigid polymer structure of the self-assembled PDA, most of the nanofiber samples showed improved tensile strength and higher modulus with the increase of PDA content. In AFM force spectrometry, the PU-PDA fibers sustained higher indentation force than the PEO-PDA fibers. The PU-PDA fiber showed elastic response and the PEO-PDA fiber exhibited plastic deformation at an external force. The results indicated potential applications of PDA-based composite nanofibers in wound care.

Chapter 5

SYNTHESIS OF PLGA NANOPARTICLES

5.1 Introduction

The techniques that are commonly used to synthesize drug-encapsulated PLGA nanoparticles are 1) chemistry based processes such as emulsion polymerization, miniemulsion polymerization and interfacial polymerization, and 2) physicochemical processes such as multiple emulsion techniques, spray drying, emulsion solvent diffusion and layer by layer process [Iqbal et al., 2015]. Ogawa et al. developed a basic emulsion solvent evaporation technique in 1998 for nanoparticle synthesis [Ogawa et al., 1988] and since then different variations of the technique were developed. Water-in-Oil-in-Water (w1/o/w2) double emulsion technique is commonly used for hydrophilic drug entrapment because the method is relatively simple, convenient in controlling process parameters, and does not require expensive instruments [Ruan et al., 2002]. In the w1/o/w2 technique, small water (w1) droplets are dispersed in oil or organic (o) phase, resulting in a primary emulsion (w1/o). The primary emulsion (w1/o) is then dispersed in another continuous aqueous (w2) phase to form large droplets, resulting in a double emulsion. In this study, a double emulsion method was used to synthesize PLGA nanoparticles that were embedded with gentamicin for antibiotic release applications. PLGA that was dissolved in an organic solvent was the oil phase (o). The gentamicin that was hydrophilic dissolved in water was w1 phase. The second aqueous phase (w2) was polyvinyl alcohol (PVA) solution that was a surfactant. PVA was able to help the formation of double emulsion by covering the surface of primary emulsion (w1/o) droplets. PLGA nanoparticles were formed via the diffusion of the solvent from the oil phase to the external aqueous phase (w2), which left the PLGA to precipitate around the internal aqueous phase (w1) [Bilati et al., 2005, Khoee and Yaghoobian, 2009]. In general, the surfactants are present in continuous phase of the emulsion (w2). A surfactant for emulsion is amphiphilic and it has one part that attracts water and the other part that has affinity for oil phase. If the surfactant remains at the liquid-liquid

interface during the diffusion and its encapsulating effect is adequate, the nanoparticles will be formed after the complete diffusion of the solvent from the oil phase. Then the elimination of the solvent will result in the transformation of each droplet into a hard particle of smaller size.

In the current study, a variety of formulation parameters have been investigated. They included 1) molecular weight of PLGA, 2) copolymer ratios of lactide to glycolide, 3) stabilizing agents (surfactants), 4) PLGA concentration, and 5) volume and concentration of both aqueous and organic phase [Li et al., 2008, SEZGIN BAYINDIR et al., 2009, Rosca et al., 2004, Cui et al., 2005]. It was found that the surfactant played an important role in determining particle size and size distribution. The surfactant was able to decrease interfacial tension between the hydrophobic (oil phase) and hydrophilic portion (aqueous phase) of the emulsion and improves emulsion stability [Zhang and Feng, 2006, Salager, 2002]. It has been reported that partially hydrolyzed polyvinyl alcohol (PVA) is a good surfactant that is commonly used to formulate nanoparticles [Jeffery et al., 1991].

The objectives of Chapter 5 are to synthesize and to characterize PLGA nanoparticles containing hydrophilic antibiotics using different formulation conditions. The morphologies and size of the resulting nanoparticles were studied. The results showed that we were able to prepare spherical PLGA nanoparticles that incorporated gentamicin. The diameter of the nanoparticles is in the range of 200-300 nm.

5.2 Methods

In this study, gentamicin was encapsulated into PLGA nanoparticles by both water-in-oil-in-water (w/o/w) and solid-in-water-in-oil (s/w/o) double emulsion solvent evaporation methods. Polyvinyl alcohol (PVA) was used as a surfactant. PVA powder (Mw 13,000-31,000 g/mol was purchased from Sigma-Aldrich) was first dissolved in distilled water by applying heat for 1 hour under stirring on a hot plate. The concentrations of the PVA solution ranged from 2-7% (w/v). Temperature was raised gradually from 40-80°C and careful measurement of temperature was taken at regular intervals. The PVA solution was left overnight under stirring at 40°C. The aqueous PVA solution was then filtered using a 20µm Whatman quantitative filter paper (VWR®) and sonicated

using an ultra sonicator (Fisherbrand™ -Model 505 Sonic Dismembrator) at 20-25% amplitude for 20-30 seconds to ensure evenly dispersed PVA molecules in the solution. In w/o/w double emulsion technique, 5-10 mg of gentamicin was dissolved in distilled water with a small amount (50-100 μ l) of 2-7% (w/v) PVA solution, resulting in the aqueous phase (w1). The solution was vortexed for 2min and kept overnight until gentamicin was dissolve completely. PLGA (Resomer® RG 502H and Resomer® RG 752H were purchased from Sigma Aldrich) was dissolved in dichloromethane (DCM) and vortexed initially yielding a clear solution that was the oil/organic phase (o). After 24 hours, the gentamicin aqueous solution was added dropwise into the organic phase containing the PLGA polymer. The mixture was then sonicated (13-15 W; Fisherbrand™ -Model 505 Sonic Dismembrator) at 35-40% amplitude for 2-6 minutes, resulting in the primary emulsion (w1/o).

The PVA solution in a large beaker was under magnetic stirring to facilitate solvent evaporation. The primary emulsion (w1/o) was then added dropwise into the PVA solution (w2) that worked as an external aqueous phase. It yielded the secondary or double emulsion (w1-o-w2). Stirring rate for the PVA solution was varied from 600-1000 rpm. Stirring time was ranged in 4-18 hrs. Particles was generated at magnetic agitation. Particles were consolidated as the solvent evaporated. The particles in the solution were then centrifuged (VWR® Clinical 200 Centrifuges) at 6000 rpm for 20 minutes to get rid of the solvent residue. The particles were collected by pouring out the supernatant. Distilled water was mixed with the solution afterward. The particles were washed three times by adding 10 ml of water through centrifugation and vortexing. It helped to remove any residual free drugs and free surfactants loosely attached to the particle surface.

In the s/o/w double emulsion method, 100 mg PLGA was mixed in 2ml ethyl acetate and then vortexed for 2mins, resulting in a clear solution that was the oil/organic phase (o). 3.5mg gentamicin was dispersed into the PLGA organic solution by using a vortex mixer (Vortex-Genie 2, Fisher Scientific), which comprised the solid in oil dispersion (s/o). The solid dispersion was introduced into a large volume (20-25ml) of PVA aqueous solution (w) under stirring, which made the s/o/w double emulsion. No sonication was needed. The double emulsion solution was then stirred at 800 rpm for 4 hrs. Particles was generated at magnetic agitation. Particles were consolidated as

the solvent evaporated. The hardened particles were collected via centrifugation and washed using distilled water three times.

A variety of formulation parameters were experimented using the w/o/w double emulsion solvent evaporation technique, including monomer ratios of PLGA, molecular weight of PVA, sonication amplitude and time, aqueous phase volume, stirring rate and time, drug amount, and centrifugation speed. Table 5.1 and Table 5.2 shows the formulation parameters used in our experiments.

Table 5.1: Formulation parameters used for PLGA (50:50) nanoparticle synthesis by double emulsion technique.

Double Emulsion Method with Lactide to Glycolide ratio 50:50									
ID	PLGA (50:50)	Dichloro methane (ml)	Gentamicin (mg)	Water (µl)	PVA (internal phase)	Sonication	PVA (external phase)	Stir (rpm)	Centrifugation (rpm)
NP 1	200	12	5	200	N/A	35% 1 min	Mw= 89-98k 4%, 40ml	1500 for 45min	5000 15 min
NP 2	200	10	5	200	Mw= 89-98k 0.5%, 45 µl	35% 2 min	Mw= 89-98k	700 for 5.5hrs,3	4000 15min
NP 3	300	4	10	200	Mw= 89-98k 0.5%, 45 µl	35% 2 min	Mw= 89-98k	1000 for	4000 15min
NP 4	300	6	10	200	Mw= 89-98k 0.5%, 2ml	25%- 30%- 35% for 3min	Mw= 89-98k 0.2%, 75 ml	1000 for 16 hrs	5000 for 5min
NP 5	200	12	10	200	Mw= 89-98k 0.5%, 2ml	35% 3min	Mw= 89-98k, 0.2%, 40ml	8000 for 4hrs	5000 for 5min
NP 6	100	6	10	200	Mw=13-23k 100 µl, 6%	35% 4min	6% Mw= 13-23k 20ml	600 for 4 hrs	5000 for 5min
NP 7	100	6	10	150	No PVA	25% 2min 35% 2min	6% Mw= 13-23k 20ml	600 for 4hrs	4000 for 5min
NP 8	100	6	10	150	6%, Mw=13-23k Filtered (F) + sonicated (S) 20% 15s	25% 2 min 35% 2min	Mw= 13-23k 20ml	827, 4hrs	4000 for 5min
NP 9	100	6	10	300	Mw=13-23k 6% PVA (F + S)	35% 3min	Mw=13-23k 6%, 20ml	800 for 4hrs	5000 for 5min
NP 10	100	6	10	200	100ul Mw=31k 6%	40% 3min	Mw=31k 6%	700, 4hrs	3500 for
NP 11	100	6	10	200	100ul Mw=31k 6% (F+S)	30% 3min 40% 3min	Mw=31k 5%, 20ml	400, 4hrs	3500 for 10min

Table 5.2: Formulation parameters used for PLGA (75:25) nanoparticle synthesis by double emulsion technique.

Double Emulsion Method with Lactide to Glycolide ratio 75:25									
ID	PLGA (75:25)	Dichloro methane (ml)	Gentamicin (mg)	Water (µl)	PVA (internal phase)	Sonication	PVA (external phase)	Stir (rpm)	Centrifugation (rpm)
NP 12	100 mg	6	10	200	100 µl Mw=31k 4% Sonicated (S)	25% 3min 30% 2min 35% 2min	Mw=31k 4% 20ml	700 at 30°C	6000 rpm 10 min
NP 13	100 mg + 2ml EA	6	10	200	100 µl Mw=13-23k 4%, Filtered	35% 3min	13-23k 4% 20ml	800 for 4 hrs	5500 rpm 10 min
NP 14	100 mg	6	10	150	100 µl, 4% Mw=13-23k Filtered (F)	35% 3min	13-23k 4% 30ml	10min - 1000 Overnight-800	5500 rpm 10 min
NP 15	100 mg	4	5	150	Mw=31k 6% 50 µl (F)	35% 5min 30% 5min	31k 6% 25 ml	Overnight at 1000	5000rpm 10min
NP 16	100 mg	6	5	150	Mw=31k 6% 50 µl (F)	35% 5min 39%	31k 6% 20ml	Mixed @800rpm	4000rpm 10min
NP 17	100 mg	4	5	150	Mw=31k 6%, 50 µl (F+S)	35% 5min 39%	31k 6%	Mixed @pt3	4000rpm 10min
NP 18	100 mg	4	5	200	Mw=31k 5%, 50 µl (F+S)	35% 5min 40% 5min	13k 5% 25ml	1000 rpm 500 rpm	3500 for 10min
NP 19	100 mg	6	5	200	Mw=31k 5%, 50 µl (F+S)	35% 5min 40% 5min	13k 5% 25ml	Mixed @pt3 on stir plate	3500 for 10min

Characterization of PLGA nanoparticles

The PLGA nanoparticles were examined using a scanning electron microscopy (SEM; JEOL 6400, Tokyo, Japan). A microparticle suspension was dropped on a silicon wafer and was kept overnight to air dry. The silicon wafer was then taped with copper tape onto the copper stub. A 10nm thick gold layer was sputter-coated on the particle surface. The gold coating inhibited surface charging, reduced thermal damage and improved the signal required in the SEM. The samples were scanned at 5 kV accelerating voltage to reduce the damage of polymeric surface.

5.3 Results and Discussions

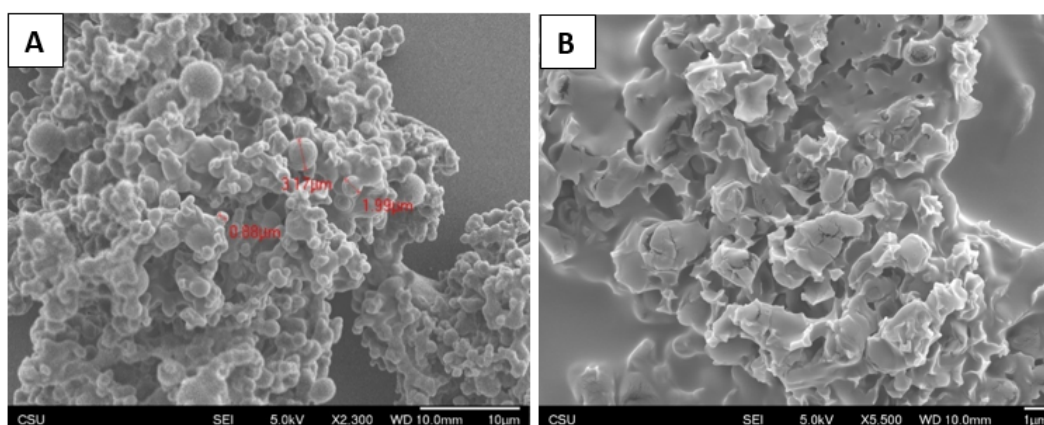


Figure 5.1: PLGA nanoparticles produced from high molecular weight (89,000-98,000 g/mol) PVA by A. water-in-oil-in-water (w1/o/w2) and B. solid-in-oil-in-water (s/o/w) double emulsion solvent evaporation method.

In general, the water-in-oil-in-water double emulsion method produced more uniform particles than the solid-in-oil-in-water double emulsion method. Figure 5.1 shows the SEM images of the particles prepared using w1/o/w2 and s/o/w double emulsion evaporation method respectively. The particles synthesized by the w1/o/w2 double emulsion method were shown in Figure 5.1A. Small and large particle agglomeration was observed. The shape of the particles was roughly spherical with uneven surface structures. Figure 5.1B shows the particles synthesized by the s/o/w double emulsion method. The particles were not in spherical shape rather deformed in shape

with flakes and porous structures. Different formulation parameters were tested but no significant improvement in the particle size was found. Due to high molecular weight the PVA might not well dispersed into the continuous phase in the emulsion and thus resulted in inefficient cover of the emulsion droplets. In addition, the concentration of PVA was low (2-4% (w/v)) which also affected the formation of individual particles.

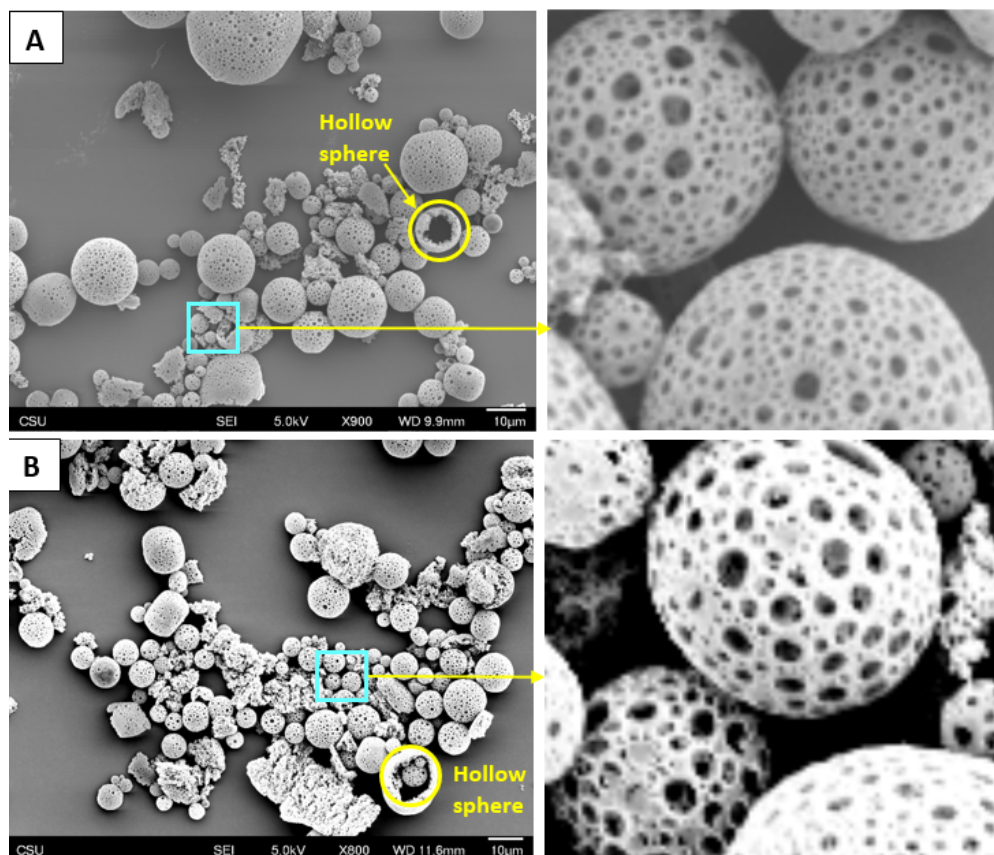


Figure 5.2: SEM micrographs of PLGA A.NP18 and B. NP19 prepared from low molecular weight (13,000-31,000 g/mol) PVA by the double emulsion solvent evaporation method.

Significant improvement in particle morphology was found when a low molecular weight of PVA (13,000-31,000 g/mol) and a high concentration of PVA (4-7% (w/v)) were used. However, the size distribution of the particles was large. NP18 and NP19 (Figure 5.2A and 5.2B) were synthesized using a large external aqueous volume (25 ml) that attributed to the large and porous structure in the particles due to rapid solvent evaporation from the organic phase. In addition, high

sonication amplitude might have generated air bubbles during the dispersion of primary emulsion. At the solvent evaporation stage, the air bubbles might have diffused through the polymer layer to create pores on particle surface. It was also noticed that some particles exhibited hollow-like spheres with a collapsed shell.

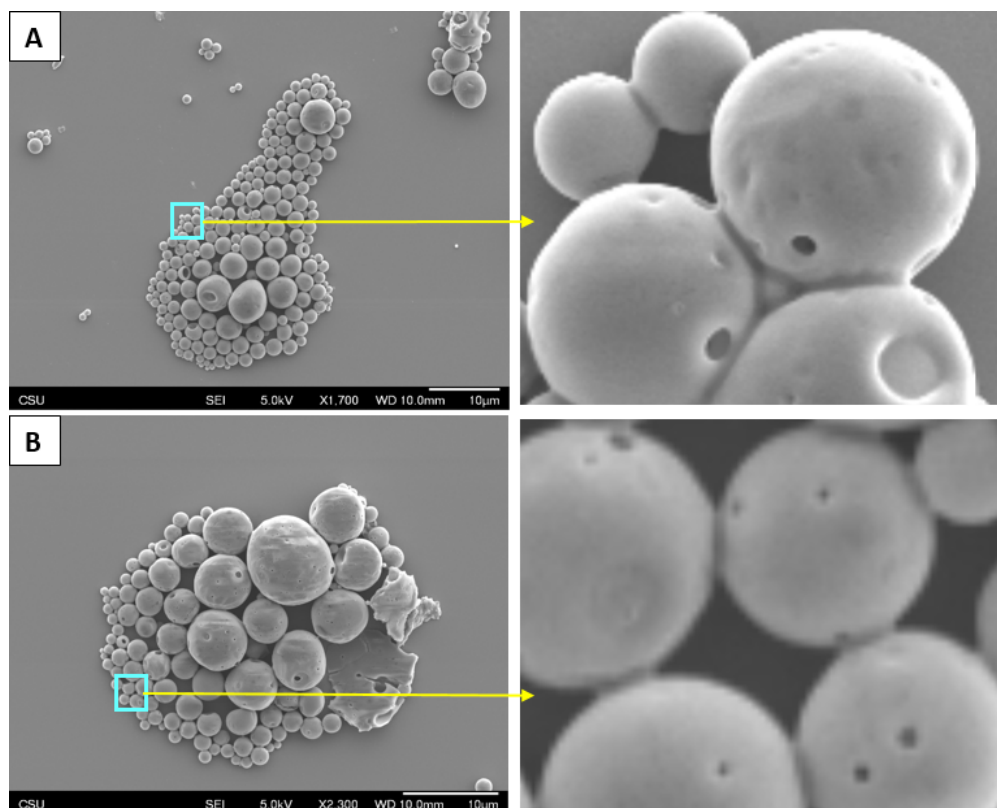


Figure 5.3: SEM micrographs of PLGA A.NP10 and B.NP 11 prepared by the emulsion solvent evaporation method.

Spherical particles with smooth surface were obtained with a large volume of the PVA (surfactant) solution ($100 \mu\text{l}$) in the primary emulsion and a high PVA concentration (5-6% (w/v)) in the secondary emulsion during solvent evaporation step. Figure 5.3A shows the SEM images of NP10 with individual small particles circled around the large particles. No agglomeration of particles was observed. The surface of the particles was quite smooth with a few small pits. The average particle size was around $1\sim 2\mu\text{m}$. The largest particle size was $6\mu\text{m}$ and smallest particle size was 300 nm . No significant pores were seen on the surface. The NP11 shown in Figure 5.3B had

quite similar surface structure except with larger particle size than the NP10. For NP10 extra 5ml of water was added in the external PVA solution after the initial particle hardening. That helped the diffusion of residual solvents and made smaller particles. Also, in case of NP11 stirring of secondary emulsion was low which might result in larger particles. Slow precipitation of PLGA polymer is known to cause smooth particle surface as reported by Luan et al. [Luan et al., 2006]. There was a very low affinity between dichloromethane and non-solvent water. It helped the slow diffusion of solvent and slow precipitation of polymer layer around the drug particles resulted in a smooth particle surface.

5.3.1 Mechanism of PLGA Nanoparticle Formation in Double Emulsion

Method

The emulsification of the water phase into the oil phase was the first step in double emulsion solvent evaporation technique. It yielded the primary emulsion (w1/o). The primary emulsion (w1/o) was again dispersed into a large volume of aqueous phase containing the surfactant molecules (PVA) to form the double emulsion (w1/o/w2).

5.3.1.1 Primary emulsion formation (w1/o)

The size and shape of dispersed phase in the primary emulsion determined the final size and shape of the polymeric nanoparticles. Careful observation was done during the primary emulsion formulation under complex optical microscope. In order to reduce the solvent evaporation during observation, a glass cover was used to protect the emulsion drops. Figure 5.4 shows an image at an optical microscope of the primary emulsion that consisted of water or aqueous phase (containing gentamicin) dispersed in the organic or oil phase (PLGA polymer dissolved in organic solvent). The aqueous droplets were randomly dispersed with various size distribution. Some aqueous droplets came close together and transformed into larger droplets. Air bubbles might also be present in the continuous phase (oil phase) due to high sonication amplitude. At an optical microscope, it was observed that as the solvents evaporated the size of the primary emulsion was reduced and also the number of droplets was minimized. It was due to the air bubbles present in

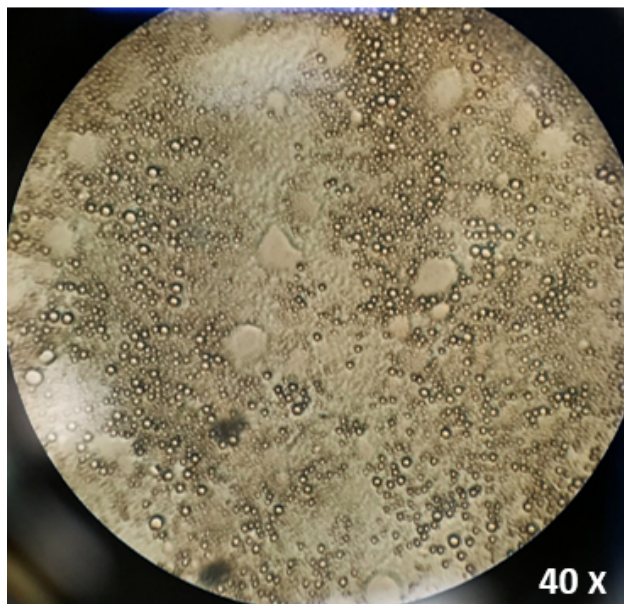


Figure 5.4: Primary emulsion (w/o) with aqueous droplets dispersed into organic/continuous phase.

the emulsion were broken during solvent drying. After the primary emulsion formation, the aqueous phase was saturated with solvent and the solvent started to evaporate and polymer precipitated around the aqueous droplets. Therefore, it is necessary to transfer the primary emulsion immediately to the second aqueous phase (external aqueous phase) before the solvent starts to evaporate.

5.3.1.2 Secondary emulsion formation (w1/o/w2)

A secondary emulsion or double emulsion was formed by immediately transferring the primary emulsion into the external aqueous phase (PVA solution). In the external aqueous phase that contained the surfactant PVA, the primary emulsion was covered with surfactant molecules. The surfactant molecules had the hydrophobic tail inserted in to the organic layer and hydrophilic head oriented to the outer/external water phase. The surfactant molecules kept the double emulsion droplets separated from each other and provided emulsion stability. Thus, the final nanoparticle formation and their morphology also depends on the formation of double emulsion droplets with different amount of inner aqueous phase entrapped inside it. In Figure 5.5A and 5.5B we can see double emulsion droplets with single and multiple aqueous droplets respectively. The different do-

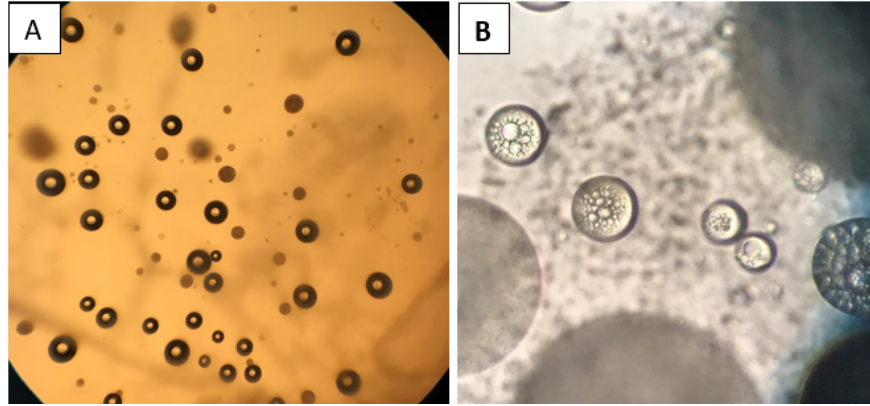


Figure 5.5: Double emulsion droplets with single and multiple aqueous droplets inside it.

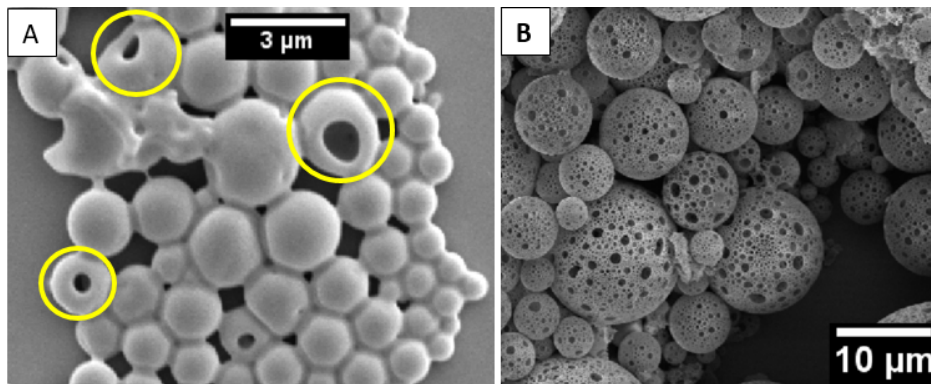


Figure 5.6: PLGA microparticles with A. capsule (yellow circle) and B. honeycomb structure observed under SEM.

Double emulsion droplets structures behaved differently during solvent evaporation and resulted in different particle morphologies. The emulsion droplets without inner aqueous droplet transformed into plain polymer particles. If there was one inner aqueous droplet, the particle exhibited an open or closed microstructure depending on the size of the inner aqueous phase. When the diameter of the inner aqueous phase was close to the diameter of the emulsion droplet, complete entrapment of the aqueous phase occurred by the polymer layer dissolved in organic phase and close structured particles formed. Emulsion droplets with more than one inner aqueous microdroplet produced capsule (Figure 5.6A) or honeycomb microstructure (Figure 5.6B) depending on the formulation parameters [Péan et al., 1998, Schwach et al., 2003]. In general, multinucleate microparticles tend to be formed by encapsulation of primary emulsion droplets under conditions of low shear rate and low surfactant concentration. As the solvent evaporation continued under magnetic stirring, the size

of the particles was reduced. During solvent evaporation, the precipitating polymer dissolved in organic phase imparted pressure onto the inner microdroplets that gradually merged and coalesced to give the final particles. When the diameter of the inner aqueous phase was much smaller than the emulsion droplet and the polymer concentration was high, then honeycomb structure on the surface was observed. The highly concentrated polymer precipitated as the solvent evaporated and produced this porous structure [Li et al., 2008]. These different kinds of particle structures were present at different proportions depending on the process variables, which includes concentration and volume of organic and aqueous phase, stirring rate, centrifugation time and rate, temperature.

5.3.2 Effects of Preparation Conditions on Particle Size and Morphology

5.3.2.1 Effect of monomer ratios in PLGA

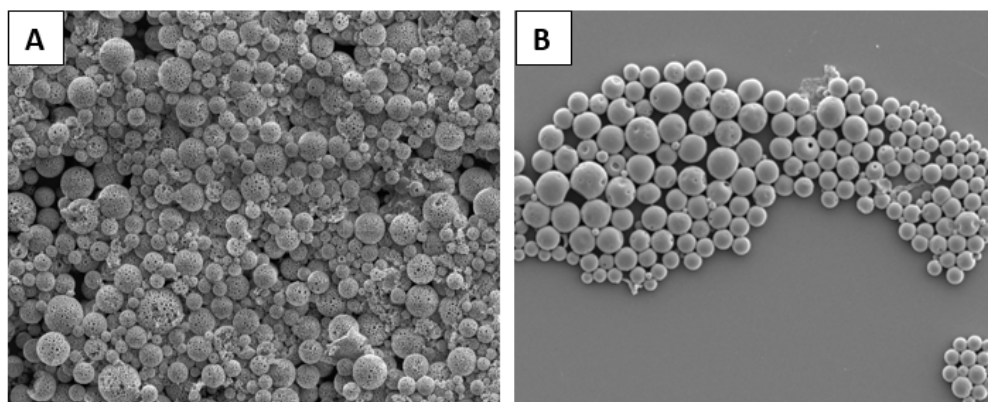


Figure 5.7: PLGA nanoparticles prepared from two different monomer ratios A. PLGA (75:25) B. PLGA (50:50)

The lactide to glycolide ratios of the PLGA polymers used in the study were 50:50 and 75:25. Figure 5.7 shows the SEM images of PLGA nanoparticles prepared from two different monomer ratios. The ratio had a significant impact on the surface morphology of the particles. The PLGA nanoparticles produced from a high lactide component (75:25) exhibited a high porous structure and a sponge-like porous structure as shown in Figure 5.7A. A smooth and nonporous surface was found in the particles prepared with a low ratio of 50:50. Similar results have also been reported in the literature [Jeffery et al., 1993]. From Figure 5.7B it can be observed that the nanoparticles

prepared from PLGA (50:50) had a smoother, denser, and nonporous surface than the particles of PLGA (75:25). It might be due to the differences in crystallinity and hydrophobicity of different formulations of PLGA [Cui et al., 2005]. Particles prepared using a PLGA with higher lactide content (increased hydrophobicity) hardened quickly due to rapid solvent evaporation from the microspheres. The quick vaporization of the solvent inside the microspheres caused the disruption of the polymer shell encapsulating the inner aqueous phase.

5.3.2.2 Effect of PLGA concentration

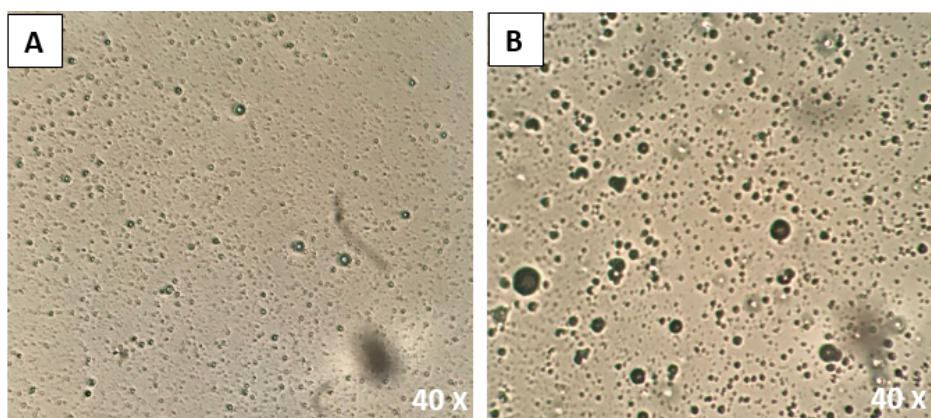


Figure 5.8: PLGA particles synthesized using A. 1.67% (w/v) and B. 2.7% (w/v) PLGA concentration in oil phase.

When the PLGA concentration was increased from 1.67% to 2.7% (w/v), it was found that the size of the particles was increased as illustrated in Figure 5.8. However, the increase in size was not significant, suggesting that the amount of surfactant was not enough to maintain the stability of the droplets. The increase in the polymer concentration was directly related to a high efficiency of the particle synthesis. At the high concentration of PLGA, the viscosity of the first emulsion was high. It was difficult for small w/o/w emulsion droplets formation and the droplets aggregated to become large particles [Cui et al., 2005]. The increase in particle size due to the increase in the PLGA concentrations has been reported previously [Kwon et al., 2001, Chorny et al., 2002]. It was likely due to be high viscous resistance against the shear forces during the emulsification process [Halayqa and Domańska, 2014].

5.3.2.3 Effect of surfactant (PVA)

The concentration and phase volume of surfactant played an important role in the emulsion droplet size and the structure of the nanoparticles. The size of the emulsion droplets depended on the amount of the surfactant as they disperse the oil-water phase and provide stabilization of the droplets during emulsification process. The role of a surfactant was to stabilize the emulsion droplets by preventing them from coalescing. In an effective stabilization, the surfactant molecules were able to cover the interface between the organic solvent and the aqueous phase for all the droplets [Manchanda et al., 2010]. It was found that an increase in PVA concentration significantly reduced the size of the nanoparticle. At high PVA concentration, the emulsifying molecules diffused to the emulsion droplet/aqueous phase interface at a high rate, resulting in a great presence of surfactants at the surface of emulsion droplets [Jeffery et al., 1993]. This efficient encirculation yields smaller particles. It was hypothesized that an insufficient amount of emulsifier failed in stabilizing all the nanoparticles and thus some of them tended to aggregate. As a result, large nanoparticles were produced [Feng and Huang, 2001]. Rafati et al. also reported the similar phenomena in size increase from 0.38 to 1.13 μm when the emulsifier (PVA) concentration was reduced from 10 to 1% w/v [Rafati et al., 1997]. However, if the PVA concentration continued to increase (>15%), the particles in the w/o system [Scholes et al., 1993] became large in size, which was considered to arise from non-uniform homogenization. Double emulsion generally gives highly polydisperse particles as compared to other techniques [Iqbal et al., 2015]. Thus, homogeneous dispersion of emulsion is very important to achieve smaller particles with low polydispersity.

Figure 5.9B shows that smaller nanoparticles were obtained by using higher PVA concentration in comparison to the nanoparticles prepared from lower PVA concentration (Figure 5.9A). At the high PVA concentration, the viscosity of the external aqueous phase prevented the coalescence of the emulsion droplets, resulting in small emulsion droplets formation. Then, the solvent in the emulsion droplets continued to evaporate and the emulsion droplets gradually hardened to form nanoparticles. Particle agglomeration was reduced when the high PVA concentration (4% w/v)

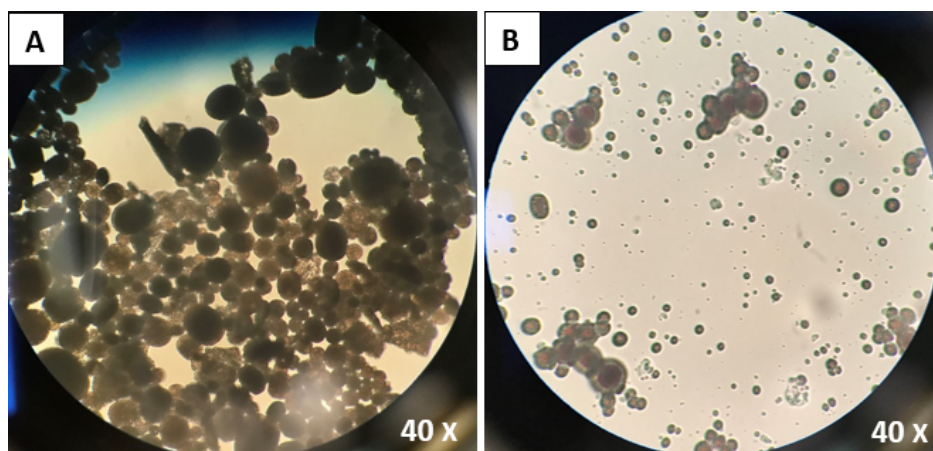


Figure 5.9: Nanoparticles prepared with A. 0.2% and B. 4% PVA solution as external aqueous phase.

was used. The particles were stabilized due to the adsorption of PVA molecules on the surface of the particles. Murakami et al. hypothesized that the hydroxyl groups of PVA molecules attached to the acetyl groups of PLGA due to hydrophobic bonding [Murakami et al., 1999], preventing particle agglomeration.

5.3.2.4 Effect of sonication time and power

In a sonicator, the particles in a dispersion are reduced in size due to random droplet disruption and fusion during sonication. Sonication amplitude is defined as peak to peak displacement at the probe tip of a sonicator. The amplitude is constant during sonication. The percentages of amplitude are in function of the maximum displacement. According to Landfester [Landfester et al., 2004] a minimum amplitude of at least 20% is necessary to reach an equilibrium state for a miniemulsion.

Figure 5.10 shows the difference in the size of the primary emulsion droplets at two different sonication power. In the current sonication experiments, the sonication effect on size was evaluated with two different amplitudes. Amplitudes of 35% and 40% were evaluated, showing a small decrease in the PLGA nanoparticles size. The nanoparticles in minimum size were obtained at 40% amplitude for five minutes. However, the effect of sonication was found significant in the primary emulsion (w1/o) formation. High sonication amplitude (40%) resulted in a smaller aqueous droplet dispersed evenly into the continuous phase (oil phase containing PLGA polymer) of the emulsion. An increase in sonication power was also able to reduce particle size due to high sonication energy.

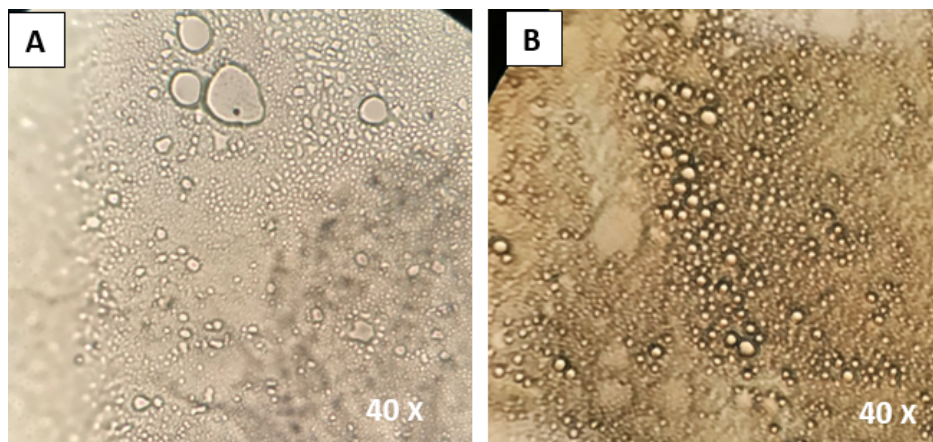


Figure 5.10: Primary emulsion (w/o) prepared at A. 35% and B. 40% sonication amplitude.

At low sonication power, agglomeration of large aqueous droplets were observed under optical microscope.

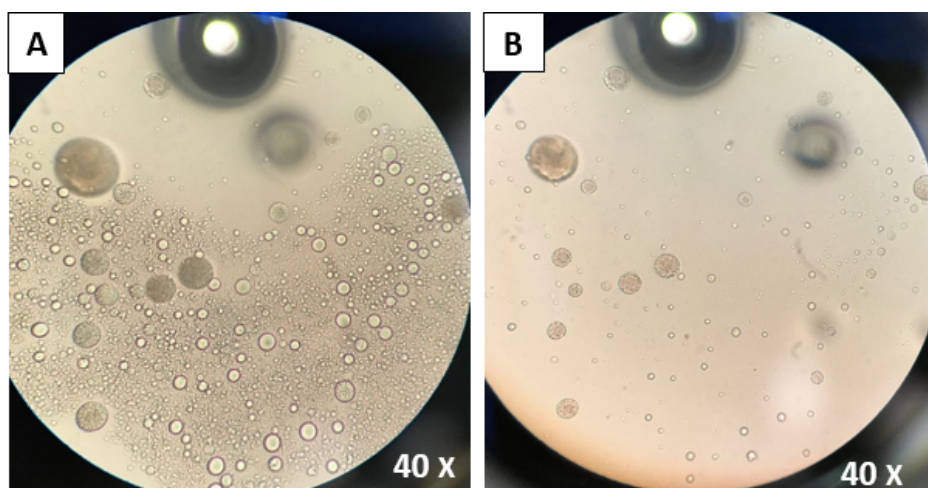


Figure 5.11: Effect of second sonication of w/o/w double emulsion droplet (A)- only large particles were retained (B), small particles broke down and mixed with external aqueous phase.

To improve the dispersion of w/o emulsion into external aqueous phase, a second sonication was introduced. Figure 5.11 reveals the effect of second sonication upon the double emulsion droplets formation. The second sonication was able to provide high energy to disrupt the emulsion structure and resulted in escape of the inner aqueous phase from the primary emulsion droplets.

The high homogenization energy broke the organic layer that was still in wet condition and surface tension of the droplet reduced resulted in releasing the drug form the emulsion droplets.

5.3.2.5 Effect of concentration of continuous phase

In the current experiments, the concentration of the oil phase was varied from 1.67%-2.7% (w/v) and the viscosity of the inner aqueous/dispersed phase was varied from 2.8-10% (w/v). With the increase of the oil phase concentration the particles size increased during the emulsification- evaporation method. With high viscosity of the inner aqueous solution larger nanoparticles were achieved with 10-20 μ m in diameter. The effect of viscosity on the size of emulsion droplets can be described by an empirical equation [Calderbank, 1958]:

$$d_{32} = A \times \left(\frac{\mu_d}{\mu_c}\right)^{0.25}$$

Where d_{32} is the average diameter (Sauter's diameter) of micro-spheres, μ_d is the viscosity of the dispersed phase, μ_c is the viscosity of the continuous phase and A is a coefficient which depends on many other factors including agitation rate, volume fraction of the dispersed phase to the continuous phase and their viscosity ratio [Davies, 1992]. From equation (1) it is evident that with the increase of viscosity of the continuous phase the emulsion droplet size decreases. At the same time, decreasing the viscosity of the dispersed phase also decreases the particle size. Increasing polymer concentration or the molecular weight of polymer increases the viscosity of continuous phase and the size decreases exponentially with viscosity.

5.3.2.6 Effect of internal aqueous phase

Figure 5.12A and 5.12B illustrates the corresponding surface morphology of particles produced by using 150 μ l and 300 μ l of inner aqueous phase, respectively. It was found that the internal aqueous phase volume had a significant impact on the surface morphology of the resulting micro-spheres. The average particle size was increased slightly and the surface of the microspheres was more irregular when the micro-spheres were prepared at a large volume of inner aqueous

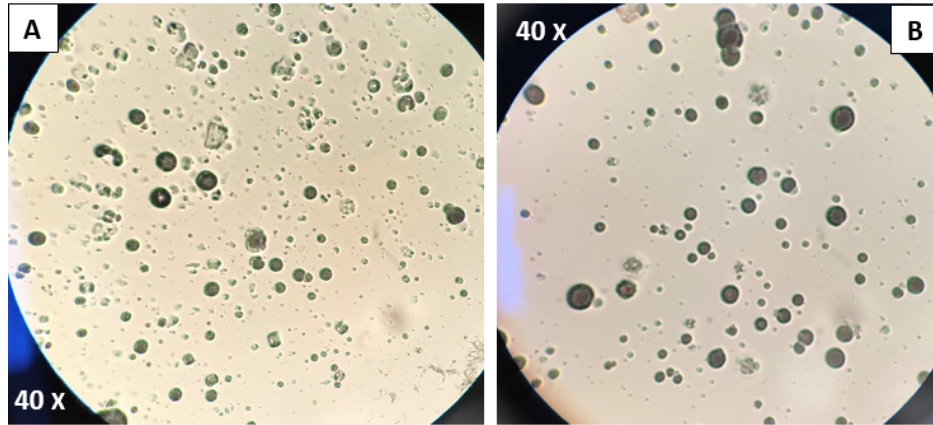


Figure 5.12: Optical microscope image of PLGA microparticles produced with A. 150 μl and B. 300 μl internal aqueous phase.

phase (water phase). The size of the inner water droplets was determined during production of the w1/o emulsions. The large volume of inner water phase led to the formation of larger emulsion droplets, followed by the formation of larger microspheres [Cui et al., 2005]. Porous structure on the particle surface was found when a large volume of the inner aqueous droplets in the emulsion. There might be two reasons for the porous structure [Cui et al., 2005]: 1) during emulsification part of the aqueous phase diffuses through the polymer-oil phase into external aqueous phase 2) residual water inside the particles evaporates during drying process.

5.3.2.7 Effect of external aqueous phase

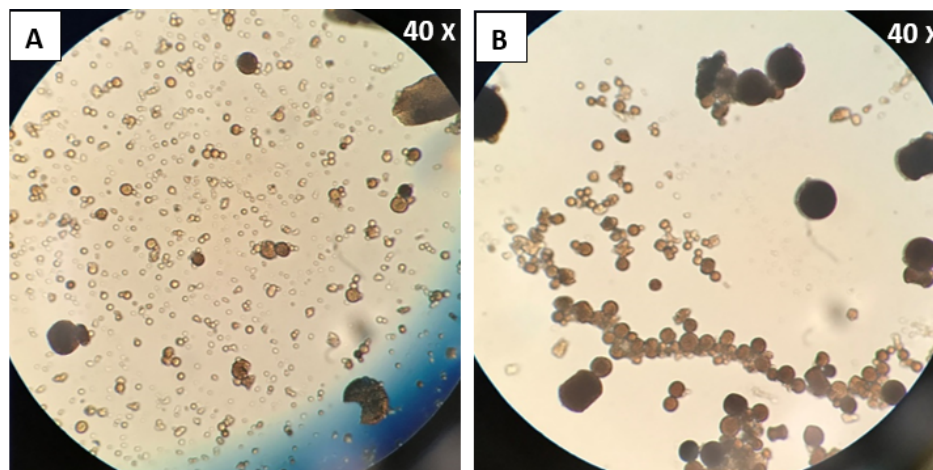


Figure 5.13: PLGA nanoparticles synthesized form A. 20 ml and B. 30 ml external aqueous volume.

Figure 5.13 illustrates the size difference of particles produced by using 20ml and 30ml external aqueous phase. An increase in the volume of the external aqueous phase resulted in an increase in particle size. The volume of external aqueous phase did not affect the surface morphology. We attributed the increase in particle size to the reduction in agitation due to the mixing efficiency of the primary emulsion droplet when using a large volume of water. A reduction in mixing efficiency produced an increase in size of the emulsion droplets formed during the preparation. However, mixing additional water to the external aqueous phase after the solvent evaporated resulted in a decreased particle size. It was due to the acceleration of solvent diffusion that remained inside the particles.

5.3.2.8 Effect of stirring speed, time, and temperature

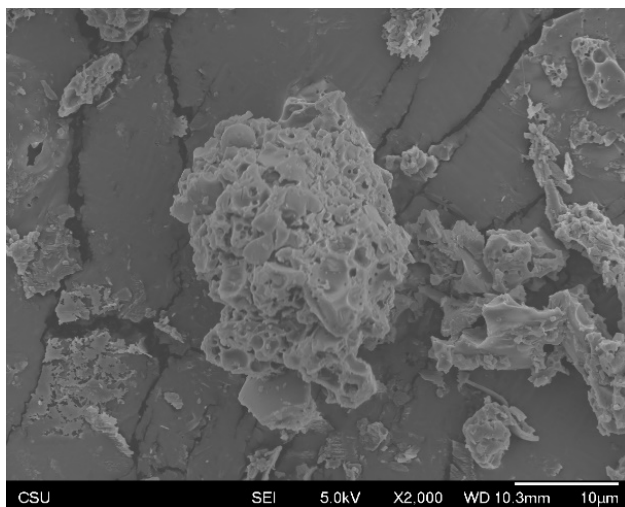


Figure 5.14: Porous honeycomb-like structure observed under SEM in nanoparticles produced at high stirring speed and temperature.

Figure 5.14 illustrates the formation of agglomerated and porous particle structure at high stirring rate and temperature. Increasing evaporation rate of organic solvent by high speed stirring at a high temperature influenced particle size and surface morphology [Feng and Huang, 2001]. At a high evaporation rate (above 800 rpm), the particles tended to aggregate and deform in shape before the emulsifier molecules covered the surface of the emulsions droplets. At a moderate stirring

rate (500-800 rpm) with magnetic bar, the solution evaporated and particles hardened gave the final product without any significant agglomeration. At a high temperature (33°C), a porous structure of the particles was found as depicted in Figure 5.14. Due to fast diffusion of solvent in the surface layer of the deformed oil droplets at the high temperature, PLGA on the particle surface solidified so quickly that the internal aqueous droplets near the oil droplet surface were promptly frozen on the surface, leading the formation of saliences on the surface of microparticle [Meng et al., 2003].

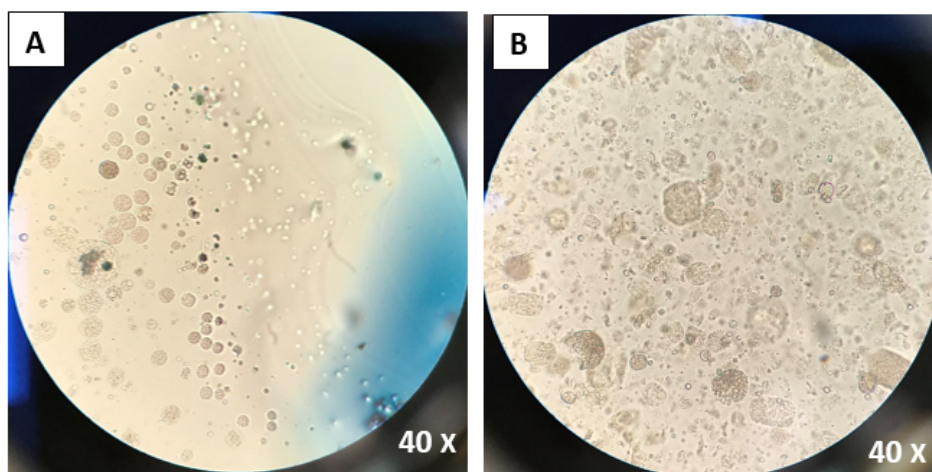


Figure 5.15: w1/o/w2 double emulsion droplet (A) after stirring for 3 hrs (B) after stirring for 6 hrs at 800rpm.

Figure 5.15 shows the particle deformation caused by stirring at a high speed for a longer period of time. The stirring rate of the secondary emulsion determined the final size distribution of the particles. In general, as the stirring rate was increased the particle size decreased. However, at high stirring rate (above 800 rpm) plain and flake structure of the particles were observed. For example- during formation of hardened nanoparticles high stirring rate and longer stirring period (18 hrs) caused the deformation of nanoparticles as demonstrated in Figure 5.15B. At high shear stress long and cylindrical particles were observed. At high rpm large amount of solvent diffused from the polymeric shell to the outer aqueous solution which increases the viscosity of the external aqueous phase [Rosca et al., 2004]. At the same time, the high-speed fluid of the external aqueous phase accelerated the diffusion of the solvent near the surface layer of oil droplets, resulting in a

rapid solidification of the polymer on the surface layer. On the other hand, the mild shear stress of 3500 rpm did not deform the w/o oil droplets resulted in spherical particles. Janssen et al. also observed that when a suspended oil droplet is subjected to a suddenly increased shear force, it stretches rapidly into a long cylindrical thread, which subsequently deformed due to the growth of interfacial tension [Janssen and Meijer, 1993].

Chapter 6

CONCLUSION

PLGA microparticles was prepared using the w/o/w emulsion solvent evaporation technique. When the microparticles were generated, an antibiotic hydrophilic drug- gentamicin was encapsulated. The microspheres with different shape and surface structure can be prepared by changing preparation conditions, such as the type of polymer, its concentration, PVA (surfactant) concentration, volume of internal water phase and level of drug loading. The microparticles were generated by solvent elimination due to the combined effects of high solvent volatility and polymer precipitation. The emulsion formation in the synthesis is critical because the droplet size of the emulsion determined the size of the final particles. The inner aqueous phase content of the emulsion droplet and the size of the inner microdroplet relative to the emulsion droplet may change particle size and contributed different morphologies such as honeycomb, capsule, and plain structure.

Chapter 7

FUTURE WORKS

The objective of this work is to prepare core-shell PDA composite nanofibers loaded with antibacterial polymeric nanoparticles for wound dressing applications. PDA was mixed with PEO and PU and the mixtures were electrospun to produce PEO-PDA and PU-PDA composite nanofibers, respectively. It was found that the PU-PDA composite fibers exhibited superior mechanical properties, which is in favor of wound dressing applications. PLGA nanoparticles loaded with gentamicin were successfully synthesized, which would be potentially used in electrospinning PDA composite nanofibers. The PLGA nanoparticles demonstrated a fairly spherical shape and a smooth surface. Further study can be focused on optimizing formulation parameters so that the particle size can be reduced to 50~100nm suitable for incorporation in core-shell nanofibers. Although significant progress was made toward understanding the composite fiber properties and PLGA nanoparticle preparation, future research should be addressed before the biosensing nanofibers could be successfully applied in a smart wound dressing.

Chemical analysis will be carried out to confirm the presence of gentamicin encapsulated inside the particle or onto the surface of the particle using a Fourier transform infrared spectroscopy (FTIR). It would also determine if there is any structural modification of the drug particles encapsulated in the PLGA nanoparticles. An elemental analysis using Energy-dispersive X-ray spectroscopy (EDX) can be also useful to determine the presence of gentamicin in the particles. As nitrogen (N) is only present in the gentamicin, presence of N map on the particles will confirm the presence of gentamicin too.

A gentamicin release study of the NPs will be carried out. Supernatant samples will be taken from the dispersion medium of the nanoparticles after an ultra-centrifugation. Gentamicin in the supernatants will be measured using a UV spectroscopy. The release study will be carried out over 24 hours and a week to understand the drug release profile of the PLGA nanoparticles.

PLGA nanoparticles with a diameter of 50~100 nm will be used in incorporation into PU-PDA nanofibers via a coaxial electrospinning technique. Fiber size and morphology will be studied and the formation of core-shell structure will be confirmed by using TEM. A gentamicin release study will be carried out to determine the efficiency of drug release from the nanofibers. Antibacterial activity of the nanofibers will also be studied using an AATCC standard method. Colony-forming unit (CFU) will also be counted to find out the minimum bacterial concentration required to make the color transformation of the PDA composite fibers.

Bibliography

- [Alam et al., 2016] Alam, A., Yapor, J. P., Reynolds, M. M., and Li, Y. V. (2016). Study of polydiacetylene-poly (ethylene oxide) electrospun fibers used as biosensors. *Materials*, 9(3):202.
- [Alemdar and Sain, 2008] Alemdar, A. and Sain, M. (2008). Biocomposites from wheat straw nanofibers: morphology, thermal and mechanical properties. *Composites Science and Technology*, 68(2):557–565.
- [Amna et al., 2012] Amna, T., Hassan, M. S., Barakat, N. A., Pandeya, D. R., Hong, S. T., Khil, M.-S., and Kim, H. Y. (2012). Antibacterial activity and interaction mechanism of electrospun zinc-doped titania nanofibers. *Applied microbiology and biotechnology*, 93(2):743–751.
- [Anhalt, 1977] Anhalt, J. P. (1977). Assay of gentamicin in serum by high-pressure liquid chromatography. *Antimicrobial agents and chemotherapy*, 11(4):651–655.
- [Astete and Sabliov, 2006] Astete, C. E. and Sabliov, C. M. (2006). Synthesis of poly (dl-lactide-co-glycolide) nanoparticles with entrapped magnetite by emulsion evaporation method. *Particulate science and technology*, 24(3):321–328.
- [Bickers et al., 2006] Bickers, D. R., Lim, H. W., Margolis, D., Weinstock, M. A., Goodman, C., Faulkner, E., Gould, C., Gemmen, E., and Dall, T. (2006). The burden of skin diseases: 2004: A joint project of the american academy of dermatology association and the society for investigative dermatology. *Journal of the American Academy of Dermatology*, 55(3):490–500.
- [Bilati et al., 2005] Bilati, U., Allémann, E., and Doelker, E. (2005). Strategic approaches for overcoming peptide and protein instability within biodegradable nano- and microparticles. *European Journal of Pharmaceutics and Biopharmaceutics*, 59(3):375–388.

- [Butt et al., 2005] Butt, H.-J., Cappella, B., and Kappl, M. (2005). Force measurements with the atomic force microscope: Technique, interpretation and applications. *Surface science reports*, 59(1-6):1–152.
- [Calderbank, 1958] Calderbank, P. (1958). Physical rate processes in industrial fermentations part i: The interfacial area in gas-liquid contacting with mechanical agitation. *Trans. Inst. Chem. Engrs*, 36:443–463.
- [Cappella et al., 2005] Cappella, B., Kaliappan, S. K., and Sturm, H. (2005). Using afm force-distance curves to study the glass-to-rubber transition of amorphous polymers and their elastic-plastic properties as a function of temperature. *Macromolecules*, 38(5):1874–1881.
- [Chae et al., 2007] Chae, S. K., Park, H., Yoon, J., Lee, C. H., Ahn, D. J., and Kim, J.-M. (2007). Polydiacetylene supramolecules in electrospun microfibers: fabrication, micropatterning, and sensor applications. *Advanced Materials*, 19(4):521–524.
- [Chakraborty et al., 2009] Chakraborty, S., Liao, I.-C., Adler, A., and Leong, K. W. (2009). Electrohydrodynamics: a facile technique to fabricate drug delivery systems. *Advanced drug delivery reviews*, 61(12):1043–1054.
- [Champion et al., 2007] Champion, J. A., Katare, Y. K., and Mitragotri, S. (2007). Particle shape: a new design parameter for micro-and nanoscale drug delivery carriers. *Journal of Controlled Release*, 121(1-2):3–9.
- [Chen et al., 2008] Chen, J.-P., Chang, G.-Y., and Chen, J.-K. (2008). Electrospun collagen/chitosan nanofibrous membrane as wound dressing. *Colloids and Surfaces A: Physico-chemical and Engineering Aspects*, 313:183–188.
- [Chen et al., 2012] Chen, X., Zhou, G., Peng, X., and Yoon, J. (2012). Biosensors and chemosensors based on the optical responses of polydiacetylenes. *Chemical Society Reviews*, 41(13):4610–4630.

- [Cherreddy et al., 2016] Cherreddy, K. K., Vandermeulen, G., and Pr eat, V. (2016). Plga based drug delivery systems: Promising carriers for wound healing activity. *Wound Repair and Regeneration*, 24(2):223–236.
- [Chorny et al., 2002] Chorny, M., Fishbein, I., Danenberg, H. D., and Golomb, G. (2002). Lipophilic drug loaded nanospheres prepared by nanoprecipitation: effect of formulation variables on size, drug recovery and release kinetics. *Journal of controlled release*, 83(3):389–400.
- [Cui et al., 2005] Cui, F., Cun, D., Tao, A., Yang, M., Shi, K., Zhao, M., and Guan, Y. (2005). Preparation and characterization of melittin-loaded poly (dl-lactic acid) or poly (dl-lactic-co-glycolic acid) microspheres made by the double emulsion method. *Journal of Controlled Release*, 107(2):310–319.
- [Danhier, 2012] Danhier, F., A. E. S. J. M. C. R. L. B. A. . P. V. (2012). Plga-based nanoparticles: an overview of biomedical applications. *ournal of controlled release*, 2:505–522.
- [Davies, 1992] Davies, G. (1992). Mixing and coalescence phenomena in liquid–liquid systems. *Science and Practice of Liquid–Liquid Extraction*, 1:244–342.
- [Day and Lando, 1981] Day, D. R. and Lando, J. B. (1981). Conduction in polydiacetylene bilayers. *Journal of Applied Polymer Science*, 26(5):1605–1612.
- [Deitzel et al., 2001] Deitzel, J. M., Kleinmeyer, J., Harris, D., and Tan, N. B. (2001). The effect of processing variables on the morphology of electrospun nanofibers and textiles. *Polymer*, 42(1):261–272.
- [Desai et al., 1997] Desai, M. P., Labhasetwar, V., Walter, E., Levy, R. J., and Amidon, G. L. (1997). The mechanism of uptake of biodegradable microparticles in caco-2 cells is size dependent. *Pharmaceutical research*, 14(11):1568–1573.
- [Desgouilles et al., 2003] Desgouilles, S., Vauthier, C., Bazile, D., Vacus, J., Grossiord, J.-L., Veillard, M., and Couvreur, P. (2003). The design of nanoparticles obtained by solvent evaporation: a comprehensive study. *Langmuir*, 19(22):9504–9510.

- [Díaz et al., 2006] Díaz, J. E., Barrero, A., Márquez, M., and Loscertales, I. G. (2006). Controlled encapsulation of hydrophobic liquids in hydrophilic polymer nanofibers by co-electrospinning. *Advanced Functional Materials*, 16(16):2110–2116.
- [Doillon and Silver, 1986] Doillon, C. J. and Silver, F. H. (1986). Collagen-based wound dressing: Effects of hyaluronic acid and firponectin on wound healing. *Biomaterials*, 7(1):3–8.
- [Felgueiras and Amorim, 2017] Felgueiras, H. P. and Amorim, M. T. P. (2017). Functionalization of electrospun polymeric wound dressings with antimicrobial peptides. *Colloids and Surfaces B: Biointerfaces*, 156:133–148.
- [Feng and Huang, 2001] Feng, S.-s. and Huang, G. (2001). Effects of emulsifiers on the controlled release of paclitaxel (taxol®) from nanospheres of biodegradable polymers. *Journal of Controlled Release*, 71(1):53–69.
- [Ferreira et al., 2006] Ferreira, M. C., Tuma Júnior, P., Carvalho, V. F., and Kamamoto, F. (2006). Complex wounds. *Clinics*, 61(6):571–578.
- [Ficheux et al., 1998] Ficheux, M.-F., Bonakdar, L., Leal-Calderon, F., and Bibette, J. (1998). Some stability criteria for double emulsions. *Langmuir*, 14(10):2702–2706.
- [Flory et al., 1981] Flory, P., Ciardelli, F., and Gusti, P. (1981). Structural orders in polymers.
- [Fong et al., 1999] Fong, H., Chun, I., and Reneker, D. (1999). Beaded nanofibers formed during electrospinning. *Polymer*, 40(16):4585–4592.
- [Fredenberg et al., 2011] Fredenberg, S., Wahlgren, M., Reslow, M., and Axelsson, A. (2011). The mechanisms of drug release in poly (lactic-co-glycolic acid)-based drug delivery systems—A review. *International journal of pharmaceutics*, 415(1-2):34–52.
- [Galiotis et al., 1984] Galiotis, C., Read, R., Yeung, P., Young, R., Chalmers, I., and Bloor, D. (1984). High-modulus polydiacetylene single-crystal fibers. *Journal of Polymer Science Part B: Polymer Physics*, 22(9):1589–1606.

- [Gao et al., 2014] Gao, Y., Bach Truong, Y., Zhu, Y., and Louis Kyrtziz, I. (2014). Electrospun antibacterial nanofibers: Production, activity, and in vivo applications. *Journal of Applied Polymer Science*, 131(18).
- [Gao and Cranston, 2008] Gao, Y. and Cranston, R. (2008). Recent advances in antimicrobial treatments of textiles. *Textile Research Journal*, 78(1):60–72.
- [Gavara, 2017] Gavara, N. (2017). A beginner’s guide to atomic force microscopy probing for cell mechanics. *Microscopy research and technique*, 80(1):75–84.
- [Ge et al., 2002] Ge, H., Hu, Y., Jiang, X., Cheng, D., Yuan, Y., Bi, H., and Yang, C. (2002). Preparation, characterization, and drug release behaviors of drug nimodipine-loaded poly (ϵ -caprolactone)-poly (ethylene oxide)-poly (ϵ -caprolactone) amphiphilic triblock copolymer micelles. *Journal of pharmaceutical sciences*, 91(6):1463–1473.
- [Goldenberg, 1959] Goldenberg, I. S. (1959). Catgut, silk, and silver—the story of surgical sutures. *Surgery*, 46(5):908–912.
- [Govender et al., 1999] Govender, T., Stolnik, S., Garnett, M. C., Illum, L., and Davis, S. S. (1999). Plga nanoparticles prepared by nanoprecipitation: drug loading and release studies of a water soluble drug. *Journal of Controlled Release*, 57(2):171–185.
- [Halayqa and Domańska, 2014] Halayqa, M. and Domańska, U. (2014). Plga biodegradable nanoparticles containing perphenazine or chlorpromazine hydrochloride: effect of formulation and release. *International journal of molecular sciences*, 15(12):23909–23923.
- [Heyer et al., 2013] Heyer, K., Augustin, M., Protz, K., Herberger, K., Spehr, C., and Rustenbach, S. (2013). Effectiveness of advanced versus conventional wound dressings on healing of chronic wounds: systematic review and meta-analysis. *Dermatology*, 226(2):172–184.
- [Hindeleh and Johnson, 1978] Hindeleh, A. and Johnson, D. (1978). Crystallinity and crystallite size measurement in polyamide and polyester fibres. *Polymer*, 19(1):27–32.

- [Hotaling et al., 2015] Hotaling, N. A., Bharti, K., Kriel, H., and Simon, C. G. (2015). Diameterj: A validated open source nanofiber diameter measurement tool. *Biomaterials*, 61:327–338.
- [Huang et al., 2006] Huang, Z.-M., He, C.-L., Yang, A., Zhang, Y., Han, X.-J., Yin, J., and Wu, Q. (2006). Encapsulating drugs in biodegradable ultrafine fibers through co-axial electrospinning. *Journal of Biomedical Materials Research Part A: An Official Journal of The Society for Biomaterials, The Japanese Society for Biomaterials, and The Australian Society for Biomaterials and the Korean Society for Biomaterials*, 77(1):169–179.
- [Huang et al., 2003] Huang, Z.-M., Zhang, Y.-Z., Kotaki, M., and Ramakrishna, S. (2003). A review on polymer nanofibers by electrospinning and their applications in nanocomposites. *Composites science and technology*, 63(15):2223–2253.
- [Imbuluzqueta et al., 2013] Imbuluzqueta, E., Gamazo, C., Lana, H., Campanero, M. Á., Salas, D., Gil, A. G., Elizondo, E., Ventosa, N., Veciana, J., and Blanco-Prieto, M. J. (2013). Hydrophobic gentamicin loaded nanoparticles are effective in brucella melitensis in mice. *Antimicrobial agents and chemotherapy*, pages AAC–00378.
- [Iqbal et al., 2015] Iqbal, M., Zafar, N., Fessi, H., and Elaissari, A. (2015). Double emulsion solvent evaporation techniques used for drug encapsulation. *International journal of pharmaceuticals*, 496(2):173–190.
- [Janssen and Meijer, 1993] Janssen, J. and Meijer, H. (1993). Droplet breakup mechanisms: Stepwise equilibrium versus transient dispersion. *Journal of Rheology*, 37(4):597–608.
- [Jeffery et al., 1991] Jeffery, H., Davis, S., and O’hagan, D. (1991). The preparation and characterisation of poly (lactide-co-glycolide) microparticles. i: Oil-in-water emulsion solvent evaporation. *International Journal of Pharmaceutics*, 77(2-3):169–175.
- [Jeffery et al., 1993] Jeffery, H., Davis, S. S., and O’hagan, D. T. (1993). The preparation and characterization of poly (lactide-co-glycolide) microparticles. ii. the entrapment of a model

- protein using a (water-in-oil)-in-water emulsion solvent evaporation technique. *Pharmaceutical research*, 10(3):362–368.
- [Jelinek and Ritenberg, 2013] Jelinek, R. and Ritenberg, M. (2013). Polydiacetylenes—recent molecular advances and applications. *RSC Advances*, 3(44):21192–21201.
- [Jeon et al., 2012] Jeon, H., Lee, J., Kim, M. H., and Yoon, J. (2012). Polydiacetylene-based electrospun fibers for detection of hcl gas. *Macromolecular rapid communications*, 33(11):972–976.
- [Jianrong et al., 2004] Jianrong, C., Yuqing, M., Nongyue, H., Xiaohua, W., and Sijiao, L. (2004). Nanotechnology and biosensors. *Biotechnology advances*, 22(7):505–518.
- [Jockenhöfer et al., 2013] Jockenhöfer, F., Gollnick, H., Herberger, K., Isbary, G., Renner, R., Stücker, M., Valesky, E., Wollina, U., Weichenthal, M., Karrer, S., et al. (2013). Bacteriological pathogen spectrum of chronic leg ulcers: Results of a multicenter trial in dermatologic wound care centers differentiated by regions. *JDDG: Journal der Deutschen Dermatologischen Gesellschaft*, 11(11):1057–1063.
- [Jorgensen, 1993] Jorgensen, W. L. (1993). Supramolecular chemistry. *Proceedings of the National Academy of Sciences*, 90(5):1635–1636.
- [Kamaly et al., 2016] Kamaly, N., Yameen, B., Wu, J., and Farokhzad, O. C. (2016). Degradable controlled-release polymers and polymeric nanoparticles: mechanisms of controlling drug release. *Chemical reviews*, 116(4):2602–2663.
- [Khil et al., 2003] Khil, M.-S., Cha, D.-I., Kim, H.-Y., Kim, I.-S., and Bhattarai, N. (2003). Electrospun nanofibrous polyurethane membrane as wound dressing. *Journal of Biomedical Materials Research Part B: Applied Biomaterials*, 67(2):675–679.
- [Khoee and Yaghoobian, 2009] Khoee, S. and Yaghoobian, M. (2009). An investigation into the role of surfactants in controlling particle size of polymeric nanocapsules containing penicillin-g in double emulsion. *European journal of medicinal chemistry*, 44(6):2392–2399.

- [Kissinger, 2005] Kissinger, P. T. (2005). Biosensors—A perspective. *Biosensors and Bioelectronics*, 20(12):2512–2516.
- [Klapperich et al., 2001] Klapperich, C., Komvopoulos, K., and Pruitt, L. (2001). Nanomechanical properties of polymers determined from nanoindentation experiments. *Journal of Tribology*, 123(3):624–631.
- [Kobayashi et al., 1987] Kobayashi, A., Kobayashi, H., Tokura, Y., Kanetake, T., and Koda, T. (1987). Crystal structure of polydiacetylene tcdv revisited. *The Journal of chemical physics*, 87(8):4962–4966.
- [Kreuter, 1994] Kreuter, J. (1994). Nanoparticles. *Colloidal drug delivery systems*, pages 219–342.
- [Kulkarni et al., 1971] Kulkarni, R. K., Moore, E., Hegyeli, A., and Leonard, F. (1971). Biodegradable poly (lactic acid) polymers. *Journal of biomedical materials research*, 5(3):169–181.
- [Kumari et al., 2010] Kumari, A., Yadav, S. K., and Yadav, S. C. (2010). Biodegradable polymeric nanoparticles based drug delivery systems. *Colloids and Surfaces B: Biointerfaces*, 75(1):1–18.
- [Kwon et al., 2001] Kwon, H.-Y., Lee, J.-Y., Choi, S.-W., Jang, Y., and Kim, J.-H. (2001). Preparation of plga nanoparticles containing estrogen by emulsification–diffusion method. *Colloids and Surfaces A: Physicochemical and Engineering Aspects*, 182(1-3):123–130.
- [Landfester et al., 2004] Landfester, K., Eisenblätter, J., and Rothe, R. (2004). Preparation of polymerizable miniemulsions by ultrasonication. *JCT research*, 1(1):65–68.
- [Lazcka et al., 2007] Lazcka, O., Del Campo, F. J., and Munoz, F. X. (2007). Pathogen detection: A perspective of traditional methods and biosensors. *Biosensors and bioelectronics*, 22(7):1205–1217.

- [Lee et al., 2014] Lee, J., Pyo, M., Lee, S.-h., Kim, J., Ra, M., Kim, W.-Y., Park, B. J., Lee, C. W., and Kim, J.-M. (2014). Hydrochromic conjugated polymers for human sweat pore mapping. *Nature communications*, 5:3736.
- [Li et al., 2010] Li, F., Zhao, Y., and Song, Y. (2010). Core-shell nanofibers: nano channel and capsule by coaxial electrospinning. In *nanofibers*. InTech.
- [Li et al., 2008] Li, M., Rouaud, O., and Poncelet, D. (2008). Microencapsulation by solvent evaporation: State of the art for process engineering approaches. *International Journal of pharmaceuticals*, 363(1-2):26–39.
- [Li et al., 2012] Li, Y., Chen, F., Nie, J., and Yang, D. (2012). Electrospun poly (lactic acid)/chitosan core–shell structure nanofibers from homogeneous solution. *Carbohydrate polymers*, 90(4):1445–1451.
- [Liang et al., 2007] Liang, D., Hsiao, B. S., and Chu, B. (2007). Functional electrospun nanofibrous scaffolds for biomedical applications. *Advanced drug delivery reviews*, 59(14):1392–1412.
- [Liechty et al., 2010] Liechty, W. B., Kryscio, D. R., Slaughter, B. V., and Peppas, N. A. (2010). Polymers for drug delivery systems. *Annual review of chemical and biomolecular engineering*, 1:149–173.
- [Lim et al., 2008] Lim, C., Tan, E., and Ng, S. (2008). Effects of crystalline morphology on the tensile properties of electrospun polymer nanofibers. *Applied Physics Letters*, 92(14):141908.
- [Lin et al., 2007] Lin, D. C., Dimitriadis, E. K., and Horkay, F. (2007). Robust strategies for automated afm force curve analysis—adhesion-influenced indentation of soft, elastic materials. *Journal of biomechanical engineering*, 129(6):904–912.
- [Luan et al., 2006] Luan, X., Skupin, M., Siepmann, J., and Bodmeier, R. (2006). Key parameters affecting the initial release (burst) and encapsulation efficiency of peptide-containing poly (lactide-co-glycolide) microparticles. *International journal of pharmaceuticals*, 324(2):168–175.

- [Mahapatra et al., 2012] Mahapatra, A., Garg, N., Nayak, B., Mishra, B., and Hota, G. (2012). Studies on the synthesis of electrospun pan-ag composite nanofibers for antibacterial application. *Journal of applied polymer science*, 124(2):1178–1185.
- [Makadia and Siegel, 2011] Makadia, H. K. and Siegel, S. J. (2011). Poly lactic-co-glycolic acid (plga) as biodegradable controlled drug delivery carrier. *Polymers*, 3(3):1377–1397.
- [Maleki et al., 2013] Maleki, M., Latifi, M., Amani-Tehran, M., and Mathur, S. (2013). Electrospun core–shell nanofibers for drug encapsulation and sustained release. *Polymer Engineering & Science*, 53(8):1770–1779.
- [Manchanda et al., 2010] Manchanda, R., Fernandez-Fernandez, A., Nagesetti, A., and McGoron, A. J. (2010). Preparation and characterization of a polymeric (plga) nanoparticulate drug delivery system with simultaneous incorporation of chemotherapeutic and thermo-optical agents. *Colloids and Surfaces B: Biointerfaces*, 75(1):260–267.
- [Martins et al., 2007] Martins, A., Araújo, J. V., Reis, R. L., and Neves, N. M. (2007). Electrospun nanostructured scaffolds for tissue engineering applications.
- [Meng et al., 2003] Meng, F. T., Ma, G. H., Qiu, W., and Su, Z. G. (2003). W/o/w double emulsion technique using ethyl acetate as organic solvent: effects of its diffusion rate on the characteristics of microparticles. *Journal of controlled release*, 91(3):407–416.
- [Menzel et al., 2000] Menzel, H., Horstmann, S., Mowery, M., Cai, M., and Evans, C. (2000). Diacetylene polymerization in self-assembled monolayers: influence of the odd/even nature of the methylene spacer. *Polymer*, 41(22):8113–8119.
- [Mitik-Dineva et al., 2008] Mitik-Dineva, N., Wang, J., Mocanasu, R. C., Stoddart, P. R., Crawford, R. J., and Ivanova, E. P. (2008). Impact of nano-topography on bacterial attachment. *Biotechnology Journal: Healthcare Nutrition Technology*, 3(4):536–544.
- [Mora-Huertas et al., 2010] Mora-Huertas, C., Fessi, H., and Elaissari, A. (2010). Polymer-based nanocapsules for drug delivery. *International journal of pharmaceutics*, 385(1-2):113–142.

- [Moreno et al., 2011] Moreno, M., Quijada, R., Santa Ana, M. A., Benavente, E., Gomez-Romero, P., and González, G. (2011). Electrical and mechanical properties of poly (ethylene oxide)/intercalated clay polymer electrolyte. *Electrochimica Acta*, 58:112–118.
- [Muffly et al., 2011] Muffly, T. M., Tizzano, A. P., and Walters, M. D. (2011). The history and evolution of sutures in pelvic surgery. *Journal of the royal society of medicine*, 104(3):107–112.
- [Murakami et al., 1999] Murakami, H., Kobayashi, M., Takeuchi, H., and Kawashima, Y. (1999). Preparation of poly (dl-lactide-co-glycolide) nanoparticles by modified spontaneous emulsification solvent diffusion method. *International journal of pharmaceutics*, 187(2):143–152.
- [Nguyen et al., 2011] Nguyen, T. T. T., Chung, O. H., and Park, J. S. (2011). Coaxial electrospun poly (lactic acid)/chitosan (core/shell) composite nanofibers and their antibacterial activity. *Carbohydrate Polymers*, 86(4):1799–1806.
- [Nguyen et al., 2012] Nguyen, T. T. T., Ghosh, C., Hwang, S.-G., Chanunpanich, N., and Park, J. S. (2012). Porous core/sheath composite nanofibers fabricated by coaxial electrospinning as a potential mat for drug release system. *International journal of pharmaceutics*, 439(1-2):296–306.
- [Ogawa et al., 1988] Ogawa, Y., Yamamoto, M., Okada, H., YASHIKI, T., and SHIMAMOTO, T. (1988). A new technique to efficiently entrap leuprolide acetate into microcapsules of polylactic acid or copoly (lactic/glycolic) acid. *Chemical and Pharmaceutical Bulletin*, 36(3):1095–1103.
- [Parsons, 2003] Parsons, S. (2003). Introduction to twinning. *Acta Crystallographica Section D: Biological Crystallography*, 59(11):1995–2003.
- [Péan et al., 1998] Péan, J., Venier-Julienne, M., Filmon, R., Sergent, M., Phan-Tan-Luu, R., and Benoit, J. (1998). Optimization of hsa and ngf encapsulation yields in plga microparticles. *International journal of pharmaceutics*, 166(1):105–115.
- [Pedicini and Farris, 2003] Pedicini, A. and Farris, R. J. (2003). Mechanical behavior of electrospun polyurethane. *Polymer*, 44(22):6857–6862.

- [Peng et al., 2009] Peng, H., Sun, X., Cai, F., Chen, X., Zhu, Y., Liao, G., Chen, D., Li, Q., Lu, Y., Zhu, Y., et al. (2009). Electrochromatic carbon nanotube/polydiacetylene nanocomposite fibres. *Nature Nanotechnology*, 4(11):738.
- [Petrović and Ferguson, 1991] Petrović, Z. S. and Ferguson, J. (1991). Polyurethane elastomers. *Progress in Polymer Science*, 16(5):695–836.
- [Pinto-Alphandary et al., 2000] Pinto-Alphandary, H., Andremont, A., and Couvreur, P. (2000). Targeted delivery of antibiotics using liposomes and nanoparticles: research and applications. *International journal of antimicrobial agents*, 13(3):155–168.
- [R. W. Warfield, 1972] R. W. Warfield, F. R. B. (1972). Elastic constants of bulk polymers. *National Technical Information Service*, 71.
- [Radke and Alocilja, 2005] Radke, S. M. and Alocilja, E. C. (2005). A high density micro-electrode array biosensor for detection of e. coli o157: H7. *Biosensors and Bioelectronics*, 20(8):1662–1667.
- [Rafati et al., 1997] Rafati, H., Coombes, A., Adler, J., Holland, J., and Davis, S. (1997). Protein-loaded poly (dl-lactide-co-glycolide) microparticles for oral administration: formulation, structural and release characteristics. *Journal of Controlled Release*, 43(1):89–102.
- [Ramalingam and Ramakrishna, 2017] Ramalingam, M. and Ramakrishna, S. (2017). Introduction to nanofiber composites. In *Nanofiber Composites for Biomedical Applications*, pages 3–29. Elsevier.
- [Ravichandran, 2009] Ravichandran, R. (2009). Nanotechnology-based drug delivery systems. *NanoBiotechnology*, 5(1-4):17–33.
- [Reneker and Chun, 1996] Reneker, D. H. and Chun, I. (1996). Nanometre diameter fibres of polymer, produced by electrospinning. *Nanotechnology*, 7(3):216.

- [Renner et al., 2012] Renner, R., Sticherling, M., Rüger, R., and Simon, J. (2012). Persistence of bacteria like *pseudomonas aeruginosa* in non-healing venous ulcers. *European Journal of Dermatology*, 22(6):751–757.
- [Rosca et al., 2004] Rosca, I. D., Watari, F., and Uo, M. (2004). Microparticle formation and its mechanism in single and double emulsion solvent evaporation. *Journal of controlled release*, 99(2):271–280.
- [Roylance, 2001] Roylance, D. (2001). Stress-strain curves. *Massachusetts Institute of Technology study, Cambridge*.
- [Ruan et al., 2002] Ruan, G., Feng, S.-S., and Li, Q.-T. (2002). Effects of material hydrophobicity on physical properties of polymeric microspheres formed by double emulsion process. *Journal of Controlled Release*, 84(3):151–160.
- [Rujitanaroj et al., 2010] Rujitanaroj, P.-o., Pimpha, N., and Supaphol, P. (2010). Preparation, characterization, and antibacterial properties of electrospun polyacrylonitrile fibrous membranes containing silver nanoparticles. *Journal of Applied Polymer Science*, 116(4):1967–1976.
- [Said et al., 2011] Said, S. S., Aloufy, A. K., El-Halfawy, O. M., Boraei, N. A., and El-Khordagui, L. K. (2011). Antimicrobial plga ultrafine fibers: Interaction with wound bacteria. *European Journal of Pharmaceutics and Biopharmaceutics*, 79(1):108–118.
- [Saito et al., 1972] Saito, Y., Nansai, S., and Kinoshita, S. (1972). Structural studies on polyurethane fibers. i. crystal and molecular structures of aliphatic polyurethanes from hexamethylene diisocyanate and some linear glycols. *Polymer Journal*, 3(2):113.
- [Salager, 2002] Salager, J.-L. (2002). Surfactants types and uses. *FIRP booklet*, (E300A).
- [Scholes et al., 1993] Scholes, P., Coombes, A., Illum, L., Daviz, S., Vert, M., and Davies, M. (1993). The preparation of sub-200 nm poly (lactide-co-glycolide) microspheres for site-specific drug delivery. *Journal of controlled release*, 25(1-2):145–153.

- [Schwach et al., 2003] Schwach, G., Oudry, N., Delhomme, S., Lück, M., Lindner, H., and Gurny, R. (2003). Biodegradable microparticles for sustained release of a new gnrh antagonist—part i: screening commercial plga and formulation technologies. *European journal of pharmaceutics and biopharmaceutics*, 56(3):327–336.
- [Scindia et al., 2007] Scindia, Y., Silbert, L., Volinsky, R., Kolusheva, S., and Jelinek, R. (2007). Colorimetric detection and fingerprinting of bacteria by glass-supported lipid/polydiacetylene films. *Langmuir*, 23(8):4682–4687.
- [Selig et al., 2012] Selig, H. F., Lumenta, D. B., Giretzlehner, M., Jeschke, M. G., Upton, D., and Kamolz, L. P. (2012). The properties of an “ideal” burn wound dressing—what do we need in daily clinical practice? results of a worldwide online survey among burn care specialists. *Burns*, 38(7):960–966.
- [SEZGIN BAYINDIR et al., 2009] SEZGIN BAYINDIR, Z., BADILLI, U., and SENDEL TÄJRK C., T. (2009). Preparation of polymeric nanoparticles using different stabilizing agents. *Ankara ĀIUniversitesi EczacÄšlÄš FakÄijltesi Dergisi*, 38:257 – 268.
- [Singh and Lillard Jr, 2009] Singh, R. and Lillard Jr, J. W. (2009). Nanoparticle-based targeted drug delivery. *Experimental and molecular pathology*, 86(3):215–223.
- [Sirc et al., 2012] Sirc, J., Kubinova, S., Hobzova, R., Stranska, D., Kozlik, P., Bosakova, Z., Marekova, D., Holan, V., Sykova, E., and Michalek, J. (2012). Controlled gentamicin release from multi-layered electrospun nanofibrous structures of various thicknesses. *International journal of nanomedicine*, 7:5315.
- [Smith, 1974] Smith, T. L. (1974). Tensile strength of polyurethane and other elastomeric block copolymers. *Journal of Polymer Science Part B: Polymer Physics*, 12(9):1825–1848.
- [Song et al., 1997] Song, C., Labhasetwar, V., Murphy, H., Qu, X., Humphrey, W., Shebuski, R., and Levy, R. (1997). Formulation and characterization of biodegradable nanoparticles for intravascular local drug delivery. *Journal of Controlled Release*, 43(2-3):197–212.

- [Sonnenschein, 2015] Sonnenschein, M. F. (2015). Theoretical concepts and techniques in polyurethane science. *Polyurethanes: Science, Technology, Markets, and Trends*, pages 127–159.
- [Spathis, 1991] Spathis, G. (1991). Polyurethane elastomers studied by the mooney–rivlin equation for rubbers. *Journal of applied polymer science*, 43(3):613–620.
- [Srikar et al., 2008] Srikar, R., Yarin, A. L., Megaridis, C., Bazilevsky, A., and Kelley, E. (2008). Desorption-limited mechanism of release from polymer nanofibers. *Langmuir*, 24(3):965–974.
- [Staudinger, 1960] Staudinger, H. (1960). Die hochmolekularen im festen zustand. In *Die Hochmolekularen Organischen Verbindungen*, pages 105–123. Springer.
- [Stebbins et al., 2014] Stebbins, N. D., Ouimet, M. A., and Uhrich, K. E. (2014). Antibiotic-containing polymers for localized, sustained drug delivery. *Advanced drug delivery reviews*, 78:77–87.
- [Su et al., 2012] Su, Z., Li, J., Li, Q., Ni, T., and Wei, G. (2012). Chain conformation, crystallization behavior, electrical and mechanical properties of electrospun polymer-carbon nanotube hybrid nanofibers with different orientations. *Carbon*, 50(15):5605–5617.
- [Subbiah, 2004] Subbiah, T. (2004). *Development of nanofiber protective substrates*. PhD thesis, Texas Tech University.
- [Sun et al., 2006a] Sun, A., Lauher, J. W., and Goroff, N. S. (2006a). Preparation of poly (diiododiacetylene), an ordered conjugated polymer of carbon and iodine. *Science*, 312(5776):1030–1034.
- [Sun et al., 2006b] Sun, B., Duan, B., and Yuan, X. (2006b). Preparation of core/shell pvp/pla ultrafine fibers by coaxial electrospinning. *Journal of Applied Polymer Science*, 102(1):39–45.

- [Sun et al., 2003] Sun, Z., Zussman, E., Yarin, A. L., Wendorff, J. H., and Greiner, A. (2003). Compound core-shell polymer nanofibers by co-electrospinning. *Advanced materials*, 15(22):1929–1932.
- [Tachibana et al., 2001] Tachibana, H., Kumai, R., Hosaka, N., and Tokura, Y. (2001). Crystal structures, polymerization, and thermochromic phase changes in urethane-substituted diacetylenes crystals with varying alkyl chain lengths. *Chemistry of materials*, 13(1):155–158.
- [Taha et al., 2013] Taha, M., Chai, F., Blanchemain, N., Goube, M., Martel, B., and Hildebrand, H. (2013). Validating the poly-cyclodextrins based local drug delivery system on plasma-sprayed hydroxyapatite coated orthopedic implant with toluidine blue o. *Materials Science and Engineering: C*, 33(5):2639–2647.
- [Tan et al., 2005] Tan, S., Inai, R., Kotaki, M., and Ramakrishna, S. (2005). Systematic parameter study for ultra-fine fiber fabrication via electrospinning process. *Polymer*, 46(16):6128–6134.
- [Tanaka, 2008] Tanaka, M. (2008). Glossary of TEM Terms. <http://www.jeol.co.jp/en/words/emterms/>. [Online; accessed 19-December-2017].
- [Thakur et al., 2008] Thakur, R., Florek, C., Kohn, J., and Michniak, B. (2008). Electrospun nanofibrous polymeric scaffold with targeted drug release profiles for potential application as wound dressing. *International journal of pharmaceutics*, 364(1):87–93.
- [Thein et al., 2013] Thein, E., Tabin, U. F., Betrisey, B., Trampuz, A., and Borens, O. (2013). In vitro activity of gentamicin-loaded bioabsorbable beads against different microorganisms. *Materials*, 6(8):3284–3293.
- [Tissue, 2015] Tissue, A. (2015). Wound infection and the dangers of sepsis. *Wound infections*, 14.
- [Tong et al., 2011] Tong, L., Cheng, B., Liu, Z., and Wang, Y. (2011). Fabrication, structural characterization and sensing properties of polydiacetylene nanofibers templated from anodized aluminum oxide. *Sensors and Actuators B: Chemical*, 155(2):584–591.

- [Tsuji et al., 2000] Tsuji, H., Mizuno, A., and Ikada, Y. (2000). Properties and morphology of poly (l-lactide). iii. effects of initial crystallinity on long-term in vitro hydrolysis of high molecular weight poly (l-lactide) film in phosphate-buffered solution. *Journal of Applied Polymer Science*, 77(7):1452–1464.
- [Verstraete et al., 2016] Verstraete, L., Greenwood, J., Hirsch, B. E., and De Feyter, S. (2016). Self-assembly under confinement: nanocorrals for understanding fundamentals of 2d crystallization. *ACS nano*, 10(12):10706–10715.
- [Wei, 2012] Wei, Q. (2012). *Functional nanofibers and their applications*. Elsevier.
- [Weisenhorn et al., 1989] Weisenhorn, A., Hansma, P., Albrecht, T., and Quate, C. (1989). Forces in atomic force microscopy in air and water. *Applied Physics Letters*, 54(26):2651–2653.
- [Weisenhorn et al., 1993] Weisenhorn, A. L., Kasas, S., Solletti, J., Khorsandi, M., Gotzos, V., Roemer, D., and Lorenzi, G. (1993). Deformation observed on soft surfaces studied with an afm. In *Scanning Probe Microscopies II*, volume 1855, pages 26–35. International Society for Optics and Photonics.
- [Xiong et al., 2014] Xiong, M.-H., Bao, Y., Yang, X.-Z., Zhu, Y.-H., and Wang, J. (2014). Delivery of antibiotics with polymeric particles. *Advanced drug delivery reviews*, 78:63–76.
- [Yao et al., 2014] Yao, J., Bastiaansen, C. W., and Peijs, T. (2014). High strength and high modulus electrospun nanofibers. *Fibers*, 2(2):158–186.
- [Yoon et al., 2009] Yoon, B., Lee, S., and Kim, J.-M. (2009). Recent conceptual and technological advances in polydiacetylene-based supramolecular chemosensors. *Chemical Society Reviews*, 38(7):1958–1968.
- [Zahedi et al., 2010] Zahedi, P., Rezaeian, I., Ranaei-Siadat, S.-O., Jafari, S.-H., and Supaphol, P. (2010). A review on wound dressings with an emphasis on electrospun nanofibrous polymeric bandages. *Polymers for Advanced Technologies*, 21(2):77–95.

- [Zhang et al., 2009] Zhang, J.-F., Yang, D.-Z., Xu, F., Zhang, Z.-P., Yin, R.-X., and Nie, J. (2009). Electrospun core-shell structure nanofibers from homogeneous solution of poly (ethylene oxide)/chitosan. *Macromolecules*, 42(14):5278–5284.
- [Zhang et al., 2005] Zhang, Y., Lim, C. T., Ramakrishna, S., and Huang, Z.-M. (2005). Recent development of polymer nanofibers for biomedical and biotechnological applications. *Journal of Materials Science: Materials in Medicine*, 16(10):933–946.
- [Zhang and Feng, 2006] Zhang, Z. and Feng, S.-S. (2006). Nanoparticles of poly (lactide)/vitamin e tpgs copolymer for cancer chemotherapy: synthesis, formulation, characterization and in vitro drug release. *Biomaterials*, 27(2):262–270.
- [Zhou et al., 2013] Zhou, J., Patel, T. R., Sirianni, R. W., Strohbehn, G., Zheng, M.-Q., Duong, N., Schafbauer, T., Huttner, A. J., Huang, Y., Carson, R. E., et al. (2013). Highly penetrative, drug-loaded nanocarriers improve treatment of glioblastoma. *Proceedings of the National Academy of sciences*, 110(29):11751–11756.
- [Ziabicki and KÈłdzierska, 1962] Ziabicki, A. and KÈłdzierska, K. (1962). Studies on the orientation phenomena by fiber formation from polymer melts. iii. effect of structure on orientation. condensation polymers. *Journal of Applied Polymer Science*, 6(19):111–119.